TECHNISCHE UNIVERSITÄT DRESDEN

Fakultät Umweltwissenschaften

# Reactive transport simulation of contaminant fate and redox transformation in heterogeneous aquifer systems

Dissertation for awarding the academic degree

Doctor of Engineering (Dr.-Ing)

Submitted by

**M.Sc. Eunseon Jang**

06.10.1986 in Ulsan, South Korea

Supervisor

Prof. Dr. –Ing. Olaf Kolditz, Technical University of Dresden

Prof. Dr. Christoph Schüth, Technical University of Darmstadt

Prof. Dr. Seong-Taek Yun, Korea University, South Korea

Date of defense: 17.03.2017

Leipzig, July 2017

Note on the commencement of the doctoral procedure

(1) I hereby assure that I have produced the present work without inadmissible help from third parties and without aids other than those stated; ideas taken directly or indirectly from external sources are identified as such.

(2) When selecting and evaluating the material and also when producing the manuscript, I have received support from the following persons: Dr. Thomas Kalbacher (UFZ), Wenkui He (UFZ/TUD), and Heather Savoy(UC Berkeley)

(3) No further persons were involved in the intellectual production of the present work. In particular, I have not received help from a commercial doctoral adviser. No third parties have received monetary benefits from me, either directly or indirectly, for work relating to the content of the presented dissertation.

(4) The work has not previously been presented in the same or a similar format to another examination body in Germany or abroad, nor has it-unless it is a cumulative dissertation-been published.

(5) If this concerns a cumulative dissertation in accordance with Section 10 Para. 2, I assure compliance with the conditions laid down therein.

(6) I confirm that I acknowledge the doctoral regulations of the Faculty of Environmental Sciences of the Technische Universität Dresden.

Declaration of conformity:

I hereby confirm that this copy conforms with the original dissertation on the topic:

„Reactive transport simulation of contaminant fate and redox transformation in heterogeneous aquifer systems"

Place, Date

Leipzig, 05.07.2017

Signature (surname, first name)

Jang, Eunseon

# ABSTRACT

The transport of contaminants in groundwater system is strongly influenced by various aquifer heterogeneity factors such as spatial aquifer heterogeneity of hydraulic conductivity and reactive substances distribution. The contaminants transport can be simulated by using numerical reactive transport models, and their fate can be possibly even predicted. Furthermore, reactive transport modeling is an essential tool to get a profound understanding of hydrological-geochemical complex processes and to make plausible predictions of assessment.

The goal of this work is to improve our understanding of the groundwater contaminants fate and transport processes in heterogeneous aquifer systems, with a focus on nitrate problems. A large body of knowledge of the fate and transport of nitrogen species has been achieved by previous works, however, most previous models typically neglect the interrelation of physical and chemical aquifer heterogeneities on the contaminant fate and redox transformation, which is required for predicting the movement and behavior of nitrate and quantifying the impact of uncertainty of numerical groundwater simulation, and which motivates this study. The main research questions which are answered in this work are how aquifer heterogeneity influences on the nitrate fate and transport and then, what is the most influential aquifer heterogeneity factor must be considered. Among the various type of aquifer heterogeneity, physical and chemical aquifer heterogeneities are considered.

The first part of the work describes groundwater flow system and hydrochemical characteristics of the study area (Hessian Ried, Germany). Especially, data analyses are performed with the hydrochemical data to identify the major driving force for nitrate reduction in the study area. The second part of the work introduces a kinetic model describing nitrate removal by using numerical simulation. The resulting model reproduces nitrate reduction processes and captures the sequence of redox reactions. The third and fourth parts show the influence of physical and chemical aquifer heterogeneity with varying variance, correlation length scale, and anisotropy ratio. Heterogeneous aquifer systems are realized by using stochastic approach. Results, in

short, show that the most influential aquifer heterogeneity factors could change over time. With abundant requisite electron donors, physical aquifer heterogeneity significantly influences the nitrate reduction while chemical aquifer heterogeneity plays a minor role. Increasing the spatial variability of the hydraulic conductivity increases the nitrate removal efficiency of the system in addition. If these conditions are reversed, nitrate removal efficiency varies by the spatial heterogeneity of the available initial electron donor. The results indicate that an appropriate characterization of the physical and chemical properties can be of significant importance to predict redox contamination transport and design long-term remediation strategies and risk assessment.

# KURZFASSUNG

Der Transport von Verunreinigungen in Grundwasserleitern werden, neben dem hydraulischen Gradienten, in erster Linie durch räumlich uneinheitlich verteilte Aquifermaterialeigenschaften, wie z.B. die heterogene Verteilung der hydraulische Leitfähigkeit und reaktiver Substanzen, gesteuert. Der Transport der Schadstoffe kann durch durch reaktive Transportmodellierung simuliert und deren Verbleib gegebenenfalls auch vorhergesagt werden. Die reaktive Transportmodellierung ist darüber hinaus auch ein wesentlicher Ansatz, um ein tieferes Verständnis für komplexe hydrogeochemische Prozesse zu erhalten.

Das Ziel dieser Arbeit ist es, Modellstudien zur Verbesserung des Verständnisses über Grundwasserschadstoffverbleib und –transport in heterogenen Aquifersystemen zu unterstützen, mit einem Fokus auf Nitratprobleme. Obwohl es bereits eine umfangreiche Fachliteratur gibt, mangelt es noch immer an ausreichender Information und Verständnis über den Zusammenhang von physikalischer und chemischer Aquiferheterogenität mit dem Schadstoffverbleib und den Redox-Reaktionen, und das insbesondere auf größeren Skalen.

Folgende zentrale Forschungsfrage wird in dieser Arbeit aufgegriffen: Wie beeinflusst Aquiferheterogenität die Nitratabbaukapazität? Unter den verschiedenen Typen von Aquifereigenschaften werden physikalische und chemische Aquiferheterogenitäten betrachtet.

Der erste Teil der Arbeit beschreibt das Grundwasserströmungssystem und die hydrogeochemischen Eigenschaften des Untersuchungsgebietes (Hessisches Ried, Deutschland). Dazu wurden Datenanalysen mit den hydrogeochemischen Daten ausgeführt, um die Hauptantriebskraft für die Nitratreduktion im Untersuchungsgebiet zu identifizieren. Im zweiten Teil der Arbeit wird ein kinetisches Modell eingeführt, das den Nitratabbau mittels numerischer Simulation beschreibt. Das entwickelte Modell reproduziert Nitratreduktionsprozesse einschließlich des Verbrauchs von Nitrat und der Auflösung / Ausfällung von Mineralien. Die Abfolge von Redox-Reaktionen wird

erfasst. Der dritte und vierte Teil der Arbeit zeigen den Einfluss der physikalischen und chemischen Aquiferheterogenität bei unterschiedlichen Varianzen und Korrelationslängen. Heterogene Aquifersysteme wurden unter Verwendung eines stochastischen Ansatzes realisiert. Die Ergebnisse zeigen, dass sich die Relevanz der Heterogenitätsfaktoren mir der Zeit verändern kann, bzw. stark vom betrachteten Zeitraum abhängt. Wenn z.B. ausreichend Elektrodonatoren vorhanden sind, wird die Nitratreduktion insbesondere durch die physikalische Aquiferheterogenität beeinflusst, . die chemische Aquiferheterogenität spielt dann eine eher untergeordnete Rolle. Eine Vergrößerung der räumlichen Variabilität der hydraulischen Leitfähigkeit erhöht den Wirkungsgrad des Nitratabbaus zusätzlich. Bei umgekehrten Bedingungen variiert die Effizienz des Nitratabbaus durch die räumliche Heterogenität der verfügbaren Elektronendonatoren. Die Ergebnisse zeigen, dass eine ausreichende Charakterisierung der Varianz der physikalischen und chemischen Eigenschaften von großer Bedeutung ist, um Schadstofftransport und Redox-Reaktionen vorherzusagen um insbesondere langfristige Sanierungsstrategien und Risikobewertungen zu planen.

# ACKNOWLEDGEMENTS

From my deepest heart, I would like to thank all those who have supported me to complete my dissertation.

First and foremost, I would like to express my sincere thanks to my supervisors Prof. Dr.-Ing Olaf Kolditz (Helmholtz-Centre for Environmental Research-UFZ, Department of Environmental Informatics-ENVINF) and Dr. Thomas Kalbacher (UFZ, ENVINF) who provided excellent support and expert guidance throughout my studies. Without their help, I could not have achieved my goals in the Ph.D. work in this field. I also greatly appreciate Prof. Rubin Yoram (University of California, Berkeley) bring me a deeper understanding of stochastic groundwater hydrology with his helpful scientific discussions and Prof. Christoph Schüth (Technische Universität Darmstadt) for insightful comments during my paper writing. Special recognition is given to Dr. Wenkui He (Dr. Knoell Consult GmbH) and Heather Savoy (University of California, Berkeley) for proofreading and many valuable discussions.

Also, I would like to express my gratitude to all of my colleagues at the Department of Environment Informatics and the OpenGeoSys Community, especially Dr. Wenqing Wang, Dr. Norihiro Watanabe and Jun.-Prof. Dr. Haibing Shao for their kind advice and help in numerical simulation matters and Dr. Chan-Hee Park, Dr. Byoung-Ohan Shim, Dr. Yuanyuan Sun and Prof. Seong-Taek Yun (Korea University) for being my special mentors and encouraging me a lot. Additionally, I would like to extend my thanks to Leslie Jacob and Barbara Kolditz, who helped me to improve my English and German language for my publication.

I would like to further gratefully acknowledge all my fellow Ph.D. students for their support throughout my graduate school experience, Yonghui Huang, Haiyang Yi, Xing-Yuan Miao, Renchao Lu, Erik Nixdorf, Christoph Lehmann, Tianyuan Zheng, and Philipp Hein. I also thank the graduate school of the UFZ (HIGRADE) and Barbara Timmel (UFZ, International Office) for providing convenience for my studying and staying in UFZ.

Last but not the least; I must thank my beloved family and wonderful friends who continuously supported me during the last three years. Thank you all!

*Leipzig July 2017*

*Eunseon Jang*

# CONTENTS

# LIST OF TABLES

# LIST OF FIGURES

# Acronyms

| | |
|---|---|
| **ADE** | Advection-Dispersion Equation |
| **CV** | Covaraince Function |
| **DDC** | Domain Decomposition |
| **ED** | Electron Donor |
| **EA** | Electron Acceptor |
| **FEM** | Finite Element Method |
| **MPI** | Message Passing Interface |
| **OGS** | OpenGeoSys |
| **PDF** | Partial Differential Function |
| **REV** | Representative Elementary Volume |
| **RTM** | Reactive Transport Modeling |
| **SNIA** | Sequential Non-Iterative Approach |
| **SRF** | Spatial Random Function |

# 1. INTRODUCTION

## 1.1. Background and motivation

Groundwater is an essential natural resource. In the environment, groundwater is a source of recharge for lakes, rivers, and wetlands. In many rivers across Europe, more than 50 % of the annual flow is provided from groundwater (European Commission, 2008). That means the deterioration of groundwater quality may directly affect related surface water and terrestrial ecosystems. Groundwater is also a source of drinking water and still more use it to supply factories with process water or farms with irrigation water. Approximately one-third of the world's populations use groundwater for drinking (UNEP, 2013) and about 75% of EU inhabitants depend on groundwater for their water supply (European Commission, 2008). The quality of groundwater is therefore of the utmost importance for the functioning of the hydrological cycle and ecological systems, and also for the human life. However, groundwater can easily become polluted, primarily because of human activities such as waste disposal, mining, and agricultural operations. Any addition of undesirable substances to groundwater is considered to be groundwater contaminants. When these substances reach the aquifer, they trigger dis-equilibrium of groundwater and deteriorate water quality. Since groundwater moves very slowly that contaminants can take a long-time to appear. This means that the pollution that occurred some decades ago may still last and be threatening groundwater quality today or even near future (European Commission, 2008). Therefore, a thorough understanding of the groundwater contaminant fate and transport is fundamental for the management of groundwater resources.

Various studies have been conducted to understand the behavior of the groundwater contaminants. Identifying and monitoring the groundwater contamination can be verified through comparison with *in situ* field measurement and laboratory experiments. However, such experiments are necessarily limited to relatively short time scale, and coupled physical-geochemical systems are difficult to elucidate. A numerical simulation

could be used to help understand and predict the movement of the contaminants, as well as, to develop a better understanding of these complexities. Since the 1980s, a variety of numerical reactive transport modeling has been implemented and applied to simulate groundwater contamination problems, such as BIOMOC (Essaid and Bekins, 1997), CFPv2 with UMT3D (Xu et al., 2015), GeoSysBRNS (Centler et al., 2010), MODFLOW-PHT3D (Zhang et al., 2013), MODFLOW-UZF and RT3D (Bailey et al., 2013), OpenGeoSys-ChemApp (Li et al., 2013), OpenGeoSys-GEM (Kosakowski and Watanabe, 2014), OpenGeoSys-IPhreeqc (He et al., 2015), ParCrunchFlow (Beisman et al., 2015), RISK-N (Oyarzun et al., 2007), SF-Monod (Cui et al., 2014), and TOUGHREACT-N (Maggi et al., 2008).

The majority of the efforts have been conducted; however, characterization of the subsurface is still a challenge since the structure and properties of the subsurface are inherently heterogeneous and variable at various scales (Bayer et al., 2015; Elfeki et al., 1997). Various types of heterogeneity have been suggested to affect the contaminant fate and transport. For example, heterogeneous hydraulic conductivity field can cause a broad range of groundwater travel times and flow patterns which significantly influence transport and distribution of mobile species. Heterogeneous aquifer mineralogy or reactive substances distribution also affect local geochemical conditions that contribute to the redox reactions. Most existing models neglect the effect of the heterogeneity and assumed the subsurface properties as a single value throughout the entire domain or represented by the multi-layered system. Furthermore, the value is often uncertain due to the scarcity of information. Even if we can observe these heterogeneous characteristics without observation errors, we cannot possibly measure them everywhere. Obviously, these imperfect representations of parameters lead to errors in model results (Bierkens and Geer, 2012). For a better understanding of the behavior of the contaminants in the subsurface system, the influence of various types of aquifer heterogeneity must be considered while very few of modeling studies include the aquifer heterogeneity.

The intention of the thesis is to improve our understanding of the groundwater contaminants fate and transport processes in heterogeneous aquifer systems. The

application of coupled hydrological-geochemical models with stochastic approach allows the evaluation of the influence of the aquifer heterogeneity on the fate of contaminant and can help to delineate risk areas and design remediation strategies.

## 1.2. Research question and objectives

The objective of this study is to describe the influence of the aquifer heterogeneity on the contaminant fate and transport. The two main research questions are:

1. How aquifer heterogeneity (e.g. physical and chemical) influences the groundwater contaminant transport and geochemical reactions (i.e. redox transformation processes)?
2. What is the most influential aquifer heterogeneity factor must be considered? Physical or chemical?

Results for this study can be interpreted from two different perspectives. First, one might be interested in contaminant reactive transport modeling, especially in the heterogeneous aquifer systems. This study can show how reactive transport processes with coupled physical and chemical aquifer heterogeneity have been achieved. The second perspective involves designing remediation strategy and risk assessment. Because of inherent complexities, quantifying the uncertainty of the prediction has been considered as a crucial point. This research gives how aquifer heterogeneity influences the contaminant behavior and suggests that the most influential aquifer heterogeneity factor must be considered beforehand its impact.

## 1.3. Dissertation organization

This dissertation is organized in the following. Chapter 2 describes the basic principles, and Chapter 3 presents the general information of the methods. In Chapter 4, a description of the study area and nitrate reduction simulation is presented. Finally, simulation results and discussion are presented in Chapter 5. The summary and outlook of the work are given at the end.

# 2. THEORY

The contamination problem of major interest within this work is nitrate in groundwater systems. Nitrate ($NO_3^-$) is a ubiquitous groundwater contaminant found in aquifers, particularly shallow unconfined aquifers in rural areas (Nolan et al., 1997). A brief description of nitrate contamination is presented in Chapter 2.1. Modeling nitrate reactive transport in the groundwater involves the coupling of multiple processes, which mainly consists of water flow, solute transport, and geochemical reactions. The governing equations of each problem are described separately in Chapter 2.2 and 2.3. Detailed spatial resolutions of the heterogeneous distribution of hydrological and geochemical parameters are not possible in numerical models in general due to the complexity and lack of information. Therefore, a method has developed to handle the aquifer heterogeneity in a stochastic manner described in Chapter 2.4.

## 2.1. Nitrate contamination in groundwater

Nitrogen is the most abundant gas in the atmosphere and essential for all living things, as it is an essential component of protein. Nitrogen exists in many forms and is transformed into reactive forms, typically like nitrate ($NO_3^-$), ammonium ($NH_4^+$), ammonia ($NH_3$), and organic nitrogen as it moves through the nitrogen cycle. Nitrate can get into the groundwater systems from various point and non-point sources and persist for decades as a predominant form of reactive nitrogen due to its high soluble and mobile characteristics (Korom, 1992). Ammonium also can exist, but less prevalent in the water because it is incorporated into organic matter and adsorbed by predominantly negatively charged clay particles.

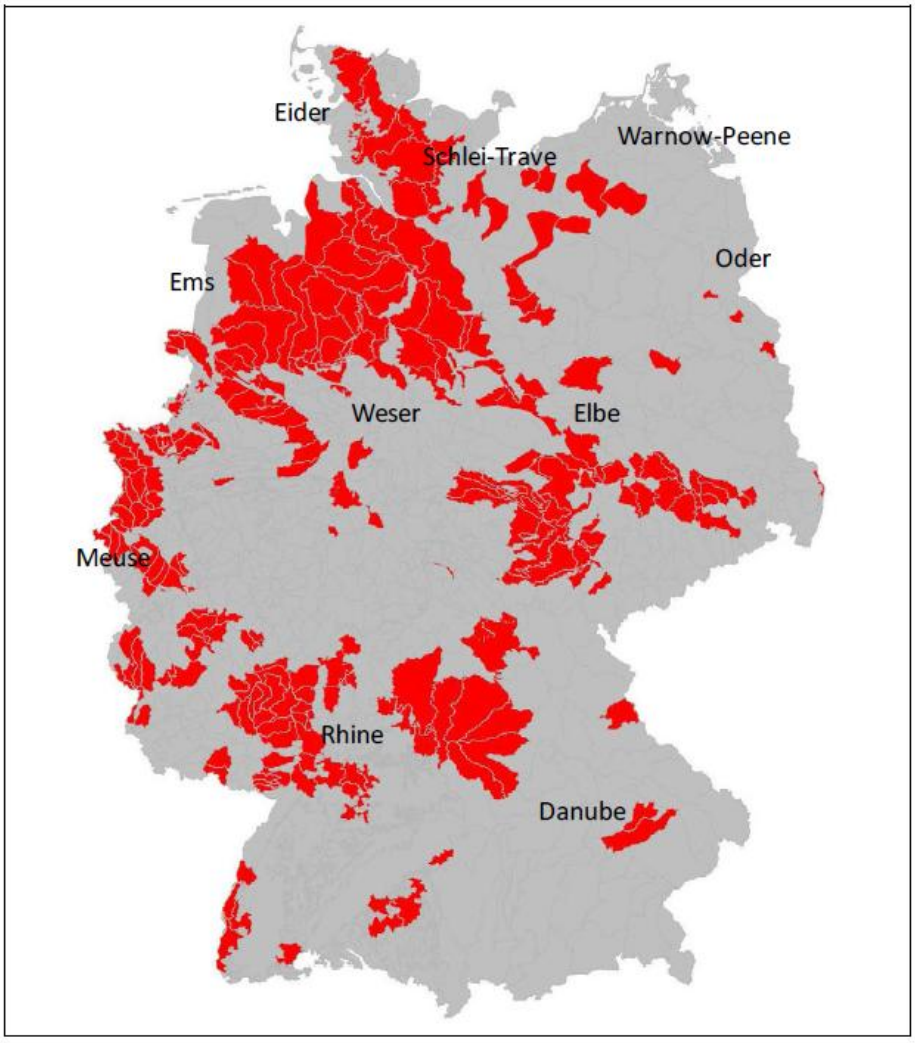


Figure 1 Bodies of groundwater in Germany which do not have good chemical status due to excessive nitrate concentrations (> 50mgL$^{-1}$) (from SRU (2015))

Background nitrate concentrations unaffected by human activities are usually less than 2 mg/L (Mueller et al., 1995). Nevertheless, it can reach high levels due to the intensive use of fertilizers or contamination with human and/or animal waste (e.g. septic discharge, fertilization using manure or synthetic nitrogen sources, and concentrated animal feeding operations) (Korom, 1992; Rivett et al., 2008). Excessive concentrations of nitrate in drinking water can trigger health problems such as gastric cancer and

methemoglobinemia [1] (Fan and Steinberg, 1996), and nitrate contaminants from domestic and industrial wastewaters are responsible for promoting the eutrophication in lake and rivers (Rinke et al., 2013; Zan et al., 2011). Therefore the European Union (EU) Drinking Water Directive (98/83/EC) and Nitrate Directive (91/676/EEC) require protection of all natural waters and set a maximum allowable concentration for nitrate of 50mg$L^{-1}$ (European Union, 1998) and US Environmental Protection Agency (EPA)'s maximum contaminant level (MCL) for nitrate (as nitrate-N) is 10 mg$L^{-1}$ (USEPA, 2009). Even so, the application of fertilizer has led to significant nitrate pollution of shallow groundwater in many countries since the middle of the last century (Böhlke and Denver, 1995; Chae et al., 2009; Kim et al., 2015; Knipp, 2012; Miotliński, 2008; Zhang et al., 2009). For example, the groundwater in Germany by the Water Framework Directive (WFD) shows that 27% fail to achieve good chemical status because of a high concentration of nitrate (SRU, 2015). In Figure 1, the nitrate pollution is generally spread over all areas of the country; however, the high concentrations of nitrate can be identified in northwest Germany which shows a clear influence of agricultural operations. According to the National Institute of Environmental Research (NIER), in South Korea a medium groundwater nitrate–concentration is 5.4mg$L^{-1}$ for 1500 wells (including 1032 domestic and 468 agricultural wells) in rural cropping-livestock farming area, and 19.6% of the sample are exceeded the 10mg$L^{-1}$ allowable limit for drinking water (NIER, 2012). Most of the nitrate pollution in groundwater bodies in South Korea is highly related with non-point sources with relation to agricultural activities (e.g. chemical fertilizers and manure composts) (Kim et al., 2015). Moreover, various researchers reported that a new interest in biofuel crops to meet energy needs is likely to elevate nitrate concentration in the shallow groundwater resources (Li and Merchant, 2013; Liao et al., 2012; Twomey et al., 2010).

[1] i.e., "blue baby syndrome", when ingested, nitrate is converted to nitrite by the body and reacts with hemoglobin (which carries oxygen to all parts of the body) in the bloodstream to form methemoglobin (which does not carry oxygen) resulting in suffocation of the victim Comly, H.H., 1945. Cyanosis in infants caused by nitrates in well water. Journal of the American Medical Association, 129(2): 112-116.

## 2.1.1. Redox reaction

An Oxidation-reduction reaction, commonly known as a redox reaction, plays an important role in the distribution of dissolved substances in the natural groundwater systems. Redox reactions are defined as reactions in which electrons are transferred from one species (electron donor: ED) to another (electron acceptor: EA). Since these reactions determine the redox species speciation and their mobility, they also exert a major role for aquifer contaminant problems such as leaching of nitrate from agricultural land, contaminants leaching from landfill sites, and so on (Appelo and Postma, 2005; Christensen et al., 2000). The sequence of redox reactions can be predicted by standard equilibrium thermodynamics; however, their reaction rates are often very slow (e.g. kinetic reaction) or mediated by bacterial catalysis and rather variable (Appelo and Postma, 2005). Figure 2 shows the distribution of the redox zones in response to a contaminant plume moving through the aquifer. The plume, which moves with groundwater flow, develops distinct redox zones. Once EA is depleted, a new redox reaction using a new electron acceptor is initiated.

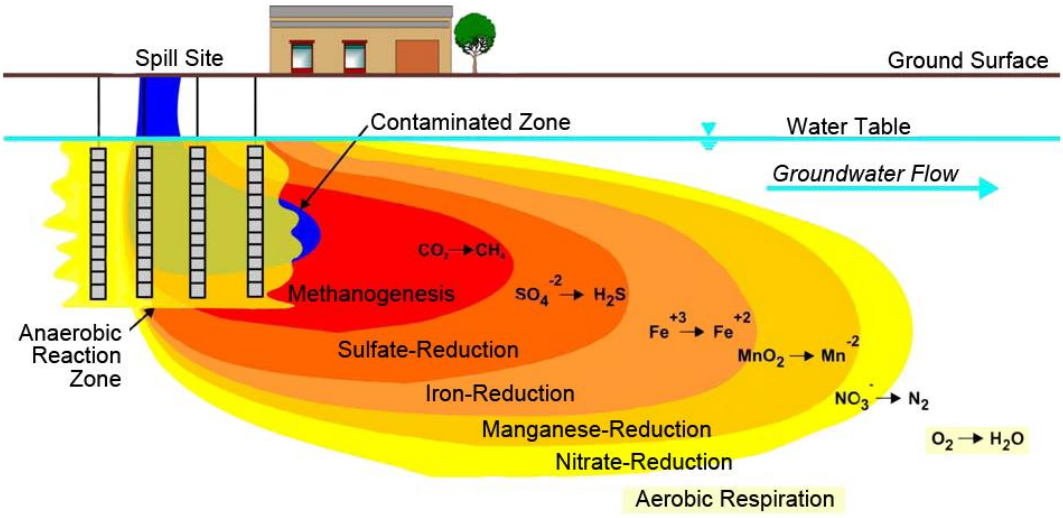


Figure 2 Redox zones of a typical contaminant plume. The redox reaction sequence is commonly seen along groundwater flow lines in landfill leachate plumes (from Parsons (2005))

## 2.1.2. Denitrification

Excessive nitrate can be migrated naturally under anaerobic condition by reduction processes, so-called denitrification, which reduces nitrate ($NO_3^-$) to nitrous oxide ($N_2O$) and dinitrogen ($N_2$) (Figure 3).

$$(+5) \rightarrow (+3) \rightarrow (+2) \rightarrow (+1) \rightarrow 0$$

$$NO_{3\,(aq)}^- \rightarrow NO_{2(aq)}^- \rightarrow NO_{(gas)} \rightarrow N_2O_{(gas)} \rightarrow N_{2(gas)} \quad (2.1.1)$$

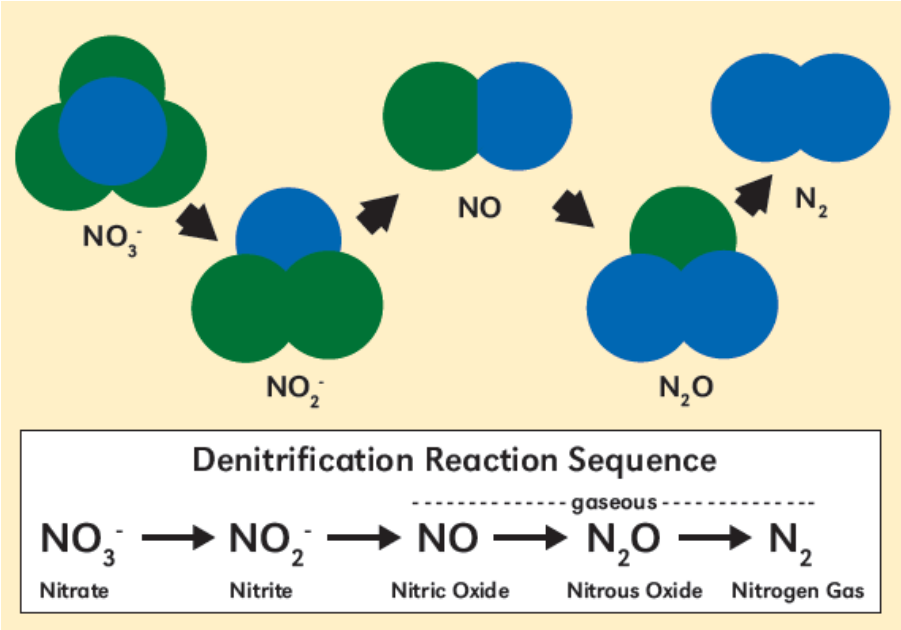


Figure 3 Denitrification reaction sequence (from NPNI)

The nitrate reduction reaction can be written as a half-equation that describes the role of electron ($e^-$) transfer:

$$2NO_3^- + 10e^- + 12H^+ \rightarrow N_2 + 6H_2O \quad (2.1.2)$$

The produced $N_2$ gas remains until groundwater discharges to surface water and equilibrates with the atmosphere (Heaton and Vogel, 1981).

Denitrification can occur in both unsaturated soils and groundwater aquifer where the following principle conditions are matched; 1) nitrate present, 2) microbes with metabolic capacity for nitrate reduction, 3) restricted dissolved oxygen (< 2~5mgL$^{-1}$)

condition, and 4) reactive substances such as organic matters or reduced inorganic species (reduced iron, or reduced sulfur compounds or uranium (IV)) as requisite electron donors (Korom, 1992; Wriedt and Rode, 2006). The most common microbes with metabolic capacity to couple the oxidation of reduced iron and reduced sulphur compounds are *Thiobacillus denitrificants* and *Rhodopseudomonas sphaeroides* (autotrophic denitrifying bacterium) (Beller et al., 2006). *Pseudomonas, Alcligenes,* and *Azospirilum* are typical microbes for nitrate reduction by organic matter (Beauchamp et al., 1989). Although these microbes are essentially ubiquitous in the subsurface (Rivett et al., 2008), nitrate is still the most common contaminants in the shallow groundwater system due to lack of suitable electron donors or redox environment to accelerate nitrate reduction (Critchley et al., 2014).

## 2.1.3. Denitrification coupled to pyrite oxidation

Two major denitrification reactions have been suggested; heterotrophic denitrification by oxidation of organic carbon sources and autotrophic denitrification by oxidation of chemoautotrophic energy sources (Rivett et al., 2008). Heterotrophic denitrification occurs mainly in shallow unsaturated or saturated zones, where organic matter is present due to decaying crop material and leaching from the soil profile (Bailey et al., 2012). Various studies have been extensively conducted both in field and laboratory experiments and reported that nitrate reduction by heterotrophic denitrification is thermodynamically more favored than reductions coupled to chemoautotrophic energy sources (e.g. reduced iron, reduced sulfur and methane) (Korom, 1992). However, the latter pathway may also be utilized by denitrifying organisms in the presence of pyrite ($FeS_2$). Autotrophic denitrification is supported by laboratory scale experiments (Juncher Jørgensen et al., 2009; Torrentó et al., 2010) and also field studies that pyrite oxidation decrease the nitrate concentrations while sulfate is release to the groundwater (Hayakawa et al., 2013; Torrentó et al., 2010; Zhang et al., 2009). For example, Zhang et al.,(2009) conducted a geochemical analysis of both sediment and groundwater in a sandy aquifer located underneath cultivated fields and an

adjacent forested area at Oostrum, The Netherlands. They reported that denitrification coupled to pyrite oxidation is possibly a major nitrate reduction pathway. Torrentó at al., (2011) and Otero et al., (2009) also revealed that denitrification processes is mainly related to pyrite oxidation in Osona area (NE Spain) and suggested that the addition of pyrite is a feasible remediation strategy for the nitrate-contaminated aquifer as well.

Under anaerobic conditions, when electron acceptors (nitrate) are present, pyrite oxidation can be described corresponds to redox reactions (Eq. 2.1.3)

$$5FeS_2 + 14NO_3^- + 4H^+ \rightarrow 5Fe^{2+} + 7N_2 + 10SO_4^{2-} + 2H_2O \qquad (2.1.3)$$

The nitrate depletion is associated with an increase of dissolved sulfate ($SO_4^{2-}$) and ferrous ion ($Fe^{2+}$). The second pathway of pyrite oxidation is by reaction with ferric iron ($Fe^{3+}$):

$$FeS_2 + 14Fe^{3+} + 8H_2O \rightarrow 15Fe^{2+} + 2SO_4^{2-} + 16H^+ \qquad (2.1.4)$$

The reaction between pyrite and ferric iron is fast and produces a low pH value. The produced $Fe^{2+}$ may become oxidized by oxygen or nitrate to $Fe^{3+}$. If the $Fe^{2+}$ produced is oxidized:

$$5Fe^{2+} + NO_3^- + 7H_2O \rightarrow 5FeOOH + 0.5N_2 + 4H^+ \qquad (2.1.5)$$

The produced $Fe^{3+}$ can be precipitated as Goethite. Overall reaction where denitrification mediated by pyrite oxidation:

$$5FeS_2 + 15NO_3^- + 10H_2O \rightarrow 7.5N_2 + 10SO_4^{2-} + 5FeOOH + 5H^+ \qquad (2.1.6)$$

## 2.2. Flow and mass transport

In the simulation of flow and mass transport of the contaminants in porous media, the representative elementary volume (REV) (Bear and Bachmat, 1990) is introduced since it is impossible to describe the complex geometry of the soil matrix at the microscopic scale. The volume which is big enough to describe the porous medium at that scale is called REV (Figure 4). The detailed structure of the medium is neglected and becomes a continuous field. Relative parameters (e.g. porosity, storativity, permeability, and dispersivity) are considered constant and averaged within the concept of REV. In the following sections, described theories are based on this REV concept.

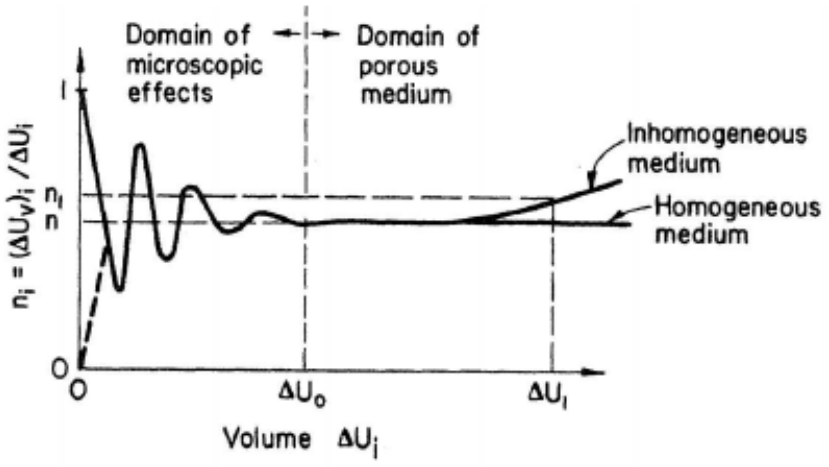


Figure 4 Representative elementary volume concept (from Bear and Bachmat (1990))

## 2.2.1. Groundwater flow

*Darcy's law*

Darcy's law was formulated by French engineer Henry Darcy based on experimental results, in the mid-1800s. Darcy found that if the soil column with the length L $[L]$ is set with hydraulic head $h_A$ $[L]$ and $h_B$ $[L]$ on the inlet and outlet side respectively, then the volumetric flow rate $Q$ $[L^3T^{-1}]$ in the column is proportional to the cross-sectional area of the column $A[L^2]$, and the hydraulic gradient, $\nabla h$ $(= h_A - h_B)$. The formula can be given by Eq. (2.2.1).

$$Q = -KA\left(\frac{h_A - h_B}{L}\right) = -KA\nabla h \tag{2.2.1}$$

where $K[LT^{-1}]$ is hydraulic conductivity, and $h_A - h_B$ is the hydraulic head gradient [-]. It is one of the basic equations in hydrogeology to describe water movement in a porous media. This may also be expressed in a more general term as Eq. (2.2.2)

$$Q = -KA\left(\frac{dh}{dl}\right) \tag{2.2.2}$$

Where *dh/dl* $(= h_A - h_B)$ is known as the hydraulic gradient [-]. The quantify *dh* represents the change in hydraulic head between two points that are very close together, and *dl* is the small distance between these two points. The negative symbol means that the flow direction is from the high hydraulic head position to the low one. If the flow rate $[LT^{-1}]$ is expressed in per unit cross section Eq. (2.2.3),

$$q = \frac{Q}{A} = -K\nabla h \tag{2.2.3}$$

*Governing Equation for confined aquifer.*

The governing equation for flow in the confined aquifer is based on the law of mass conservation and Darcy's law. Let's assume a very small piece of the confined aquifer,

called a controlled volume, the three sides of the length $dx, dy$ and $dz$, respectively (Figure 5). The area of the faces to the x-axis is $dydz$; the area of the faces to the z-axis is $dxdy$, and the area of the faces to the y-axis is $dxdz$. If the aquifer is homogenous with an isotropic condition and the fluid moves in only one direction through the controlled volume, the actual fluid motion can be subdivided on the basis of the components of flow parallel to the three principle axes. If $q$ is flow per unit cross-sectional area, $\rho_\omega q_x$ is the portion parallel to the x-asis, where $\rho_\omega$ is the water density $[M/L^3]$. The mass flux into the controlled volume is $\rho_\omega q_x dydz$ along the x-axis. The mass flux out of the controlled volume due to movement parallel to the x-axis is equal to the inflow less than the outflow, or $-\frac{\partial}{\partial x}(\rho_\omega q_x)dx\, dydz$. Since there are flow components along all three axes, similar terms can be determined for the other two directions: $-\frac{\partial}{\partial y}(\rho_\omega q_y)dy\, dxdz$ and $-\frac{\partial}{\partial z}(\rho_\omega q_z)dz\, dxdy$. Combining these three terms yields the net total accumulation of mass in the controlled volume:

$$-\left(\frac{\partial}{\partial x}\rho_\omega q_x + \frac{\partial}{\partial y}\rho_\omega q_y + \frac{\partial}{\partial z}\rho_\omega q_z\right) dxdydz \tag{2.2.4}$$

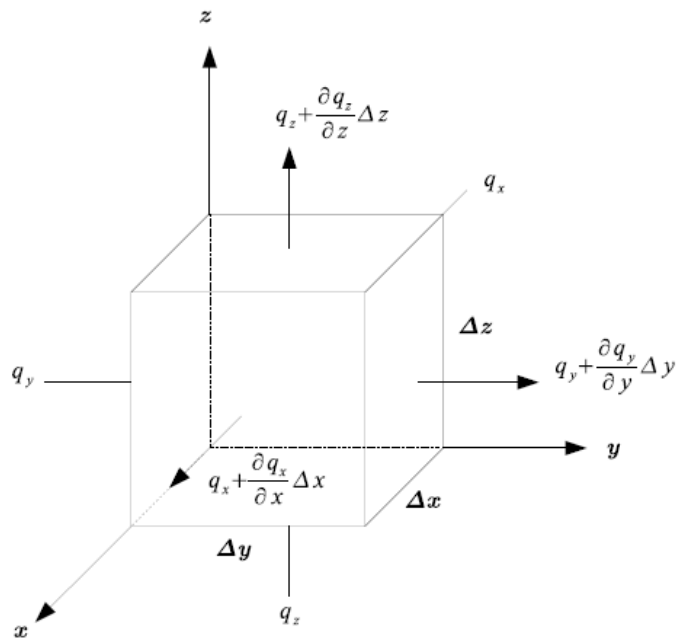


Figure 5 The control volume for water flow through porous media (from Sun (2011))

The confined aquifer is generally considered as saturated, then its volume is equal to $n\Delta x\Delta y\Delta z$ , where $n$ [-] is the porosity. The initial mass of the water is thus $\rho_\omega n dxdydz$. The volume of soil material is $(1-n)dxdydz$. Any change in the mass of water $M$ $[kg]$, with respect to (increment) time $t$ $[s]$ is given as

$$\frac{\partial M}{\partial t} = \frac{\partial}{\partial t}\left(\rho_\omega n dxdydz\right) \tag{2.2.5}$$

When the water and the aquifer are considered compressible, the fluid density will change, and also the porosity of the aquifer as the pressure in the control volume changes. The compressibility of water $\beta_\omega$ is defined as the rate of change in density with regards to the pressure, $\rho_\omega$ $[\frac{M}{L^3}\ ; Pa]$:

$$\beta_\omega = \frac{1}{dp}\frac{d\rho_\omega}{\rho_\omega} \implies d\rho_\omega = \rho_\omega \cdot \beta_\omega \cdot dp \tag{2.2.6}$$

And if we assume the relative changes of volume is only vertical, the bulk aquifer material compressibility $\alpha$ can be given by

$$\alpha d\rho_\omega = \frac{d(dz)}{dz} \tag{2.2.7}$$

As the aquifer compresses or expands, the porosity *n* will change, while the volume of the solids, $Vs$ will be constant. Likewise, if the only deformation is in the z-direction, $d(dx)$ and $d(dy)$ will be equal to zero:

$$V_s = 0 = d[(1-n)dxdydz] \tag{2.2.8}$$

Differentiation of the above equation yields

$$dzdn = (1-n)d(dz) \tag{2.2.9}$$

$$dn = \frac{(1-n)d(dz)}{dz} \tag{2.2.10}$$

The pressure $P$, at a point in the aquifer, is equal to $P_0 + \rho_\omega gh$, where $P_0$ is atmospheric pressure, and h is the height of a column of water above the point. Therefore, $dP = \rho_\omega g dh$, and Eq. (2.2.7) become

$$d\rho_\omega = d\rho_\omega \beta_\omega (\rho_\omega g dh) \tag{2.2.11}$$

And

$$d(dz) = dz\alpha(\rho_\omega g dh) \tag{2.2.12}$$

Eq. (2.2.10) can be rearrange if $d(dz)$ is replaced by Eq. (2.2.12).

$$dn = (1-n)\alpha\rho_\omega g dh \tag{2.2.13}$$

If $dx$ and $dy$ are constant, the equation for change of mass with time in the control volume, Eq. (2.2.5) can be expressed as

$$\frac{\partial M}{\partial t} = \left[\rho_\omega n \frac{\partial(dz)}{\partial dt} + \rho_\omega dz \frac{\partial n}{\partial t} + ndz \frac{\partial(\rho_\omega)}{\partial t}\right] dxdy \tag{2.2.14}$$

Substitution of Eq. (2.2.11), Eq. (2.2.12) and Eq. (2.2.13) into Eq. (2.2.14) yields

$$\frac{\partial M}{\partial t} = (\alpha\rho_\omega g + n\beta_\omega \rho_\omega g)\rho_\omega dxdydz \frac{\partial h}{\partial t} \tag{2.2.15}$$

The net accumulation of material expressed as Eq. (2.2.14) is equal to Eq. (2.2.15), the change of mass with time:

$$\left[\frac{\partial(q_x)}{\partial x} + \frac{\partial(q_y)}{\partial y} + \frac{\partial(q_z)}{\partial z}\right]\rho_\omega dxdydz = (\alpha\rho_\omega g + n\beta_\omega \rho_\omega g)\rho_\omega dxdydz \frac{\partial h}{\partial t} \tag{2.2.16}$$

From Darcy's law in Eq. (2.2.3)

$$q_x = -K\frac{\partial h}{\partial x} \tag{2.2.17}$$

$$q_y = -K\frac{\partial h}{\partial y} \tag{2.2.18}$$

$$q_z = -K\frac{\partial h}{\partial z} \tag{2.2.19}$$

Substituting these into Eq. (2.2.16) yields the governing equation of flow in a confined aquifer:

$$K\left(\frac{\partial^2 h}{\partial x^2}+\frac{\partial^2 h}{\partial y^2}+\frac{\partial^2 h}{\partial z^2}\right)=(\alpha\rho_\omega g+n\beta_\omega\,\rho_\omega g)\frac{\partial h}{\partial t} \tag{2.2.20}$$

It is a general equation for three dimensional flows for an isotropic, homogeneous porous medium.

## 2.2.2. Solute transport

The transport and retardation of solutes can be described by mass transport such as advection, dispersion, adsorption, and so on. These processes will be influenced by various factors such as flow field, physical-chemical characteristics of the solutes, and as well as the properties of the fluid and the porous media through which the flow and solutes transport occur.

*Advection*

Dissolved solids are transported along with the flowing water. This process is called advection transport, or convection. The solids are traveling at the same rate as the average linear velocity of the water (Eq. 2.2.21) if the solids are not subject to any sort of reactions with the porous media. Since the groundwater flow only occurs in the void space of the porous media, the actual velocity (i.e. seepage velocity) $\upsilon$ $[LT^{-1}]$ is:

$$\upsilon = \frac{q}{n} \tag{2.2.21}$$

Where $q[LT^{-1}]$ is the specific discharge and *n* is the porosity [-].

*Dispersion and Diffusion*

Not all solute transport is with the advection process. Dispersion causes "spreading" of the solute plume and is composed of both molecular and mechanical dispersion ($D = D_{mech} + D_{mol}$). The mechanical dispersion is caused by the different flow paths in a geological medium. Some of the flow paths are faster if they involve a more direct path or large pores. Other flow paths may be slower if they are closer to the grain boundaries. The different flow paths cause the mechanical dispersion, mechanical mixing, and dilution of the solute within the bulk movement of water (Schulze-Makuch, 2009). Three directions of the mechanical dispersion are possible: 1) longitudinal dispersion (parallel to flow direction) 2 and 3) transverse dispersion (perpendicular to flow; two directions). The dispersive flux of the solute can be described by a Fickian type law

$$J_{dis} = -D \cdot \nabla C \tag{2.2.22}$$

$D$ is the coefficient of mechanical dispersion $\alpha_i v_i$ where $\alpha_i$ is a dynamic dispersivity, and $v_i$ is an average linear groundwater flow in the $i$-direction. The dispersivity ($\alpha_i$) is a characteristic property of the geological medium and differs in value for each of the spatial components.

Molecular diffusion describes the fact that a solute in water will move from an area of higher concentration towards areas where it is lower concentrated. That means the molecular diffusion is the spreading of solute in the fluid (e.g. water) as a result of the random walk of molecules, which can produce a solute flux in response to its concentration gradient. The values of the coefficient of molecular diffusion depend on the type of solute in the groundwater medium, but for major anions and cations, it usually ranges between 1E-9 to 1E-10 (See in Table 1). Similar like the mechanical dispersion, based on Fick's law, Bear and Bachmat (1990) derived the equation for diffusion flux

$$J_{dif} = -D_d^* \cdot \nabla C \tag{2.2.23}$$

Where $J_{dif}$ is the flux vector of solute [$ML^{-2}T^{-1}$], $D_d^*$ is the coefficient of molecular diffusion [$L^2T^{-1}$], and $\nabla C$ is the concentration gradient of solute.

Table 1 Diffusion coefficients in water at 25℃ (data from Schulze-Makuch (2009))

| Cations | $D_d$ ($m^2s^{-1}$) | Anions | $D_d$ ($m^2s^{-1}$) |
|---|---|---|---|
| $H^+$ | 9.31 E-9 | $OH^-$ | 5.27 E-9 |
| $Na^+$ | 1.33 E-9 | $F^-$ | 1.46 E-9 |
| $K^+$ | 1.96 E-9 | $Cl^-$ | 2.03 E-9 |
| $Ca^{2+}$ | 7.93 E-10 | $Br^-$ | 2.01 E-9 |
| $Mn^{2+}$ | 6.88 E-10 | $HCO_3^-$ | 1.18 E-9 |
| $Fe^{2+}$ | 7.19 E-10 | $SO_4^{2-}$ | 1.07 E-9 |
| $Fe^{3+}$ | 6.07 E-10 | $CO_3^{2-}$ | 9.55 E-10 |

The term hydrodynamic dispersion is used to denote the spreading phenomenon. Combining diffusive and dispersive flux can be denoted as

$$J_{dif} + J_{dis} = -(D_d^* + D) \cdot \nabla C = -D_h \cdot \nabla C \quad (2.2.24)$$

Where $D_h$ is the coefficient of hydrodynamic dispersion.

*Advection-Dispersion Equation*

The advection-dispersion equation is based on the principle of conservation of mass of solute flux into and out of a REV of porous media. The solute transported by advection and hydrodynamic dispersion can be expressed as $v_i nCdA$ (Advective transport) and $nDi\frac{\partial C}{\partial t}dA$(Dispersive transport), respectively. Where $A[L^2]$ is the cross-sectional area of the control volume, and $i$ direction is normal to that cross-sectional face. $C$ is the concentration of solute [$M$]. The total mass of solute per unit cross-sectional area transported in the *i* direction per unit time,

$$F_i = v_i nC - nD_i\frac{\partial C}{\partial t} \quad (2.2.25)$$

Where the negative sign indicates that the dispersive flux is from areas of higher to areas of lower concentration. The total mass of solute entering the control volume is

$$F_x dydz + F_y dxdz + F_z dxdy \quad (2.2.26)$$

And the total mass of solute leaving the control volume (=REV) is

$$\left(F_x + \frac{\partial F_x}{\partial x}\right) dydz + \left(F_y + \frac{\partial F_y}{\partial y}\right) dxdz + \left(F_z + \frac{\partial F_z}{\partial z}\right) dxdy \tag{2.2.27}$$

The net mass accumulation in the volume is

$$-\left(\frac{\partial F_x}{\partial x} + \frac{\partial F_y}{\partial y} + \frac{\partial F_z}{\partial z}\right) dxdydz \tag{2.2.28}$$

The rate of mass change in the control volume is

$$n\frac{\partial F_x}{\partial x} dxdydz \tag{2.2.29}$$

Consider the law of mass conservation, the net mass accumulation in the volume (REV) equal to the rate of mass change

$$-\left(\frac{\partial F_x}{\partial x} + \frac{\partial F_y}{\partial y} + \frac{\partial F_z}{\partial z}\right) = n\frac{\partial C}{\partial t} \tag{2.2.30}$$

Substitute equation (Eq. (2.2.25) into Eq. (2.2.30) yields

$$\frac{\partial C}{\partial t} = \left[\frac{\partial}{\partial x}\left(D_x \frac{\partial C}{\partial x}\right) + \frac{\partial}{\partial y}\left(D_y \frac{\partial C}{\partial y}\right) + \frac{\partial}{\partial z}\left(D_z \frac{\partial C}{\partial z}\right)\right] - \left[\frac{\partial}{\partial x}(v_x C) + \frac{\partial}{\partial y}(v_y C) + \frac{\partial}{\partial z}(v_z C)\right] \tag{2.2.31}$$

Which is the governing equation of mass transport for a conservative solute in porous media (Bear and Bachmat, 1990). If the Laplace operator is applied, the above equation can be written in a vector form as

$$\frac{\partial C}{\partial t} = \nabla \cdot (D\nabla C) - \nabla \cdot (vC) \tag{2.2.32}$$

Where $C$ is the concentration ($ML^{-3}$), $v$ is the pore velocity vector ($ML^{-1}$), and $D$ is the hydrodynamic dispersion tension ($L^2T^{-1}$), $t$ is time ($T^2$), $\nabla$ is the gradient operator, and $\nabla \cdot$ is the divergence operator.

## 2.3. Chemical calculation

For the chemically non-reactive species (conservative species), only physical processes are needed to be modeled. However, most groundwater contaminants and solutes are reactive, and chemical reactions can retard the mitigation of the contaminant or transform. Chemical reactions can often be described by two types of reaction pathways, equilibrium and kinetic. Reactions, which occur fast and evolve the equilibrium states in an "ignorable" time, can be considered as the equilibrium reaction. In contrary, if a reaction is rather "slow" then its reaction kinetics has to be taken into consideration by the kinetic reaction pathway (Kehew, 2001).

### 2.3.1. Equilibrium reaction

The equilibrium reactions between the primary and secondary species can often be described as Eq. (2.3.1).

$$A_i \leftrightarrow \sum_{j=1}^{N_c} v_{ij} A_j \tag{2.3.1}$$

Where $Aj$ and $Ai$ are the chemical formulas of the primary and secondary species, respectively, and $v_{ij}$ is the number of moles of primary species $j$ in one mole of secondary species $i$. $N_c$ is the total number of aqueous species (primary or basis species). At the equilibrium state, the distribution of secondary and primary species can be linked via coefficients called equilibrium constant $K_i$, which can be obtained by using Eq. (2.3.2).

$$K_i = \alpha_i^{-1} \cdot \prod_{j=1}^{Nc} \alpha_j^{v_{i,j}} \tag{2.3.2}$$

Where $\alpha_i$ and $\alpha_j$ are the activity of secondary and primary species, respectively. Eq. (2.3.2.) is called the law of mass action, which is the fundamental theory for equilibrium reactions. The molarity of species $A_i$ (i.e. $C_i$) can be calculated by Eq. (2.3.3)

$$C_i = K_i^{-1}\gamma_i^{-1}\prod_{j=1}^{N_c}(\gamma_j C_j)^{v_{ij}} \qquad (i = 1, \dots, N_x) \tag{2.3.3}$$

Where $\gamma_j$ and $\gamma_i$ are the activity coefficients for the primary and secondary species, respectively, and $K_i$ is the equilibrium constant for the reaction. The activity coefficient can be calculated by different approaches such as extended Debye-Hückel equation (Appelo and Postma, 2005) (Eq. 2.3.4) and Davies equation (Davies, 1962) (Eq. 2.3.5).

$$log\gamma_i = -\left(\frac{Az_i^2\sqrt{I}}{1+Ba\sqrt{I}}\right) + b_i I \tag{2.3.4}$$

$$log\gamma_i = -Az_i^2\left(\frac{\sqrt{I}}{1+\sqrt{I}} - 0.3I\right) \tag{2.3.5}$$

In Eq. (2.3.4) and Eq. (2.3.5), *A* and *b* are constantly dependent on the temperature, $z_i^2$ is the ion charge number, $\alpha_i$ and $b_i$ are ion-specific fit parameters and *I* is the ionic strength. The equilibrium constant $K_i$ is temperature dependent. In a standard state (at a pressure of 1 bar and temperature of 25°C), $K_i$ can be calculated based on the standard Gibbs free energy (Eq. 2.3.6).

$$K_i = e^{-\frac{\Delta rG_i^\circ}{RT}} \tag{2.3.6}$$

Where R is the ideal gas constant, T is a temperature in Kelvin and $\Delta rG_i^\circ$ is the standard Gibbs free energy for the reaction. Based on the equilibrium constant at the standard state, those for other temperature, $K_i$(T) can be calculated based on Van't Hoff equation (Eq. 2.3.7) or a polynomial expression (Eq. 2.3.8).

$$logK_i\,(T) = logK_i\,(T_o) - \frac{\Delta H}{Rln10}\left(\frac{1}{T} - \frac{1}{T_0}\right) \tag{2.3.7}$$

Where $K_i\,(T_o)$ is the equilibrium constant at temperature $(T_o)$ and $\Delta H$ is the reaction enthalpy.

$$logK_i\,(T) = A + B\cdot T + \frac{C}{T} + D\cdot logT + \frac{E}{T^2} \tag{2.3.8}$$

Where $A, B, C, D$ and $E$ are constant.

## 2.3.2. Kinetic reaction

Equilibrium reactions expressed by the mass-action law are thermodynamically reversible and independent of time. In contrast, kinetic processes are time dependent reactions (Kehew, 2001). Introducing the factor time in a reaction, where A convert to B ($A \rightarrow B$) in a certain time and at a certain reaction rate. The reaction rate, the change of A as function of time, can be calculated as following

$$rate = -\frac{dC_A}{dt} \tag{2.3.9}$$

The concentration of A is inversely proportional to the concentration of B. If there is a decrease of A, the rate is given a negative sign, where the rate of B and the corresponding slope of the tangent are positive.

$$rate = -\frac{dC_A}{dt} = \frac{dC_B}{dt} \tag{2.3.10}$$

Reactions, where the reaction rate is independent of the concentration of its reactions, are called zeroth order reactions (Figure 6). First order reaction is determined by the rate constant or specific rate, k. This reaction generally used to calculate radioactive decay reactions. The overall order of reactions is determined by the sum of the different reaction orders of its reactants.

$$A + 2B = 3C \tag{2.3.11}$$

The rate is

$$rate = -\frac{dC_C}{dt} = 3\frac{dC_A}{dt} = 3/2\frac{dC_B}{dt} \tag{2.3.12}$$

$$rate = k \cdot C_A^{\alpha} \cdot C_B^{\beta} \tag{2.3.13}$$

The overall order n of this reaction is:

$$n = \alpha + \beta \tag{2.3.14}$$

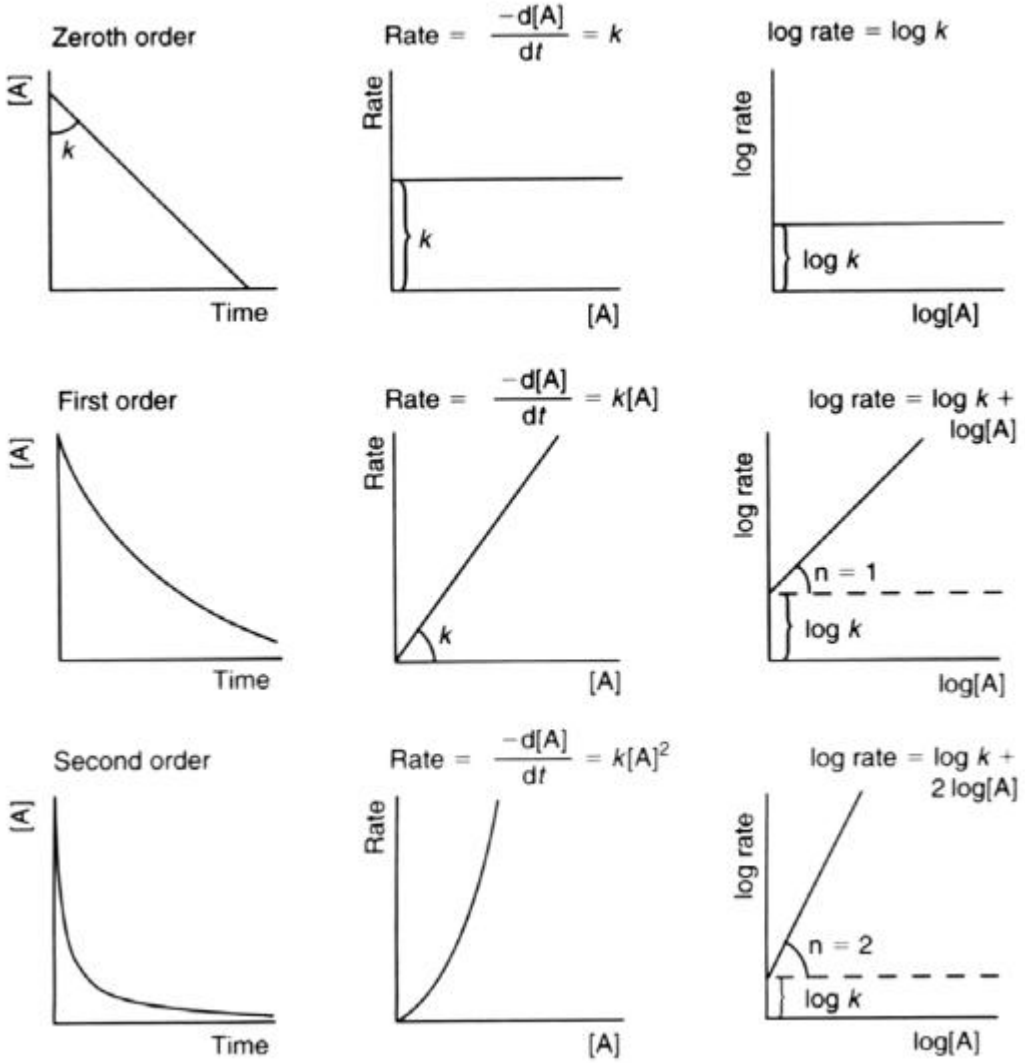


Figure 6 Zeroth, first, and second order rate laws for the reaction A (from Appelo and Postma (2005))

## 2.3.3. Calculation of saturation states

Comparing the ion activity product (IAP) with the equilibrium constant K leads to an expression of the saturation conditions, called saturation state Ω

$$\Omega = \frac{IAP}{K} \tag{2.3.15}$$

When the system is equilibrium state Ω = 1, super-saturation Ω >1 and for sub-saturation Ω <1. The logarithmic scale is useful for larger derivations from equilibrium, given by the saturation index SI (Appelo and Postma, 2005). In the saturation index can be defined in the input file for selected species, and will also be shown in the output file for the referring species.

$$\mathrm{SI} = \log\left(\frac{IAP}{K}\right) \tag{2.3.16}$$

SI = 0 reflects equilibrium between the mineral and the solution; SI > 0 super-saturation and SI < 0 sub-saturation..

## 2.4. Stochastic approach

One of the main challenges of numerical reactive transport modeling is a characterization of subsurface since the structure and properties of the subsurface are inherently heterogeneous and variable over many scales. To account for the heterogeneous subsurface characteristics, a stochastic approach can be applied. The stochastic approach aims at predicting the value of an unknown variable at non-observed times or non-observed locations, while also starting how uncertain we are when making these predictions (Bierkens and Geer, 2012; Rubin, 2003).

### 2.4.1. Why stochastic approach?

The spatial variability in the subsurface is a result of complex geological processes. Physical and chemical processes (such as structural deformation and deposition) may influence on the geometry and texture of sedimentary deposits. There are two distinct ways of hydrological models; Deterministic and Stochastic approach (Bierkens and Geer, 2012; Rubin, 2003). The deterministic approach (also called as a process-based approach) describes the most probable pictures of the formation based on the interpolation of the field measurements data (e.g. well longs) and the calibration (Elfeki et al., 1997). After the calibration of the model, the errors are not explicitly taken into account while performing with the model. Thus, errors in model outcomes are ignored. The deterministic approach needs the estimation of a number of parameters for the interpolation and calibration processes, while only a limited number of direct measurements information are usually available. The imperfect (or incomplete) representations of the measurement parameters lead to errors in model results.

Stochastic approach not only tries to use models for predicting hydrological variables (e.g. hydraulic conductivity, transmissivity, hydraulic head, solute concentration, fracture density, dispersivity, and so on), but also tries to quantify the errors in model outcomes. Although we do not know the exact values of the parameters and errors of

the model prediction, usually from the few measurements that we can take, we often can get some probability distribution of the errors. Let's assumed that hydrological parameter (as a target parameter) is represented as the variable z (whose value is calculated at some location and time) and we do not know the exact value of z. The model output is denoted as $\check{z}$. Then, the error ($e$) can be calculated as:

$$e = \check{z} - z \tag{2.4.1}$$

Because the exact value is unknown, it can be considered as so-called random variable *B* (note that the capital means the random variables) with a possible probability distribution. In case of deterministic hydrology modeling approach would only yield $\check{z}$ (upper figure of Figure 7-a), while stochastic hydrology modeling approach would yield $\check{z}$ (lower figure of Figure 7-a) with a possible probability distribution of the random variable. According to Bierkens and Geer (2012), most of the methods used in the stochastic approach do not consider errors in model outcomes explicitly. Instead, it is assumed that the hydrological variable z itself is a random variable Z. Thus, although we do now know the hydrological variable z exactly, we know that it is more likely to be around between 0.3 and 0.4. Stochastic models provide a probability distribution of the random variable instead of single value. Based on the probability distribution, it is possible to obtain the best prediction $\hat{z}$ (Figure 7-b). Incidentally, the value of the best prediction does not have to be the same the deterministic model outcome $\check{z}$. These were described in great details in Rubin (2003) and Bierkens and Geer (2012).

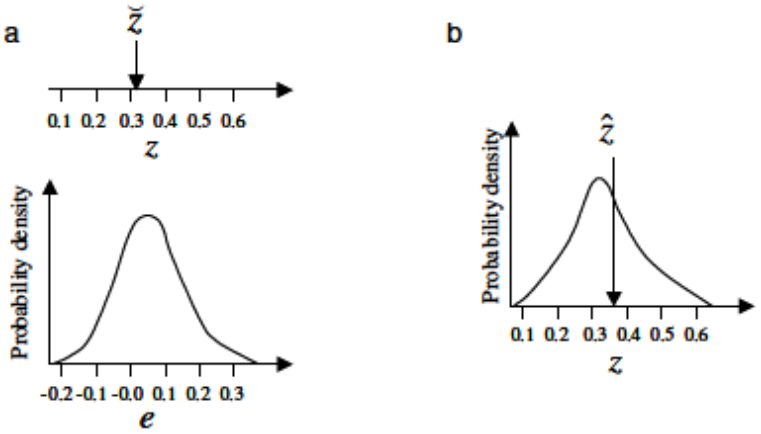


Figure 7 Deterministic approach (a) and stochastic approach (b) (from Bierkens and Geer (2012))

## 2.4.2. Concept of Spatial Random Function (SRF)

The stochastic approach representing subsurface heterogeneity is realized by statistical models using Spatial random function (SRF), with a given mean value, variance, covariance structure, and correlation scale (Rubin, 2003). SRF is mostly an employed method to represent aquifer heterogeneity and to account for the fact that subsurface properties at a point in space are correlated depending on their distance apart (Fiori et al., 2011). Field measurements have shown that this statistical model is effective in the representation of the subsurface properties (Graham and McLaughlin, 1991; Simmons et al., 2001; Sudicky, 1986). According to Freeze (1975), hydraulic conductivity (*K*) is often log-normally distributed (the probability density of *lnK* is normally distributed) and can be described by using the SRF concept.

There are random variables (such as hydrological parameters such as hydraulic conductivity) that depend on the location and exhibit the stochastic spatial structure. That means that these characteristics can be captured by the spatial random fields (e.g. *Z(x)* fields if *Z* is a function of space) characterized by the spatial laws with the expected value or arithmetic mean, variance, and the covariance. Here, *Z* is a function of space, and it is also referred to as a spatial random function. In this presented work, the spatial framework *Z(x)* is only defined in space. For example, the interdependency of random variable values is covered by the model of spatial correlation, which is expressed by the covariance function. In most cases, stationarity is often assumed. That means the statistics do not change over space. Thus the mean is constant, and the correlation does not depend on $x$ but on the separation distance of any two points $r$ ( $r = |x_1 - x_2|$).

## 2.4.3. Covariance model

The three most common covariance models used in groundwater modeling are Gaussian, exponential, and spherical (Figure 8).

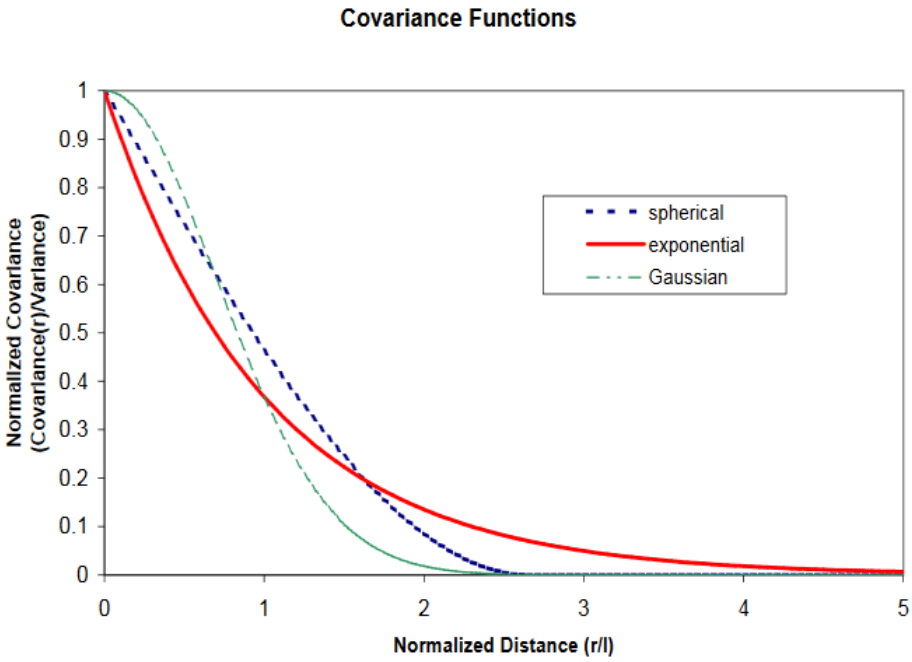


Figure 8 Spatial correlation model (from Bierkens and Geer (2012))

The spatial distribution of a random variable $B$, modeled by the Gaussian covariance function, is described by the following equation:

$$C(h) = \sigma_B^2 * e^{(-h^2)} \tag{2.4.2}$$

$$h = \left| \sqrt{\sum_{i=1}^{m} \left( {}^{r_i}/_{l_i} \right)^2} \right| \quad \text{with } i = 1,\ldots, m \ (m \text{ is space dimensionality}) \tag{2.4.3}$$

where $r_i$ = a separation vector between two points, $\sigma_B^2$ = the variance of $B$, and $l_i$ = a scaling length parameter in the $i^{th}$ dimension. The scaling length parameter in a Gaussian model is equal to $2\lambda_i/\sqrt{\pi}$ where $\lambda_i$ is represented as the correlation length scale in the $i^{th}$ dimension. The correlation length scale represents the average length over which a variable is positively correlated at neighboring points (Smith and Freeze, 1979). When the Gaussian covariance function is used, the variable $B$ will be normally

distributed, i.e., the probability density function (pdf) will be Gaussian. The Gaussian covariance function is both continuous and differentiable at the origin, which indicates a smooth transition of the variable between closely situated nodes. Therefore, this model, which creates visually continuous fields, is best used for gradually changing subsurface properties (Rubin, 2003).

The exponential covariance model is written as

$$C(h) = \sigma_B^2 * e^{-|h|} \tag{2.4.4}$$

It is worth to note that the scaling length parameter in this model is equal to the correlation length scale ($r_i = l_i$). This means that when we have two points with distance $r_i$, the two-point correlation follows an exponential function of distance. The exponential model is best suited for a rugged subsurface in which porous media properties might vary greatly. In this case, the model is a better fit for modeling of larger domains, as sharp transitions occur between neighboring nodes. Also, the spatial correlation decreases more rapidly than in both the Gaussian and spherical models (Rubin, 2003).

The spherical covariance function is given as:

$$C(h) = \begin{cases} \sigma_B^2\,[1 - 3h/2 + h^3/2], h \leq 1 \\ 0 \quad otherwise \end{cases} \tag{2.4.5}$$

Its most distinctive difference from the exponential covariance function is that the correlation length is equal to zero at a finite separation distance determined by the scaling length parameter. The scaling length parameter,$l_i$, in the spherical model is equal to $8\lambda_i/3$ (Bierkens and Geer, 2012). More fundamental details on spatial random functions can be found in Rubin (2003).

Table 2 Summary of several commonly-used covariance functions. Modified from Murphy (2006) and Bierkens and Geer (2012)

| Covariance function | Expression |
|---|---|
| Constant | $\sigma_0^2$ |
| Linear | $\sum_{d=1}^{D} \sigma_d^2 x_d x'_d$ |
| Polynormial | $(x \cdot x' + \sigma_0^2)^p$ |
| Squared exponential | $exp\left(-{r^2}/{2l^2}\right)$ |
| Martérn | ${1}/{2^{v-1}\Gamma(v)}\left({\sqrt{2v}}/{l} \cdot r\right)^v K_v\left({\sqrt{2v}}/{l} \cdot r\right)$ |
| Exponential | $exp\left(-{r}/{l}\right)$ |
| $\gamma$-exponential | $exp\left(-\left({r}/{l}\right)^\gamma\right)$ |
| National quadratic | $\left(1 + {r^2}/{2\alpha l^2}\right)^{-\alpha}$ |
| Gaussian | $C(h) = \sigma_B^2 * e^{(-h^2)}$ |
| Spherical | $\mathrm{C(h)} = \begin{cases} \sigma_B^2\,[1 - 3h/2 + h^3/2], h \le 1 \\ 0 \quad otherwise \end{cases}$ |

- The covariance are written either as a function of $x$ and $x'$, or as a function of $r = |x - x'|$ and $l = correlation\ length$.

# 3. METHOD

In this following Chapter, an overview of the methods and numerical tools will be described. First, a brief description of the numerical reactive transport simulation will be introduced, and a concept and implementation of the coupling interface between OGS and PHREEQC will be described (Chapter 3.1). Lastly, a random field generator which used in this study will be introduced (Chapter 3.2).

## 3.1. Numerical reactive transport simulation

The concentrations of reactive solutes (e.g. groundwater contaminants such as nitrate) are altered by geochemical and (micro)-biological transformation reactions and hydrological processes (Centler et al., 2010; Steefel et al., 2014). Their fate and transport can be predicted by using Reactive transport modeling (RTM). RTM has been emerged as an essential tool to get a profound understanding of these complex processes and to make plausible predictions of assessments for various applications (Steefel et al., 2014; Yabusaki et al., 2011). RTM has been widely used for many geotechnical applications, e.g. risk assessment of nuclear waste disposal (Bea et al., 2013; Kosakowski and Watanabe, 2014), evaluation of geological sequestration of carbon dioxide (Beyer et al., 2012; Li et al., 2013), and remediation strategies of contaminated site (Beisman et al., 2015; Cui et al., 2014; Kinzelbach et al., 1991; MacQuarrie et al., 2001). RTM also can provide a platform for testing concepts and hypothesis derived from experimental observations (from field and laboratory), and for integrating new experimental, observational, and theoretical findings (Regnier et al., 2003). Moreover, RTM can bridge a gap between fundamental, process-oriented research and results from laboratory experiment/field measurements (Yabusaki et al., 2011; Zhang et al., 2013).

A great number of RTM for the simulation of soil- and groundwater processes have been developed (Table 3) and applied to simulate reactive multispecies transport

coupled with geochemical reactions (Table 4). Among these existing tools, OpenGeoSys (OGS) (Kolditz et al., 2012) coupling with PHREEQC (Charlton and Parkhurst, 2011; Parkhurst and Appelo, 1999) was chosen in this study because of its capability to simulate variably saturated flow in the heterogeneous aquifer systems with an unlimited number of geochemical reactions and compounds.

Table 3 A comparisons the key flow and transport features of reactive transport modeling codes. Modified from : Steefel et al. (2014)

| Capabilities/features | PHREEQC | PHT3D | OpenGeoSys | TOUGHREACT | CrunchFlow | MIN3P |
|---|---|---|---|---|---|---|
| Dimensions | 1D | 1,2,3D | 1,2,3D | 1,2,3D | 1,2,3D | 1,2,3D |
| Flow | | | | | | |
| Saturated flow | Yes | Yes | Yes | Yes | Yes | Yes |
| Richards equation | No | No | Yes | Yes | No | Yes |
| Multiphase-multicomponent flow | No | No | Yes | Yes | No | No |
| Variable density flow | No | Yes | Yes | Yes | Yes | Yes |
| Transport | | | | | | |
| Advection | Yes | Yes | Yes | Yes | Yes | Yes |
| Molecular diffusion | Yes | Yes | Yes | Yes | Yes | Yes |
| Gas phase advection | No | No | Yes | Yes | Yes | Yes |
| Gas phase diffusion | NO | No | Yes | Yes | Yes | Yes |
| Geochemistry | | | | | | |
| Ion exchange | Yes | Yes | Yes | Yes | Yes | Yes |
| Kinetic mineral precipitation/dissolution | Yes | Yes | Yes | Yes | Yes | Yes |
| Mineral nucleation | Yes | Yes | Yes | No | Yes | No |
| Equilibrium isotope fractionation | Yes | Yes | Yes | Yes | Yes | No |
| Kinetic isotope fractionation | Yes | Yes | No | Yes | Yes | Yes |
| Aqueous kinetics | Yes | Yes | Yes | Yes | Yes | Yes |

Table 4 Features of existing reactive multispecies transport code coupled with geochemical reactions. Modified from Cui et al. (2014)

| Reference | Code name | Transport numerical /analytical method | Dimension | Saturated/ unsaturated | Transport reactions | Multispecies reactions |
|---|---|---|---|---|---|---|
| Essaid and Bekins (1997) | BIOMOC | Hybrid-particle tracking for advection, finite-difference for dispersion | 2D | Saturated | Retardation, first-order decay | Monod equations |
| Gu et al. (2012) | - | Finite-element | 2D | Variably saturated | None | Monod equations |
| Gusman and Mariño (1999) | RISK-N | Analytical | 1D, top soil layer | Variably saturated | First-order decay, retardation | GropSyst model |
| Kinzelbach et al. (1991) | - | Finite-difference | 2D | Saturated | First-order decay | Monod equations |
| Kinzelbach (1988) | - | RWPT | 2D | Saturated | Kinetic sorption | None |
| MacQuarrie et al. (2001) | - | Finite-element | 3D | Variably saturated | Retardation | Monod and kinetic reactions |
| Maggi et al. (2008) | TOUGHREACT-N | Integrated finite difference | 3D | Variably saturated | Multiphase flow, sorption, first-order decay | Monod and kinetic reactions |
| Peyrard et al. (2011) | - | Finite-difference | 1D | Saturated | None | Monod equations and kinetic reactions |
| Steefel (2009) | CrunchFlow | Integral finite difference | 3D | Variably saturated | Radioactive chain reactions | Monod equations, multicomponent aqueous complexation |
| Yabusaki et al. (2011) | eSTOMP | Integrated-volume finite-difference | 3D | Variably saturated | First-order decay, radioactive | Equilibrium, conservation, and kinetic reactions, Mood equations for |

| | | | | | | |
|---|---|---|---|---|---|---|
| | | | | | decay, dissolution | biomass growth and biogeochemical reactions |
| Widdowson et al. (1988) | - | Hybrid-particle tracking for advection, finite-difference for dispersion | 1D | Saturated | None | Monod equations |
| Wriedt and Rode (2006) | RT3D | Hybrid-particle tracking for advection, finite-difference for dispersion | 3D | Saturated | First-order decay | Monod equations |
| Cui et al. (2014) | SF-Monod | RWPT | 1D, 2D, 3D | Variably saturated | None Reactive air-phase transport | Multiple-Monod equations |
| Zhang et al. (2013) | MODFLOW-PHT3D | Finite-difference | 3D | Variably saturated | Retardation | Monod and First order kinetics, volatilization |
| Bailey et al. (2015) | MODFLOW-UZF and UZF-RT3D | | | | | |
| Beisman et al. (2015) | ParCrunchflow | | | | | |
| Atchley et al. (2013) | SLIM-FAST and CrunchFlow | Finite-difference | 3D | Saturated | None | Kinetic reactions |
| Kosakowski and Watanabe (2014) | OpenGeosys-GEM | Finite-element | 2D | Saturated | None | Kinetic reactions |
| Centler et al. (2010) | GeoSysBRNS | Finite-element | 2D | Saturated | None | Equilibrium kinetics, Double-Monod kinetics (biomass growth and biogeochemical reactions) |

### 3.1.1. OpenGeoSys

OpenGeoSys (OGS) (Kolditz et al., 2012), used as necessary for this work, is a scientific open-source modeling software based on Finite Element Method (FEM)[2]. This code is implemented with an object-oriented FEM concept (Figure 9). OGS aims to model thermo-hydro-mechanical-chemical processes (THMC) in porous and fractured media (Kolditz et al., 2012). The OGS code is targeting applications in environmental geosciences, e.g., in the fields of contaminant hydrology (Jang et al., 2017; Sun et al., 2012), water resources management (Sun et al., 2011), waste deposits (Kosakowski and Watanabe, 2014; Shao et al., 2009), geothermal energy (Beyer et al., 2016), $CO_2$ sequestration (Beyer et al., 2012; Li et al., 2013) and energy storage (Bauer et al., 2013).

This code provides a variety of possibilities to simulate different kinds of flow processes (e.g. groundwater flow, density dependent flow, unsaturated flow, two-phase flow and overland flow). Multi-component mass transport and equilibrium/non-equilibrium heat transport models are also included in this code. Solute mass transport in fluid phase is calculated based on the Advection-Dispersion Equation (ADE). For the flow and transport processes, both implicit and explicit time discretization schemes can be applied. OGS also can handle a random-walk particle tracking (RWPT) methods (Park et al., 2008) for Euler-Lagrange simulations and incompressible/compressible flow. For the computational efficiency, OGS has been parallelized (Wang et al., 2009) to deal with computationally intensive tests in the modeling of complex problems such as the present 3D model of the Nankou area in China (Sun et al., 2011) and nitrate reduction problems in the coupled hydrological-chemical systems (Jang et al., 2017).

[2] There are several techniques for solving the partial differential equation systems such as Finite Difference (FD), Finite Element (FE), Finite Volume (FV) or boundary element method. The main advantage of the finite element method is that the element shapes are suitable for representing complex physical geometries such as geological structure.

There are two possible pathways to simulate reactive transport problems with OGS. One is to use its internal *KinReact* modules for the simulation of kinetically controlled reactions. The other way is to couple the external geochemical solvers such as PHREEQC (Xie et al., 2011), GEMs (Kosakowski and Watanabe, 2014), BRNS (Centler et al., 2010) or ChemApp (Beyer et al., 2012; Li et al., 2013).

More detailed information regarding OGS developments and benchmarking can be found at http://www.opengeosys.org/.

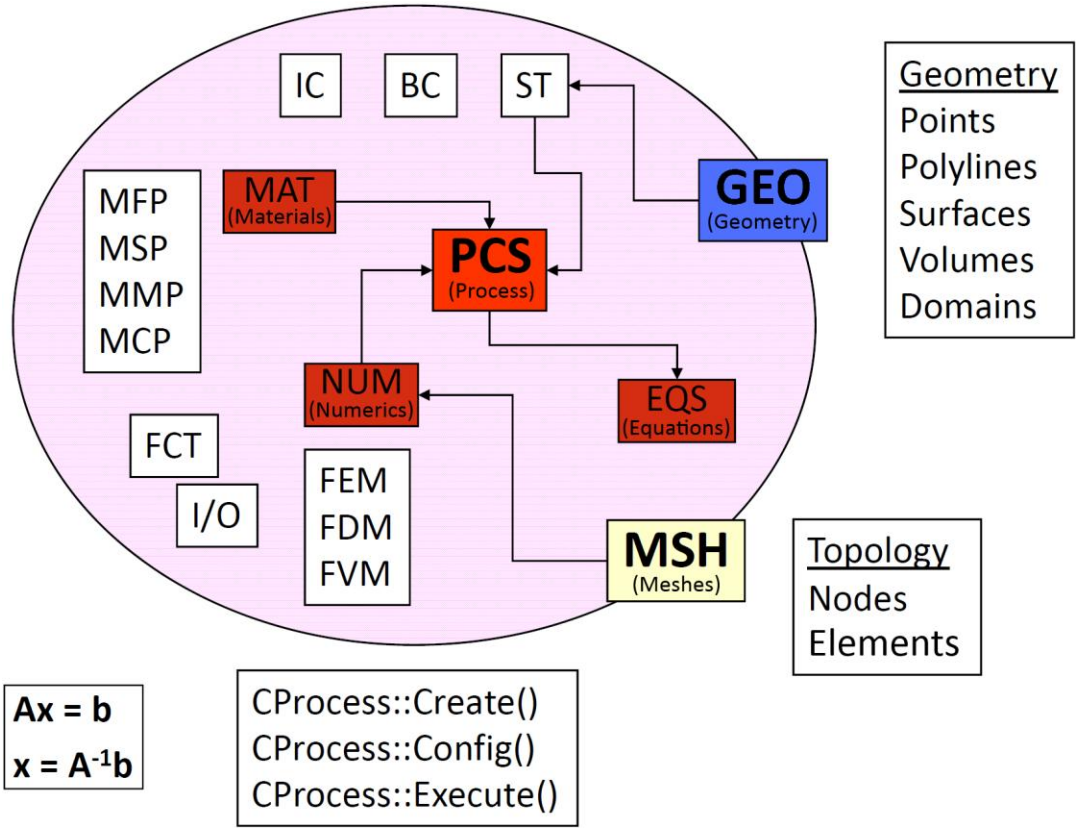


Figure 9 Object-oriented structure of OpenGeoSys Version 5 (from Kolditz et al. (2012))

## 3.1.2. PHREEQC

PHREEQC (Parkhurst and Appelo, 1999) is a geochemical solver to simulate chemical reactions and transport processes in natural or contaminated water. This code offers a wide range of equilibrium reactions (including reaction between water and minerals, ion exchange, surface complexes, solid solution, and gases) and a general kinetic formulation for a modeling of non-equilibrium mineral dissolution/precipitation, microbial reactions, decomposition of organic compounds, and so on. Several databases provide a variety of aqueous models, such as Debye-Hückel formations (*phreeqc.dat, wateq4f.dat, llnl.dat, minteq.dat, minteq.v4.dat, and iso.dat*); the Pitzer specific-ion interaction model (*pitzer.dat*), and the specific-ion interaction theory (SIT) model (*sit.dat*). Temperature dependence of activity-coefficient constant and van's Hoff or analytical expressions for equilibrium constants are available in all databases. Kinetic reactions can be defined with `RATE` expressions by using Basic programs that are evaluated with an embedded Basic interpreter. It is possible to formulate any kinds of rate expressions such as Monod or kinetics of any order, inhibition factors, rates that depend on free energy, and rate variation as a function of available electron acceptors (Parkhurst and Appelo, 1999). Various PHREEQC versions exist as well as modules that allow PHREEQC to be linked with other software. IPhreeqc (Charlton and Parkhurst, 2011) is one of these modules and provides a set of well-defined approaches for data exchange between PHREEQC and client programs. For a more detailed introduction to IPhreeqc methods can be found in (Charlton and Parkhurst, 2011).

## 3.1.3. Coupling OGS with IPhreeqc

A new coupling scheme, OGS#IPhreeqc (He et al., 2015), is realized by OGS coupling with IPhreeqc module (Figure 10). The IPhreeqc module is a C++ module of PHREEQC and designed for the coupling of PHREEQC with other codes and offers all PHREEQC capacities(Charlton and Parkhurst, 2011). The Sequential non-iterative approach (SNIA) is applied for the coupling between OGS and IPhreeqc. The non-

geochemical processes such as water flow and solute transport part are simulated by OGS in each time step and the geochemical solver, PHREEQC, is then applied to handle the local chemical systems. The coupling between these two software packages is realized at source code level, which means IPhreeqc functions can be accessed directly in the coupling interface. This is the difference between OGS-IPhreeqc and the existing coupling between OGS and PHREEQC (Xie et al., 2011), in which PHREEQC is executed externally with a system call.

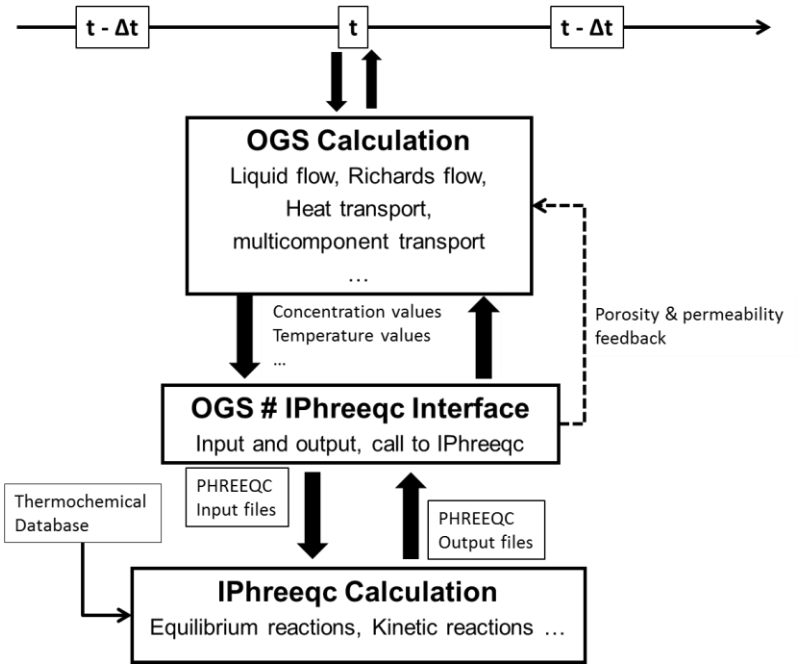


Figure 10 General concept of the coupling between OGS and Phreeqc (from He et al. (2015))

The new coupling interface is highly independent of the code updating from both software packages. When a new release from IPhreeqc is given, for example, it can be integrated efficiently by updating the IPhreeqc source code. When the IPhreeqc files are updated, only a reconfiguration of the build system is required (He, 2016). A significant reduction of the computation time is achieved by using parallelization scheme based on MPI grouping techniques (Figure 11). OGS#IPhreeqc interface is enabled to get a flexible distribution of different amounts of computer resources for the domain decomposition approach (DDC) (Wang et al., 2009) related processes and geochemical

reactions. This method allows optimizing the number of computing cores for both types of processes. More detailed information about the OGS#IPhreeqc interface and benchmarks can be found in (He et al., 2015).

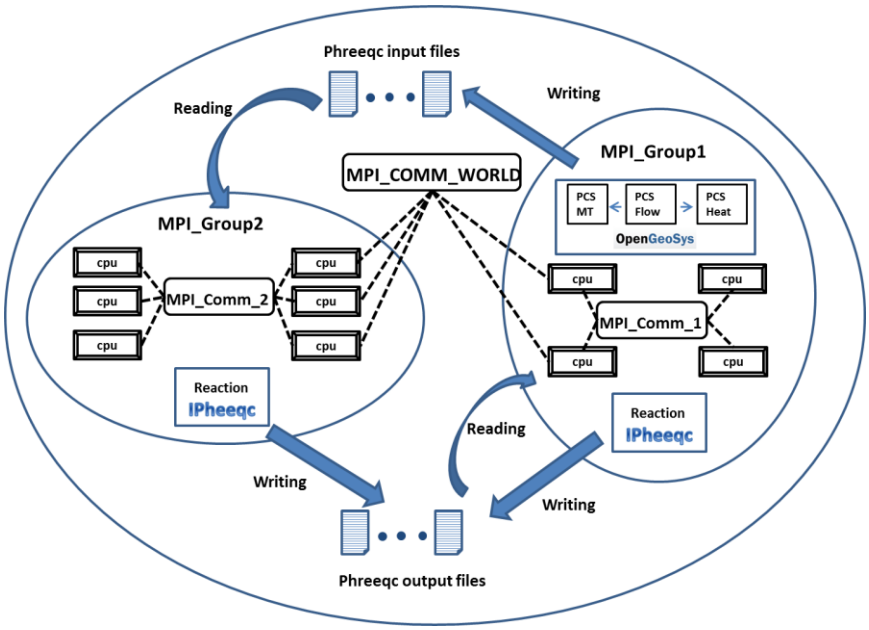


Figure 11 The concept of MPI grouping and communication of the parallelization scheme for OGS#IPhreeqc (from He et al. (2015))

## 3.2. Random Field Generation

R (R Core Team, 2014), an open-source port of the S language for statistical analysis, offers a wide variety of computational techniques (including linear and non-linear modeling, time series analysis, statistical tests, and others). It is an open source and highly extensible. This means that user can improve the base code of R and can also write extensions, so-called ―packages" that add algorithms and functions to its base implementation (R Core Team, 2014). Originally, R was developed for a statistical tool. However, it also has been applied in the field of environmental modelling (Petzoldt and Rinke, 2007), and reactive transport model applications (Soetaert and Meysman, 2012), as well.

In this presented work, gstat package is applied to generate the random fields by using RStudio (Figure 12). RStudio is a free and open-source integrated development environment for R (detailed information regarding RStudio and R can be found at https://www.rstudio.com/). Gsat (Pebesma, 2004; Pebesma and Wesseling, 1998) is one of the R packages for the modelling, prediction and simulation of geostatistical data in one, two or three dimensions. A detailed description of the R input files is given in Appendix II.

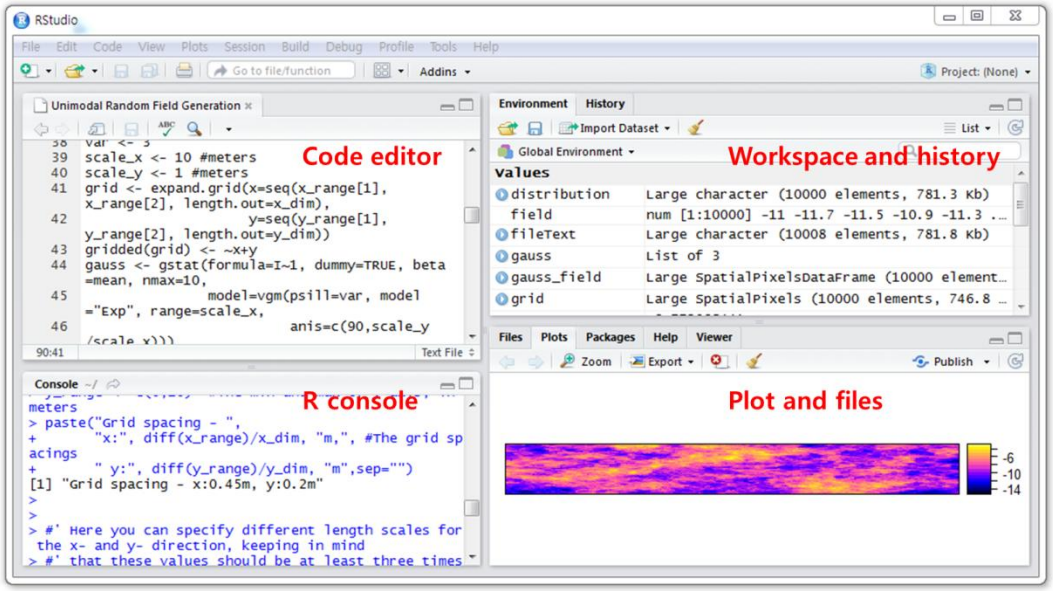


Figure 12 Generating the spatial random fields (R Studio)

# 4. SOLUTE TRANSPORT AND REDOX TRANSFORMATION IN THE HESSIAN RIED

The developed coupled reactive transport code (OGS#IPhreeqc) is applied to pyrite-driven denitrification of nitrate-contaminated groundwater scenarios based on the field measurements from the Hessian Ried, Germany. In this Chapter, the hydrological and geochemical system of the study area will be described, first (Chapter 4.1). Especially, data analyses are performed with the hydrochemical data to identify the major driving force for nitrate reduction in the study area. Then, a nitrate reactive-transport model will be developed and verified (Chapter 4.2).

## 4.1. Study Area: Hessian Ried

The study is conducted in the Hessian Ried (German: *Hessische Ried*), south of Frankfurt (Main) in Germany. The name ―Ried" stands for a natural floodplain and swampland that was created by the Rhine and its Western tributaries. However, this original landform was replaced by an intensively cultivated landscape since the late twenties of the 20th century. Since the late 1950s, the demand for drinking water and process water for industrial and agricultural irrigation had intensified enormously.

Hessian Ried is one of the most important groundwater reservoirs for densely populated Rhine-Main region in Germany. Due to the growing population and the rapid industrial development in the last sixties, the big cities in the Rhine-Main area (e.g. Frankfurt) discovered the ―Hessian Ried" as their groundwater reservoir. Many wells were built, and huge amounts of water were pumped out of this area. The groundwater level sank dramatically, especially in dry periods. Moreover, high nitrate concentration has been introduced into the aquifer by N-based fertilizers to enrich the soil fertility and to promote plant growth. Excess amounts of nitrate in the soil moved into the groundwater and had led to severe nitrate contamination of the shallow groundwater, exceeding the trigger value of 50 $mgL^{-1}$ (Knipp, 2012) (Figure 13). It has been

estimated that in these several areas about 25% of the waters show nitrate concentration close to or above the legal limit, particularly acute in the shallow groundwater aquifer (Heinelt et al., 2002; Kludt et al., 2016; Knipp, 2012). Recently, there are signs which indicate that the nitrate-removal-capacity may be exhausted, and the denitrification is slowing down (Kludt et al., 2013).

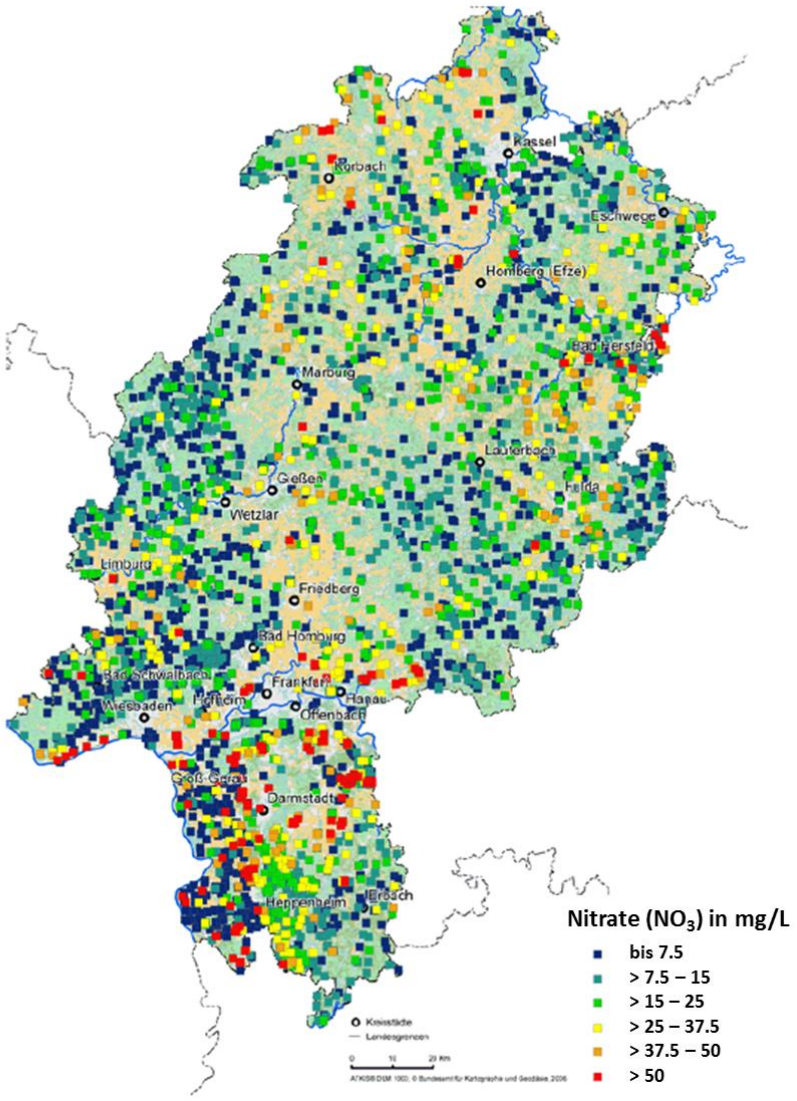


Figure 13 An overview map of nitrate concentration in Hessen (May 2012). Produced by the Hessian State Office for Environment and Geology (HLUG) and modified from Knipp (2012)

## 4.1.1. Hydrogeology

The study area is located in the Upper Rhine Graben, which is at about 300 km long and 30 km wide (Figure 14). The sediments are mainly coarse quaternary gravels and sands as a result of aggradational deposits. The aquifer of the study area consists of sandy-gravelly sediments and heterogeneously distributed silt and clay lenses. Hydraulic conductivity (*K*) comprises high values of 1E-3 to 1E-4 $ms^{-1}$ (Ludwig, 2011). The main groundwater flow is from east to west i.e. from the Eastern "Odenwald" Mountains into the Rhine River.


Figure 14 Study Area: Hessian Ried (modified from Central Intelligence Agency (2013))

## 4.1.2. Redox -Major local driving force for nitrate reduction

Preiß (2013) and Knipp (2012) conducted groundwater sampling to determine the denitrifying zone and identify the relevant nitrate degradation processes in the Hessian Ried. The groundwater sampling was collected in May to November 2012. The detailed information of the sampling and analytical procedure can be found in Preiß (2013) and Knipp (2012). In this presented study, twenty-two groundwater samples were selected with varying geochemical conditions (oxic and anaerobic condition; a definition of the oxic area Eh > 200mV and for the anaerobic area Eh < 200mV in the Hessian Ried) (Table 5). The chemical evolution of groundwater and relationship between different dissolved ions can be described by plotting the geochemical data on Piper's diagram (Piper, 1944). The major cations and anions are generally presented two faces of a Ca-$HCO_3$ and Mg-$HCO_3$ type with a partly elevated content of $NO_3^-$ and $SO_4^{2-}$ (Figure 15). The change of the major anion from bicarbonate ($HCO_3$) to nitrate (and chloride $Cl^-$) is possibly caused by the anthropogenic effect such as water pollution by agricultural activities.

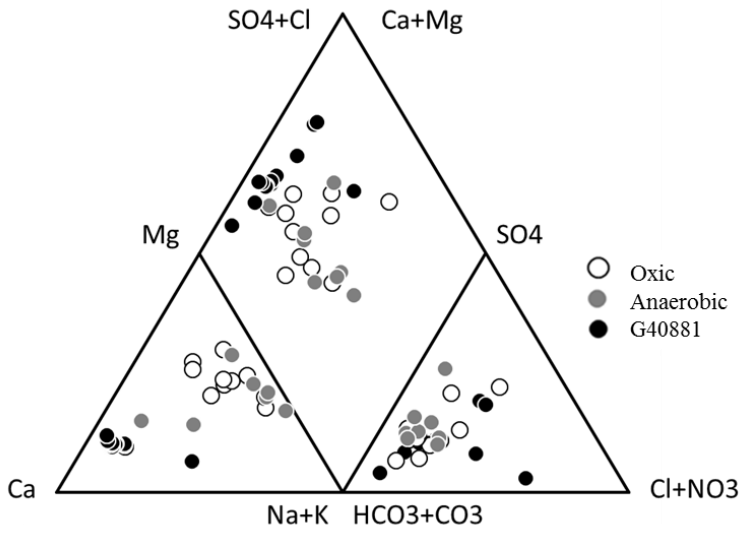


Figure 15 Piper diagram of the groundwater samples in the study area

Table 5 Groundwater data (Source from Preiß (2013))

| Sample No. | Date | FUK (m u. GOK) | Concentration (mg/L) | | | | | | | | | | | |
|---|---|---|---|---|---|---|---|---|---|---|---|---|---|---|
| | | | Na | K | Ca | Mg | $HCO_3$ | Cl | $NO_3$ | $SO_4$ | F | Fe | Mn | $NH_4$ |
| *Oxic condition* | | | | | | | | | | | | | | |
| 12101 | 04.07.2012 | 20.0 | 25.4 | 3.5 | 4.0 | 9.2 | 61.0 | 31.0 | 34.2 | 91.8 | n.a. | 0.0 | 0.0 | 2.0 |
| 12559 | 16.07.2012 | 18.5 | 23.1 | 3.0 | 3.0 | 9.9 | 274.3 | 32.0 | 40.5 | 70.7 | n.a. | 0.2 | 0.0 | 3.0 |
| 12592 | 16.07.2012 | 29.0 | 11.6 | 0.9 | 13.0 | 17.1 | 271.1 | 44.7 | 39.1 | 83.1 | n.a. | 0.0 | 0.0 | 13.0 |
| 12739 | 16.07.2012 | 21.0 | 11.6 | 1.1 | 13.0 | 15.1 | 324.8 | 40.7 | 7.9 | 97.3 | n.a. | 0.0 | 0.0 | 13.0 |
| 12924 | 26.06.2012 | 10.8 | 24.5 | 4.6 | 5.0 | 16.5 | 404.2 | 22.4 | 22.0 | 132.0 | n.a. | 0.6 | 0.1 | 5.0 |
| 13032 | 26.06.2012 | 12.0 | 23.9 | 4.1 | 12.0 | 17.3 | 369.1 | 37.0 | 6.0 | 96.8 | n.a. | 0.0 | 1.0 | 12.0 |
| 13496 | 26.06.2012 | 20.0 | 30.2 | 7.0 | 12.0 | 22.0 | 326.6 | 77.1 | 64.7 | 143.6 | n.a. | 0.2 | 0.2 | 12.0 |
| 14081 | 26.06.2012 | 15.0 | 16.1 | 5.8 | 13.0 | 12.3 | 244.3 | 43.0 | 27.8 | 192.0 | n.a. | 0.0 | 1.1 | 13.0 |
| 15146 | 27.06.2012 | 10.0 | 16.7 | 1.9 | 8.0 | 12.8 | 314.0 | 26.4 | 5.3 | 44.0 | n.a. | 0.0 | 0.1 | 8.0 |
| 15151 | 27.06.2012 | 10.0 | 23.8 | 2.0 | 9.0 | 27.7 | 398.9 | 45.8 | 15.4 | 111.8 | n.a. | 0.0 | 0.5 | 9.0 |
| Ja_3100 [a] | 24.05.2012 | 7.1 | 23.6 | 3.6 | 102.0 | 17.6 | 310.9 | 48.9 | 7.3 | 52.5 | n.a. | 0.0 | 0.1 | 0.1 |
| Ja_3111 [a] | 24.05.2012 | 7.1 | 20.1 | 3.2 | 98.0 | 0.0 | 257.5 | 45.8 | 6.5 | 54.6 | n.a. | 0.0 | 0.0 | 0.0 |
| Ja_3112 [a] | 24.05.2012 | 15.1 | 23.1 | 2.2 | n.a. | 0.3 | 209.5 | 48.8 | 0.9 | 54.1 | n.a. | 2.6 | 0.9 | 0.5 |
| *Anaerobic condition* | | | | | | | | | | | | | | |
| 12511 | 27.07.2012 | 10.0 | 42.6 | 4.0 | 5.0 | 17.7 | 374.6 | 64.8 | 0.5 | 157.0 | n.a. | 1.9 | 0.3 | 5.0 |
| 13025 | 27.07.2012 | 10.0 | 69.0 | 5.0 | 3.0 | 20.6 | 401.5 | 95.3 | 0.1 | 131.0 | n.a. | 2.0 | 0.1 | 3.0 |
| 13470 | 26.06.2012 | 15.0 | 20.1 | 2.5 | 6.0 | 20.1 | 326.9 | 49.7 | 0.3 | 348.3 | n.a. | 3.6 | 0.5 | 6.0 |
| 13581 | 04.07.2012 | 10.0 | 12.7 | 1.2 | 44.0 | 14.3 | 409.8 | 34.9 | 0.0 | 122.1 | n.a. | 5.4 | 0.4 | 43.0 |
| 13676 | 16.07.2012 | 13.0 | 18.5 | 8.4 | 23.0 | 10.4 | 272.2 | 30.3 | 9.5 | 89.1 | n.a. | 0.5 | 0.1 | 23.0 |
| 13704 | 16.07.2012 | 13.0 | 16.7 | 3.5 | 3.0 | 9.6 | 305.6 | 27.0 | 7.1 | 82.0 | n.a. | 2.5 | 0.7 | 3.0 |
| 13801 | 16.07.2012 | 15.0 | 46.1 | 1.8 | 4.0 | 19.6 | 477.3 | 112.3 | 0.0 | 132.3 | n.a. | 4.1 | 0.7 | 4.0 |
| 15153 | 27.07.2012 | 8.0 | 25.0 | 8.6 | 8.0 | 28.1 | 483.5 | 45.0 | 0.2 | 202.5 | n.a. | 4.5 | 0.7 | 8.0 |
| Ja_3373 | 12.09.2012 | 24.0 | 16.6 | 3.4 | 68.1 | 9.9 | 97.0 | 39.7 | 0.6 | 48.7 | n.a. | 0.2 | n.a. | 0.0 |

- [a] (Construction of the wells) FUK (German: *Filterunterkante*) = trailing edge of the screen in meter altitude above sea level (aasl),
  m u. GOK (German: *meter unter Geländeoberkante*) = meter under the ground level
- n.a = not analyzed [b] = Forest area

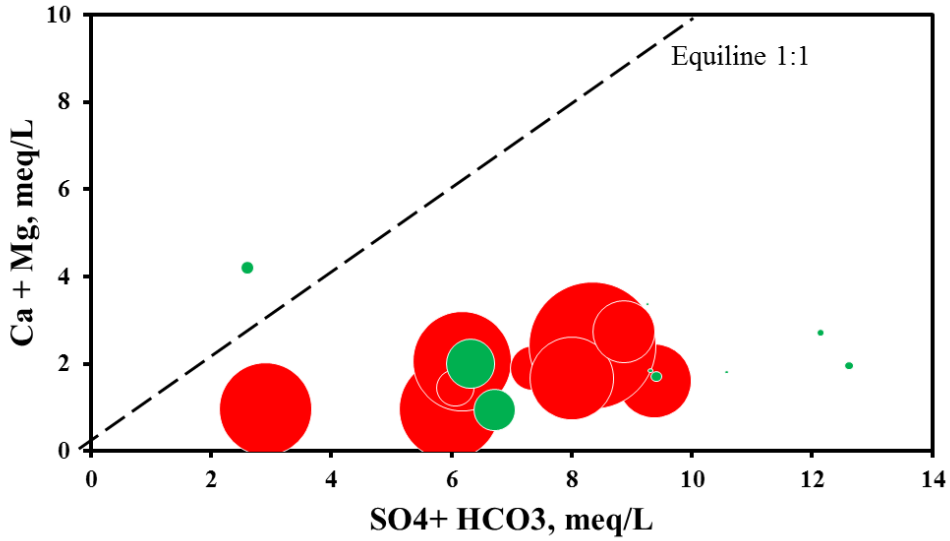


Figure 16 Relations between Ca+Mg and $SO_4$+$HCO_3$ plot. Red bubbles and green bubbles indicate oxic and anaerobic condition, respectively; Bubble sizes indicate concentration of nitrate.

If $Ca^{2+}$, $Mg^{2+}$, $SO_4^{2-}$ and $HCO_3^-$ were only resulted from the dissolution of carbonate (e.g. calcite and dolomite) and evaporate minerals (such as gypsum), ionic ratios of ($Ca^{2+}$ + $Mg^{2+}$) to ($SO_4^{2-}$ + $HCO_3^-$) should be a constant value of one (Sappa et al., 2012; Singh et al., 2013). As can be seen in Figure 16, the plotted points of the majority of the groundwater samples are clustered and fall below the 1:1 equiline. The excess of ($SO_4^{2-}$ + $HCO_3^-$) over ($Ca^{2+}$ + $Mg^{2+}$) suggests a significant contribution from non-carbonate source and indicate ion exchange processes or another source of $SO_4^{2-}$. According to Tarki et al. (2012), it is most likely the dissolution of pyrite that is relatively abundant in the aquifer.

Core samples from different field sites in the Hessian Ried were also analyzed by Knipp (2012) and Kludt et al. (2016). According to Knipp (2012), sediments under agricultural areas have much lower pyrite concentrations. These sediments having lower pyrite contents showed a much slower denitrification reaction as a result of the batch experiment. Kludt et al. (2016) analyzed sediment cores from the Hessian Ried for reactive species and revealed a heterogeneous distribution of the pyrite, specifically. In addition, they could show that autotrophic denitrification is the dominant nitrate

reduction processes. The dominance of autotrophic denitrification was verified in the field using stable isotopes ($\delta^{34}S - SO_4^{2-}$). Androulakakis (2012) also reported that the high-risk area with a low nitrate-removal capacity is mainly caused by the consumption of the pyrite during the denitrification processes in this study area. Therefore, although in situ driving forces may be both organic matter and pyrite, pyrite is the main electron donor in the Hessian Ried.

## 4.2. 1D-Nitrate reduction simulation

A nitrogen transport and redox transformation model for saturated groundwater systems is developed to assess its performance by applying it to field site contaminated nitrate. The developed model describing nitrate removal processes will be applied to simulate the fate and transport of nitrate in the heterogeneous systems in Chapter 5.

### 4.2.1. Model setup

A one-dimensional homogeneous aquifer is chosen to simulate a simple batch reaction problem (Figure 17). In the batch reaction problem, the oxidation of organic matter (denoted $CH_2O$) and pyrite ($FeS_2$) by oxygen and nitrate is considered. Additional reactions such as porosity changes due to water-rock interaction which are not directly related to the nitrate reduction reactions are not considered for simplification purpose.


Figure 17 Schematic 1D model. The column is characterized by oxidized zone with nitrate and oxygen and lower reduced zone with pyrite and organic carbon.

Flow direction is from left to right, with a mean hydraulic gradient [-] of 0.025. For this application, a mean hydraulic conductivity of 1.16E-4 $ms^{-1}$ is assumed (Table 6). The model domain is discretized with 101 nodes and 100 elements. Constant nitrate and oxygen concentration are entered from the left boundary, representing an oxygenated groundwater source exposed to the column. It means that the contaminant source (e.g. nitrate) is represented by a fixed concentration boundary condition at the source position. Neither sorption nor volatilization is accounted for. The geochemical reactions between the oxidized recharge water and the aquifer's reductants pyrite ($FeS_2$) and organic matter are kinetically controlled. Note that the initial nitrate concentration in the

domain is $C_{nitrate}$ = 0 with initially free of nitrogen species. The hydraulic parameters and specific boundary and initial conditions are listed in Table 6 and Table 7.

Table 6 Summary of aquifer hydrology, geometry and transport parameters used for simulation (Modified from Engesgaard and Kipp (1992))

| Parameters | Unit | Value | Parameter | Unit | Value |
|---|---|---|---|---|---|
| Hydraulic conductivity | $ms^{-1}$ | 1.16e-4 | Porosity | - | 0.32 |
| Column bulk density | $kgm^{-3}$ | 1.80e+3 | Flow velocity | $ms^{-1}$ | 5.78e-5 |
| Time step | Sec | 85 | Reaction time | sec | 16,150 |
| Number of node | | 101 | Number of elements | | 100 |

The mass transport in a homogeneous, saturated aquifer can be controlled by convection, diffusion, decay and biodegradation, sorption and chemical reactions (Bauer et al., 2012). The coupled set of advection-dispersion-reaction equations can be written as

$$\frac{\partial C_i}{\partial t} = -\nabla \cdot \left(\frac{V}{R_i} C_i\right) + \nabla \cdot \left(\frac{D_i}{R_i} \nabla C_i\right) + \frac{\beta_i}{R_i} \quad (i = 1,2,3 \cdots m) \tag{4.2.1}$$

$$\frac{\partial S_j}{\partial t} = \beta_j \quad (j = 1,2,3 \cdots n) \tag{4.2.2}$$

Where $R_i$ is the linear retardation factor of the $i$-th mobile component ($R = 1 + \rho K_d/n$), $\rho$ is the bulk density ($mgL^{-1}$), $K_d$ is the linear sorption constant ($Lmg^{-1}$), and $\beta_i$ and $\beta_j$ are the reactions involving mobile and immobile components, respectively. $S_j$ is the solid phases concentration (mol $kg^{-1}$).

Since the sequential non-iterative approach (SNIA) for operator splitting (OS) is applied in the OGS#IPhreeqc coupling scheme, Equation (4.2.1) is decoupled into a

transport step (Eq. 4.2.3) and a reaction step (Eq. 4.2.4) so that transport and reaction are solved sequentially.

$$\frac{\partial C_i}{\partial t} = -\nabla \cdot \left(\frac{V}{R_i} C_i\right) + \nabla \cdot \left(\frac{D_i}{R_i} \nabla C_i\right) \quad (4.2.3)$$

$$\frac{\partial \bar{C}_i}{\partial t} = \frac{\beta_i}{R_i} \; and \; \frac{\partial S_j}{\partial t} = \beta_j \quad (4.2.4)$$

The advection-dispersion terms for all mobile species (Eq.4.2.3) are solved at first before the resulting concentrations ($\bar{C}_i$) are used to calculate a set of coupled reaction terms (both mobile and immobile components, Eq.4.2.4).

Table 7 Water chemistry and reactants used for boundary and initial conditions. Modified from Engesgaard and Kipp (1992) and Preiß (2013)

| Component | Concentration (molkg$^{-1}$) | |
|---|---|---|
| | Boundary | Initial |
| pH | 5.7 | 8.67 |
| pe | 16.5 | -4.3 |
| $CO_3^{2-}$ | 2.5E-4 | - |
| $Fe^{3+}$ | 1.2E-7 | 3.61E-14 |
| $NO_3^-$ | 2.14E-3 | - |
| $Na^+$ | 2.61E-3 | 6.09E-4 |
| $O_2$ | 1.25E-3 | - |
| $SO_4^{2-}$ | 2.08E-4 | 1.46E-9 |
| $Cl^-$ | - | 5.64E-4 |
| Pyrite | - | 0.0026 |
| Organic C | - | 0.0026 |

### 4.2.2. Definition of the geochemical reaction system

Autotrophic and heterotrophic denitrification pathways are the most important nitrate turnover reaction in the groundwater system (Rivett et al., 2008). Autotrophic denitrification is based on the oxidation of reduced sulfur compounds while heterotrophic denitrification is based on the oxidation of organic matter. Related chemical reactions are described in Table 8. Note that calcite ($CaCO_3$) reaction is also considered in this study. Calcite can effectively buffer added hydrogen ions ($H^+$) provided by the oxidative formation of pyrite. This is based on the high carbonate content in the study area. In general, calcite reaction is not a requirement of the model (MacQuarrie et al., 2001). However, geochemical reactions involving carbonate minerals are particularly important in the subsurface and calcite is one of the principle carbonate minerals (Kehew, 2001). Thus, it would be reasonable to include calcite reactions, perhaps the most affected geochemical reaction as well, in the simulation. The default PHREEQC database phreeqc.dat (Parkhurst and Appelo, 2013), which contains the thermodynamic data for aqueous species and mineral phases, is used for the simulation.

Table 8 Definition of the geochemical system

| | |
|---|---|
| Pyrite oxidation and related oxidation of Fe(II) | |
| $FeS_2 + 3.5O_2 + H_2O \rightarrow Fe^{2+} + 2SO_4^{2-} + 2H^+$ | Pyrite oxidation by oxygen |
| $FeS_2 + 14Fe^{3+} + 8H_2O \rightarrow 15Fe^{2+} + 2SO_4^{2-} + 16H^+$ | Pyrite oxidation by $Fe^{3+}$ |
| $FeS_2 + 2.8NO_3^- + 0.8H^+ \rightarrow Fe^{2+} + 2SO_4^{2-} + 1.4N_{2\,(aq)} + 0.4H_2O$ | Autotrophic denitrification |
| $Fe^{2+} + 0.25\,O_2 + H^+ \rightarrow Fe^{3+} + 0.5H_2O$ and $Fe^{3+} + 2H_2O \rightarrow FeOOH + 2H^+$ | $Fe^{2+}$ oxidation by oxygen |
| $5Fe^{2+} + NO_3^- + 7H_2O \rightarrow 5FeOOH + 0.5N_2 + 9\,H^+$ | $Fe^{2+}$ oxidation by nitrate |
| Degradation of sedimentary organic matter (SOM) | |
| $CH_2O + O_2 \rightarrow 2H^+ + CO_3^{2-}$ | Mineralization |
| $CH_2O + 0.8\,NO_3^- \rightarrow 1.2H^+ + CO_3^{2-} + N_2 + 0.4\,H_2O$ | Heterotrophic denitrification |
| $CH_2O + 0.5\,SO_4^{2-} + 2.5H^+ \rightarrow CO_3^{2-} + 0.5\,HS^- + 2\,H_2O$ | Sulfate reduction |
| Carbonate equilibrium for buffer reaction | |
| $CaCO_3 \leftrightarrow Ca^{2+} + CO_3^{2-}$ | Calcite dissolution |
| $CO_3^{2-} + 2H^+ \leftrightarrow H_2CO_3$ | Carbonate equilibrium I |
| $CO_3^{2-} + H^+ \leftrightarrow HCO_3^-$ | Carbonate equilibrium II |
| $H_2O \leftrightarrow OH^- + H^+$ | Dissociation of water |

Pyrite oxidation reactions by oxygen, nitrate and sulfate as electron acceptors are assumed to follow a previously developed and applied rate expression (Appelo and Postma, 2005; Williamson and Rimstidt, 1994)

$$r_{O_2} = 10^{-8.19} * \frac{{m_{O_2}}^{0.5}}{m_{H^+}^{0.11}} \tag{4.2.5}$$

$$r_{O_{2\_Fe_3}} = 10^{-5.78} * \frac{m_{Fe^{3+}}^{0.92}}{\left(1+m_{Fe^{2+}}\right)^{0.43}} \tag{4.2.6}$$

$$r_{Fe3} = 10^{-8.84} * \frac{m_{Fe3}^{0.28}}{m_{H^+}^{0.3}\left(1+m_{Fe^{2+}}\right)^{0.52}} \tag{4.2.7}$$

$$r_{NO_3} = f_{nit} * \frac{{m_{NO_3}}^{0.5}}{m_{H^+}^{0.11}} \tag{4.2.8}$$

$$r_{pyr} = \left[A_{pyr}\left(\frac{m}{m_0}\right)_{pyr}^{0.67} * (1 - SI(\ \ yr\ t\ \ )) * \left(r_{O_2} + r_{O_{2\_Fe_3}} + r_{Fe3} + r_{NO_3}\right)\right] \tag{4.2.9}$$

Where $r$ is the reaction rate, $m$ refers to the concentration of either $O_2$, $Fe^{2+}$, $Fe^{3+}$ of $H^+$, $\left(\frac{m}{m_0}\right)_{pry}$ indicates the change in the surface area of pyrite due to its dissolution, and $A_{pyr}$ is a pyrite surface area. $SI(\ \ yr\ t\ \ )$ is Saturation Index of pyrite mineral. SI is equal to the logarithmic value of the ratio between the Ion Activity Product (IAP) and the solubility product ($K_s$) for the mineral phases. In the rate equation of Williamson and Rimstidt (1994), ${f_{nit}{m_{NO_3}}^{0.5}\ m_{H^+}^{-0.11}}$ was added for modeling oxidation by nitrate where $f_{nit}$ = 1 similar done by Eckert and Appelo (2002).

The overall organic carbon oxidation reaction is described as follows:

$$r_{SOM} = \left(ko_2 \frac{m_{o_2}}{2.94*10^{-4}+ m_{O_2}} + k_{NO_3^-} \frac{0.01\, m_{NO_3^-}}{1.55*10^{-4}+ m_{NO_3^-}} + k_{SO_4^{2-}} \frac{6.4*10^{-5}\, m_{SO_4^{2-}}}{1*10^{-4}+ m_{SO_4^{2-}}}\right) \tag{4.2.10}$$

Where $k$ is the reaction rate constant value (molL$^{-1}$s$^{-1}$) with $ko_2$ = 7.5E-12, $k_{NO_3^-}$ = 3.25 E-12 and $k_{SO_4^{2-}}$ = 1.5E-12. We look up the kinetic rate for goethite defined by Appelo and Postma (2005) based on the experiment of Zinder et al. (1986).

$$r_{goe} = \left[ A_{goe} * \left(\frac{m}{m_0}\right)_{geo} * (1 - SI(\text{Goethite})) * 10^{-11} * {\gamma_{H^+}}^{0.45} \right] \quad (4.2.11)$$

where a gamma is an activity of $H^+$ in water and $SI(\text{Goethite})$ is the Saturation ratio ($IAP/K_{sp}$) of goethite mineral. The precipitation and dissolution of calcite is simulated through the use of mass-action equations and the equation describing equilibrium with $Log\ K_{sp} = -8.48$.

### 4.2.3. Code verification

Nitrate and oxygen are electron acceptors while both pyrite and organic carbon are available as electron donors. Figure 18 and 19 show the computed results for mobile species after simulation. As oxygen is consumed at the front, $pH$ decreases while $pe$ increases. When all oxygen has been consumed, nitrate starts to be used with a further decrease in $pH$ and increase in $pe$. Reduction in nitrate is considered to be from denitrification (Figure 18).

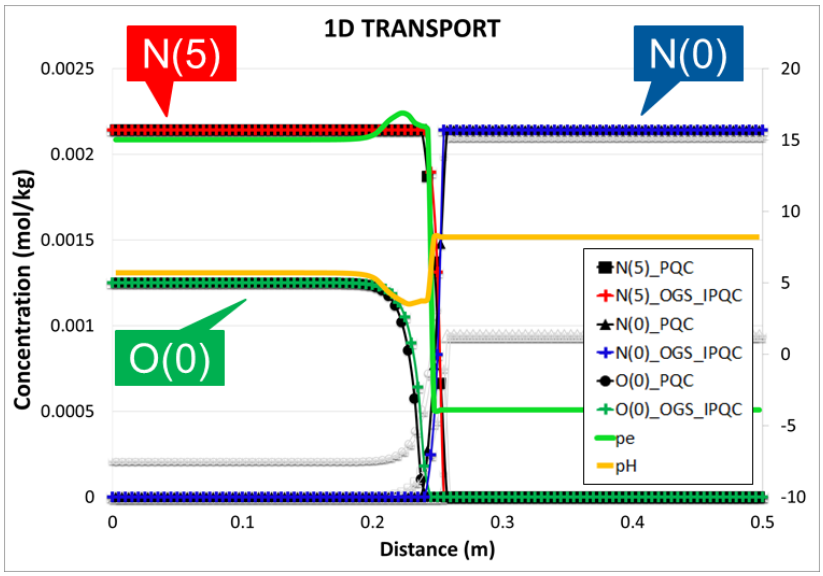


Figure 18 $NO_3$, $N_2$ and $O_2$ concentration changes in the domain. Comparison with OGS#IPhreeqc (OGS_IPQC) and PHREEQC 1D transport (PQC)

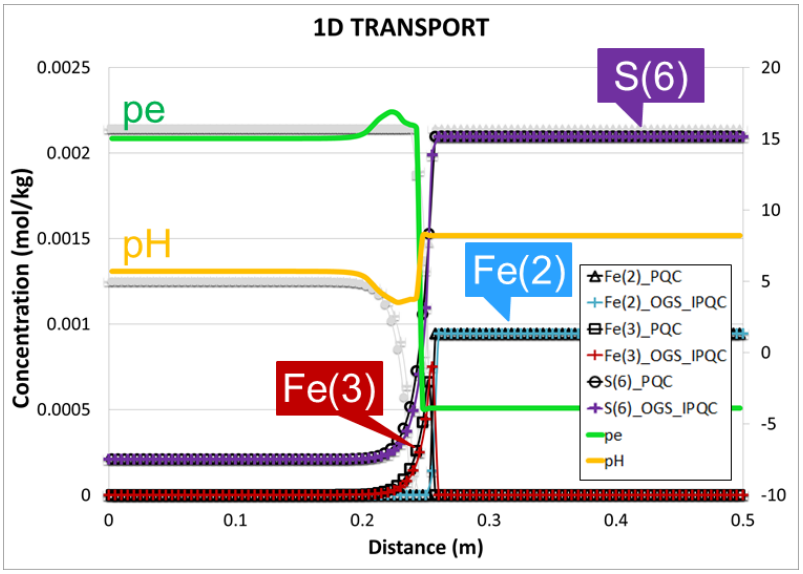


Figure 19 Distribution of the $SO_4$, $Fe^{2+}$, $Fe^{3+}$ and pe and pH changes in the domain Comaprision with OGS#IPhreeqc (OGS_IPQC) and PHREEQC 1D transport (PQC)

Figure 19 shows the distribution of some of the major redox species. The sulfate ($SO_4^-$) is the major species in the sulfur system and $Fe^{2+}$ is the major species in the iron system. The concentration of $SO_4^-$ and $Fe^{2+}$ has been increased by pyrite oxidation (Table 8-Autotrophic denitrification). If the produced $Fe^2$ is oxidized:

$$5Fe^{2+} + NO_3^- + 6H^+ \rightarrow 5Fe^{3+} + 3H_2O + 0.5N_2 \qquad (4.2.12)$$

The spatial distribution of these major redox species is similar to field measurements and the model simulations of Postma et al. (1991) and Engesgaard and Kipp (1992).

The results from OGS#IPhreeqc are compared against PHREEQC 1D transport to assess the accuracy of the mathematical formulations. It is found that all simulation results behaved identical in both models and thus proved a correct mathematical formulation.

## 4.3. Scenario model

The developed kinetic model is applied to the scenario model in 2D. The same transport parameters and turnover reactions are used. Even though the primary electron donor is pyrite in the study area (Hessian Ried), both denitrification pathways, autotrophic and heterotrophic are considered in this simulation.

### 4.3.1. Model setup

The model domain used for the numerical investigation is a two-dimensional model with 90m length, 5m depth, 200 grid cells in X and 50 cells in the Z directions (Figure 20). The simulation runs with a time step of 1 day to the total simulation time of 5000 days. The groundwater flow is simulated by OGS and fully saturated with a steady state condition is assumed. The flow direction is from right to left, i.e. from the Odenwald Forest to the Rhine River, and two constant hydraulic head boundary conditions are assigned to the right and left model boundaries, imposing a regional hydraulic gradient of 0.001 (Table 9). The flow parameters including porosity and hydraulic conductivity are specified based on the field measurement and laboratory experiment from the study area conducted by Knipp (2012) and Preiß (2013). For each time step, flow processes are calculated first and mass transport using advection-dispersion equation (ADE) is solved sequentially for each mobile component by OGS (as discussed in Chapter 2).

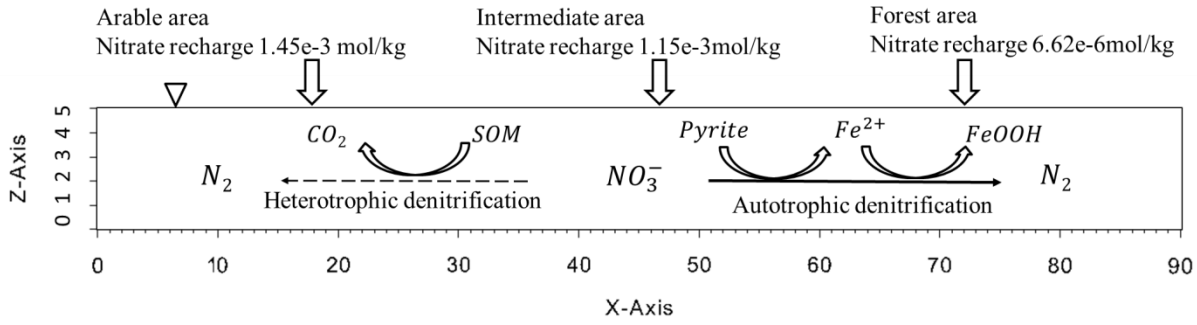


Figure 20 Two-dimensional domain used in the simulations (scale in meter) (from Jang et al. (2017)

The geochemical reaction system is defined to consider water-rock interaction affecting nitrate reduction reactions over the simulation time. Related geochemical reactions are described in Table 8 in chapter 4.2. Nitrate, as main contaminant source, is emplaced from the top boundary with various concentrations of source zones (arable, intermediate, and forest area). A solution containing oxygen and nitrate are introduced into the domain along the boundary at z = 5m (top boundary) (Figure 20). Since the aquifer's major electron donor pyrite presents to be abundant throughout the model domain, the entered nitrate is reduced to nitrogen gas by denitrification. That is, the modeling process consists of adding electron acceptors to the sediment containing electron donors.

The initial condition and boundary condition varying land use is shown in detail in Table 10 (modified from field measurement Preiß (2013)). The simulation includes eighteen aqueous species and three mineral phases in total. This is a simplification of process and certainly not the case in the nature aquifer system. In fact, nitrate reduction reactions in the nature systems are controlled by more complicated processes with spatial and temporal variations (e.g. pH, temperature, salinity, toxins, pore size and microbial acclimation). However, these simplifying approaches can be applied to evaluate the influence of the hydrological and geochemical heterogeneity on the contaminant fate and transport individually in Chapter 5.

Table 9 Flow field parameters and boundary conditions (modified from field measurement Knipp (2012) and Preiß (2013))

| *Boundary condition* | |
|---|---|
| Left | Constant head |
| Right | Constant head |
| Hydraulic gradient | 0.001 |
| *Geometrical parameters* | |
| Model longitudinal direction($x$) | 90m |
| Model thickness ($z$) | 5m |
| Grid spacing ($\Delta x$) | 0.45m |
| Grid spacing ($\Delta z$) | 0.01m |
| Longitudinal dispersivity ($\alpha_L$) | 0.1m |
| Transversal dispersivity ($\alpha_T$) | 0.01m |
| *Flow field parameters* | |
| Bulk density | 1716 $kgm^{-3}$ |
| Mean porosity ($n$) | 0.34 |
| Mean hydraulic conductivity | 1.55E-4 $ms^{-1}$ |
| Time step ($\Delta t$) | 1 day |

Table 10 Geochemical conditions for initial groundwater and sources (modified from field measurement Preiß (2013))

| Component | Initial (mol $L^{-1}$) | Source value (mol $L^{-1}$) | | |
|---|---|---|---|---|
| | | Arable | Intermediate | Forest |
| Aqueous component | | | | |
| Na | 3.67E-04 | 3.39E-04 | 3.39E-04 | 7.73E-04 |
| Ca | 2.54E-03 | 2.13E-03 | 2.13E-03 | 1.69E-03 |
| Mg | 8.64E-04 | 5.99E-04 | 5.99E-04 | 4.11E-04 |
| K | 4.99E-05 | 3.41E-03 | 3.41E-03 | 8.77E-05 |
| $HCO_3$ | 4.80E-03 | 8.30E-04 | 8.30E-04 | 8.30E-04 |
| Cl | 7.44E-04 | 1.44E-03 | 1.44E-03 | 1.17E-06 |
| $NO_3$ | - | 1.45E-03 | 1.15E-03 | 6.62E-06 |
| $SO_4$ | 9.47E-04 | 7.12E-04 | 7.12E-04 | 5.07E-04 |
| $O_2$ | - | 2.24E-04 | 2.24E-04 | 2.24E-04 |
| Tracer | - | 1.45E-03 | 1.15E-03 | 6.62E-04 |
| Solids phase (mol $kg^{-1}$) | | | | |
| Pyrite ($FeS_2$) | 0.0035 | - | - | - |
| Goethite (FeOOH) | - | - | - | - |
| Calcite ($CaCO_3$) | 0.0005 | - | - | - |
| SOM ($CH_2O$) | 0.0405 | - | - | - |

### 4.3.2. Results

Figure 21 shows the simulated reactive transport of nitrate through the study area over 5000 days. Within the upper part of the aquifer (< 2m depth), a sharp boundary is observed with high nitrate to low nitrate water corresponding to decreasing in oxidation-reduction potential ($pe$) and oxygen concentration. Excessive nitrogen gas ($N_2$ concentration above that expected from equilibrium with the atmosphere) is the comparatively conservative product of nitrate reduction and has been used as a natural tracer to identify nitrate reduction (Rivett et al., 2008). Most of the field study, the amount of nitrogen gas from nitrate reduction can be calculated by normalizing the measured dissolved concentrations as $N_2/Ar$ ratios (Singleton et al., 2007). Because natural groundwater may contain nitrogen gas beyond equilibrium concentration due to an incorporation of excessive air from physical processes. However, in this simulation, it is assumed that initial groundwater (background water) does not contain any free nitrogen species. This assumption makes it easier to calculate and evaluate the influence of the hydrological and geochemical heterogeneity on the denitrification processes. Since the initial groundwater system does not contain any free nitrogen species, so that the amount of nitrogen gas produced can be expressed regarding equivalent reduced nitrate by the input of nitrate and its reduction processes.

As nitrate removal from groundwater by pyrite oxidation increases the concentration of sulphate ($SO_4^{2-}$) and ferrous ion ($Fe^{2+}$) (Figure 22) :

$$FeS_2 + 2.8NO_3^- + 0.8H^+ \rightarrow Fe^{2+} + 2SO_4^{2-} + 1.4N_2 + 0.4H_2O$$

The produced ferrous ion ($Fe^{2+}$) is oxidized by oxygen or nitrate to ferric ion ($Fe^{3+}$) which is a relatively rapid and reversible reaction (Christensen et al., 2000). Unless pH is extremely low ferric ion is precipitated as ferric oxide or oxyhydroxide (e.g. Goethite). The goethite precipitation reaction is highly pH dependent and acts as a buffer against a decrease in pH caused by the oxidation of pyrite (Engesgaard and Kipp, 1992).

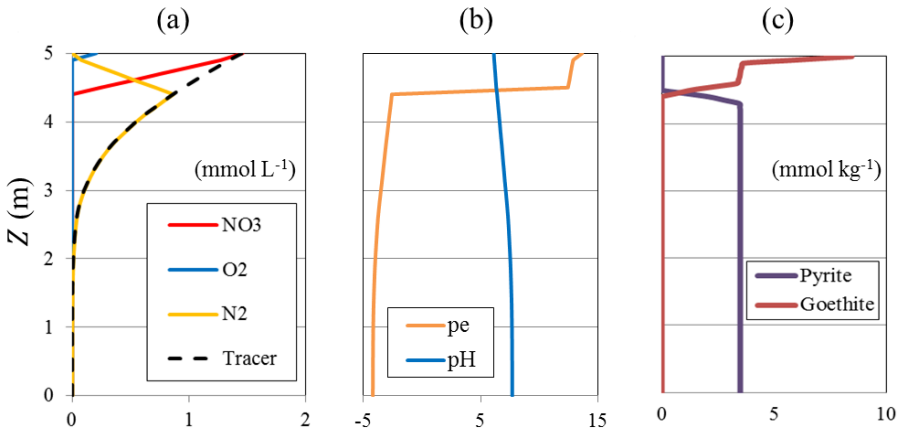


Figure 21 Chemical concentration changes below the agricultural area after 5000 days (x-x' = 15m): (a) concentration of nitrate, oxygen, excessive nitrogen and tracer, (b) pe and pH changes, and (c) goethite and pyrite concentration (from Jang et al. (2017)).

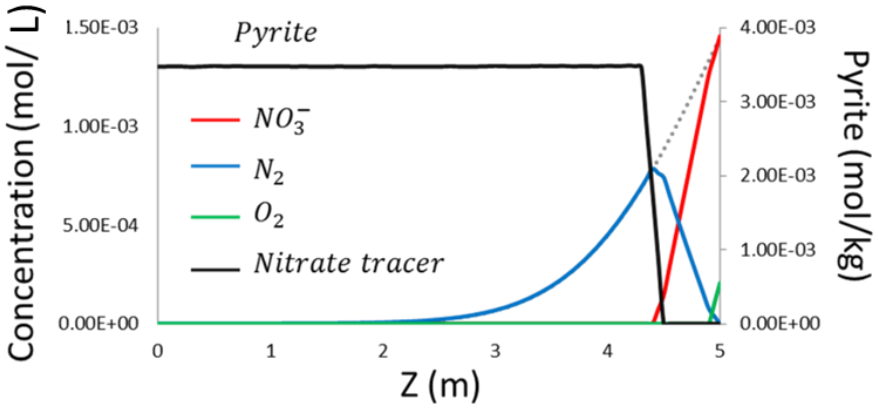


Figure 22 Concentration of $NO_3$, $N_2$, $O_2$, nitrate tracer (conservative specie) and pyrite after 5000 days along the profile x-x' (15m)

# 5. THE INFLUENCE OF AQUIFER HETEROGENEITY

The transport and fate of groundwater contaminants are strongly influenced by various heterogeneity factors of the aquifer. Thus, the criteria for the application of the redox reactions (e.g., nitrate reduction processes) is rarely met the *in situ* field measurement. In this chapter, the influence of physical and chemical aquifer heterogeneities on the redox reaction will be discussed.

## 5.1. Aquifer heterogeneities

Properties of the subsurface are inherently heterogeneous as a result of a combination of geological processes. The subsurface property involves a degree of consolidation, density, porosity, cohesion, strength, elasticity and mineralogy that may, in turn, affect the variation of other variables. Parameters of hydrological and geochemical systems are therefore highly variable in space and often also in time (Houlding, 2000).

The spatial variability of hydraulic conductivity fields, for example, can cause a wide range of groundwater travel times and flow patterns which influence transport and distribution of mobile species (Kalbus et al., 2009; Scholl, 2000; Zech et al., 2016). The spatial variability is also applied to mineral compounds of the aquifer and the distribution of the reactive substances distribution that contribute to the redox environment. As we cannot measure the spatial variability parameters everywhere by the *in situ* field measurement, these parameters are often assumed to be homogeneous, and aquifer heterogeneity is overlooked in many existing models. Obviously, the heterogeneous aquifer characteristics influence on the groundwater contaminant fate and transport processes and these imperfection representations of the parameters lead to error in model results (Bierkens and Geer, 2012). For only a few cases, physical and chemical aquifer heterogeneity has been resolved in detail such as (Atchley et al., 2013;

Beismann et al., 2015; Bosma and van der Zee, 1993; Cui et al., 2014; Mohamed et al., 2006). Most of these prior studies considered the heterogeneous hydraulic conductivity fields as the physical aquifer heterogeneity while chemical aquifer heterogeneity has been represented as spatial variability in abiotic contaminant reaction parameters, such as retardation coefficient (Bellin et al., 1993) and spatial variability in electron donor/acceptor concentrations (Mohamed et al., 2010; Mohamed et al., 2006). However, none of these studies have explored and described the contaminant fate and transport under coupled physical and chemical aquifer heterogeneity systems.

In this work, we consider physical and chemical aquifer heterogeneity represented by hydraulic conductivity and initial reactive substances distribution, respectively. As the requisite electron donor that is critical for redox reaction, pyrite is chosen since a variety of chemoautotrophic energy sources (e.g., reduced iron, reduced sulfur, methane) is of particular importance as a source of heterogeneity in subsurface environments than organic carbon (Groffman et al., 2009). Moreover, pyrite is considered as the primary energy source for denitrification in the study area (discussed in the Chapter 4.1.2).

## 5.2. Generation of heterogeneous aquifer

All scaling factors $\varphi(x, y)$ in the domain are assumed to be log-normally distributed in a two-dimensional porous medium (x-y). The distribution of the scaling factors $\varphi$ can be referred to $\varphi = e^{b}$, where $b$ is a specific point in the $\tilde{b}$, and $\tilde{b}$ is a realization of the spatial random function $B$. Within the model domain all $b(x, y)$ are arranged to be spatially correlated. This spatial correlation between any two values $b_{x1,y1}$ and $b_{x2,y2}$ with a distance of $l$ is defined by an exponential covariance function $C$ (Bellin et al., 1993; Bosma and van der Zee, 1993; Rubin, 2003)

$$C(h) = \sigma_B^2 * e^{-|h|} \tag{5.1.1}$$

$$h = \left| \sqrt{\sum_{i=1}^{m} \left( {}^{l}/_{\lambda_i} \right)^2} \right| \quad \text{with i = 1,…, } m \text{ (} m \text{ is space dimensionality)} \tag{5.1.2}$$

Where variance $\sigma_B^2$ is termed a degree of heterogeneity [-], $l$ [L] is a distance between two points in the heterogeneous domain, and $\lambda$ [L] (frequently called ―length scale" or ―correlation length scale") indicates the strength of the decrease of covariance with increasing distance in the $i^{th}$ direction between two positions. This means that the correlation length scale represents the average length over which a variable is positively correlated at nearby points. It is worth to mention that the scaling length parameter in the exponential covariance model is equal to the correlation length scale (Murakami, 2010; Rubin, 2003). Thus, when we have two points with distance $l$, the two-point correlation follows an exponential function of distance. This is the most classical and common assumption in stochastic groundwater studies (Bellin et al., 1993; Bellin et al., 1992; de Dreuzy et al., 2007; Mohamed et al., 2006; Rubin, 1990).

The mean hydraulic conductivity (*K*) and initial concentration of the electron donor (*Pyrite: P*) are regarded as random variables and assumed to be log-normally distribution with exponential covariance model. The mean hydraulic conductivity and initial pyrite concentration values are assigned on the basis of earlier parameter estimation from Knipp (2012) and Preiß (2013). The variances used in the simulations range from $\sigma^2 = 0.03$ to 3 (See Table 12). Length scale is kept as 1.5m ($\lambda_x$) and 1m ($\lambda_z$)

for all simulations since the discretization of the finite element mesh in a given direction should be at most 1/3 the integral scale, following previously established standards from (Bellin et al., 1993) and (Chin, 1997). Bellin et al. (1993) investigated solute transport in heterogeneous media numerically, and found that the spatial resolution of numerical models needs to be on the order of one -third or -fourth times of the integral scale (i.e. characteristic length of heterogeneity determined by an integral of the two-point correlation over the distance, correlation length in the exponential covariance model) of the log conductivity for capturing the effect of spatial heterogeneity on solute transport. Although the real integral scale is not known in advance, the possible integral scale can be applied. Here, the horizontal and vertical correlation length scales are assumed 1.5m and 1m, respectively. Longitudinal and transversal dispersivities are assumed to be 0.067 $\lambda_x$ and 0.01 $\lambda_z$, respectively. Summary of all input parameters used in this simulation is shown in Table 11, and examples of simulation domain are depicted in Figure 23 and 24.

Table 11 Flow field parameters and boundary conditions

| Boundary condition | |
|---|---|
| Left | Constant head |
| Right | Constant head |
| Hydraulic gradient | 0.001 |
| Geometrical parameters | |
| Model longitudinal direction($x$) | 90m |
| Model thickness ($z$) | 5m |
| Grid spacing ($\Delta x$) | 0.45m |
| Grid spacing ($\Delta z$) | 0.01m |
| Longitudinal dispersivity ($\alpha_L$) | 0.1m |
| Transversal dispersivity ($\alpha_T$) | 0.01m |
| Horizontal correlation length ($\lambda_x$) | 1.5m |
| Vertical correlation length ($\lambda_z$) | 1m |
| Flow field parameters | |
| Bulk density | 1716 kg $m^{-3}$ |
| Mean porosity ($n$) | 0.34 |
| Mean hydraulic conductivity | 1.55e-4 $ms^{-1}$ |

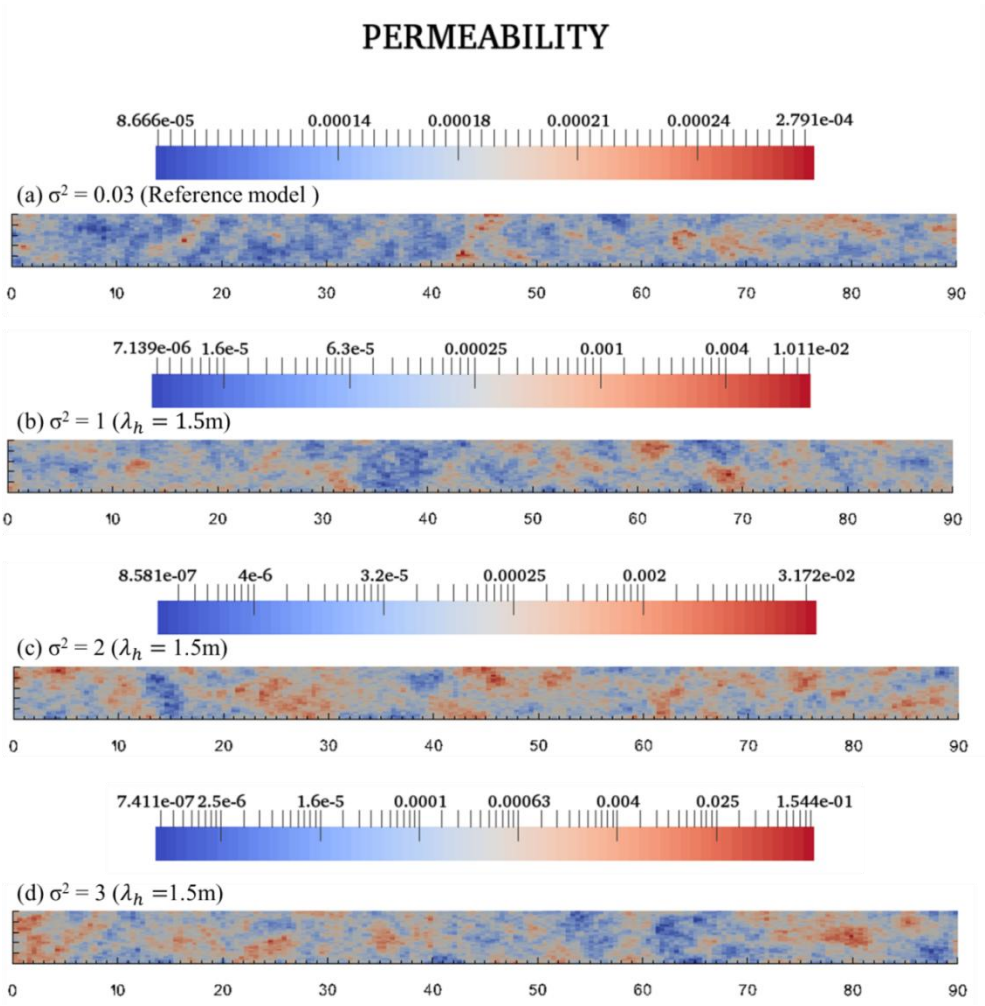


Figure 23 Hydraulic conductivity distribution ($ms^{-1}$) in heterogeneous medias with correlation length ($\boldsymbol{\lambda_h = 1.5m}$) and arithmetic mean 1.55E-4 $ms^{-1}$

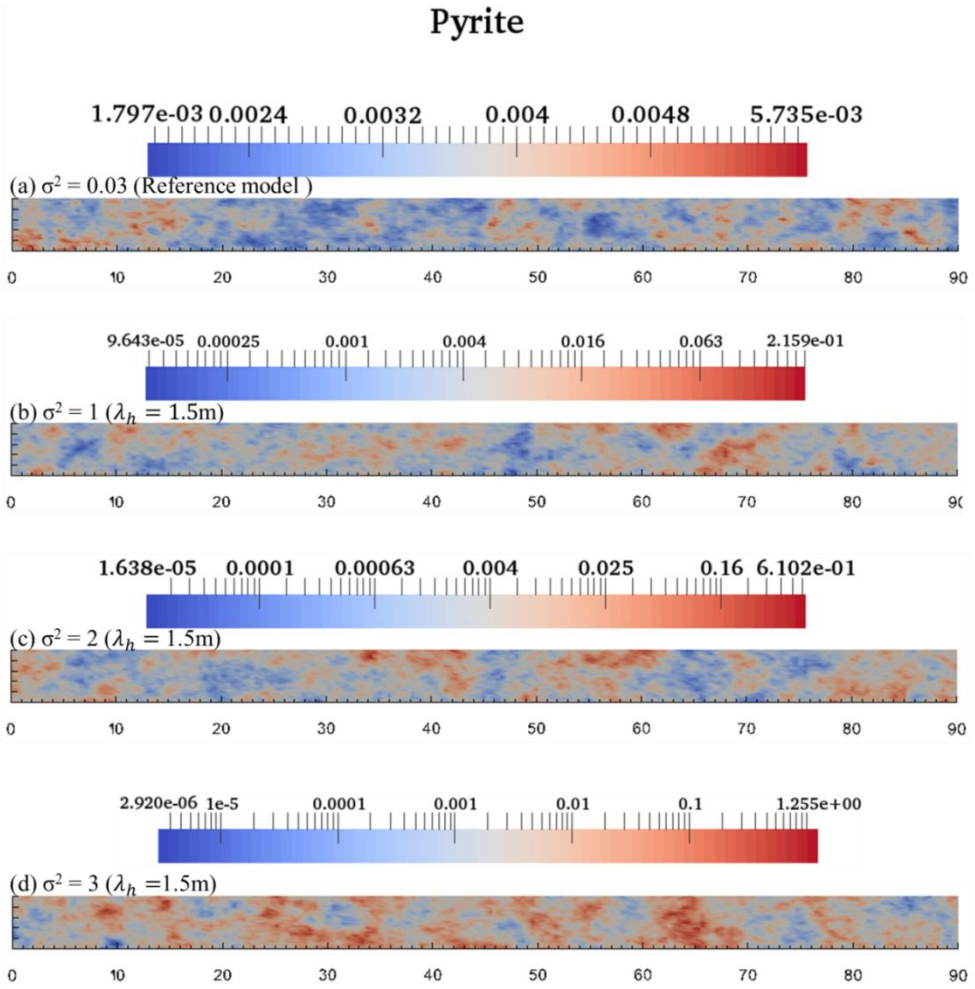


Figure 24 Initial pyrite (*P*) concentration(molkg$^{-1}$) in heterogeneous media with the same correlation length (1.5m)

## 5.3. Scenario setup

Three simulation scenarios were conducted with varying representations of physical and chemical aquifer heterogeneity. Each scenario has four different simulations with varying variance ( $\sigma^2 = 0.03, 1, 2, and\ 3$) . Note that physical and chemical heterogeneous random fields are designed by two random variables, hydraulic conductivity, and initial requisite electron donor distribution, respectively.

Scenario 1 has constant permeability throughout the domain and Scenario 2 has heterogeneous hydraulic conductivity fields. The initial pyrite concentration is homogeneously distributed throughout the model domain in both Scenario 1 and 2. Scenario 3 shows the constant permeability throughout the domain but heterogeneous initial pyrite concentration distribution. All other parameters, which are not directly related to the random variables, are constant between simulations. Overall, nine simulations were conducted, with thirty realizations in each case. The parameters used in the simulations are summarized in Table 11.

Organic matter is considered as homogeneously distributed in all simulations while pyrite is heterogeneously distributed depending on the simulation scenario. This assumption is based on the field observations from (Kludt et al., 2013; Kludt et al., 2016; Knipp, 2012). They analyzed sediment cores from the Hessian Ried (study area) for reactive species and found the heterogeneous distribution of the reactive species, specifically for pyrite. Moreover, autotrophic denitrification is typically the dominant process although organic matter is present. This assumption is also done to limit the complexity of the model. Results of the simulation are analyzed with four cases of the variance a) very weak heterogeneous ($\sigma^2$= 0.03), b) mild heterogeneous ($\sigma^2$=1), c) medium heterogeneous ($\sigma^2$=2) and d) strong heterogeneous media ($\sigma^2$ =3). Since the degree of heterogeneity $\sigma^2$= 0.03 is quite small, it directly refers to the homogeneous condition. The spatial correlation structure is identical for all different variance (1.5/1), which allows a direct comparison of realizations.

Table 12 Summary of simulation parameters

| Scenario | Simulation | Random variable | Variance of ($\sigma^2$) | | Anisotropy ratio |
|---|---|---|---|---|---|
| | | | *K* | *P* | |
| 1 | 1 | *K* and *P* (uncorrelated) | 0.03 | 0.03 | 1.5/1 |
| 2 | 2 | *K* | 0.03 | - | 1.5/1 |
| | 3 | | 1 | - | 1.5/1 |
| | 4 | | 2 | - | 1.5/1 |
| | 5 | | 3 | - | 1.5/1 |
| 3 | 6 | *P* | - | 0.03 | 1.5/1 |
| | 7 | | - | 1 | 1.5/1 |
| | 8 | | - | 2 | 1.5/1 |
| | 9 | | - | 3 | 1.5/1 |

## 5.4. Results and discussion

First, reference model (Scenario 1) is presented and then, the impacts of the physical (Scenario 2) and chemical (Scenario 3) aquifer heterogeneity factors are discussed with a focus on the nitrate reduction capacity. Besides visual comparison, a quantitative calculation is applied to support an interpretation of the simulation results. For every simulation, we calculated the extent of nitrate removal (%), which describes the efficiency of denitrification.

$$Extent\ of\ Nitrate\ removal\ (\%) = \left(\frac{C_t - C_n}{C_t}\right) * 100 \qquad (5.4.1)$$

Where $C_t$ and $C_n$ are the total concentration (molL$^{-1}$) of the conservative nitrate tracer (chemically inert) and reactive nitrate from all the finite-element nodes, respectively. Because in the OGS#IPhreeqc, geochemical reactions are calculated locally on the finite-element node (He et al., 2015), the current nitrate and tracer are extracted from all the nodes.

### 5.4.1. Scenario 1: reference model

Simulated reactive transports of denitrification processes through the study area over 5000 days are shown in Figure 25 and Figure 26.

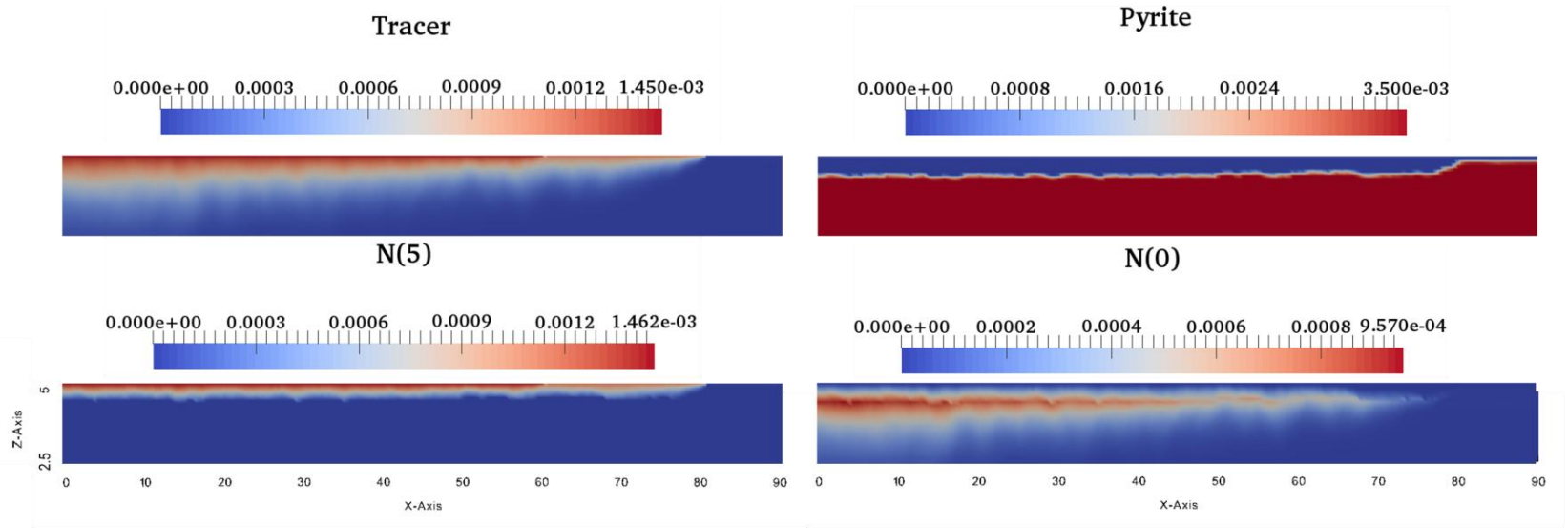


Figure 25 Spatial distribution of mobile (Tracer, $NO_3$ and $N_2$) and immobile compounds (pyrite) concentration after 5000 days (heterogeneous case $\sigma^2 = 0.03$)

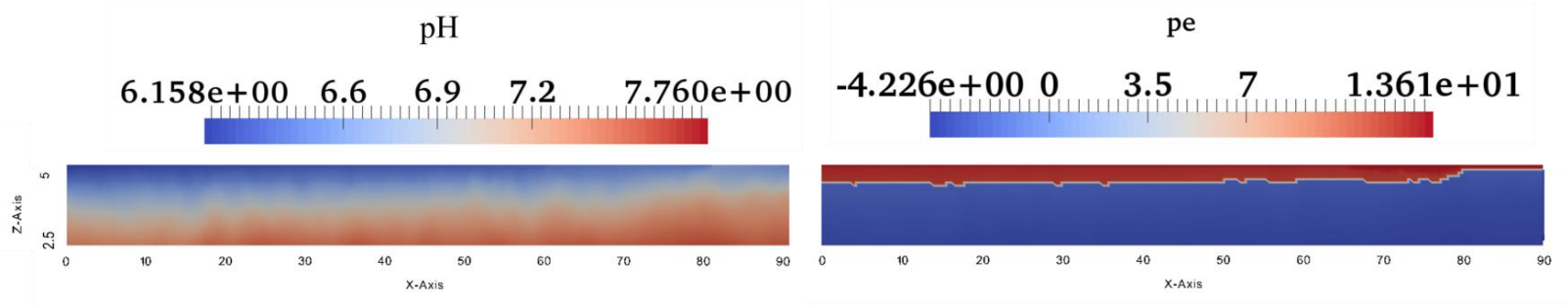


Figure 26 Spatial distribution of **pH** and **pe** after 5000 days (heterogeneous case $\sigma^2 = 0.03$)

In Figure 27, chemical species concentration changes in a vertical profile x-x' (*x*=15m, arable area representation) are shown. Case 1 represents the homogeneous model, and Case 2 represents a heterogeneous model (simulation 1) with a degree of heterogeneity of $\sigma^2 = 0.03$. Even though the case 2 is heterogeneous, it reproduces the same chemical species patterns of the classical homogeneous model, especially within the redox interface. Both simulation results indicate that the models are able to show transport and turnover of nitrogen species. It also captures fairly well the sequence of redox reactions that oxygen decreases first than nitrate (as the alternative oxidant) is reduced.

In this presented work, the simulation 1 (Case 2) will be considered as a reference model, and the results of the reference model will serve as a basis for comparison with all other scenarios. All reactive transport simulations will be based on the reference model, from which specific simulations are derived by modification of boundary condition, initial conditions and model parameters.

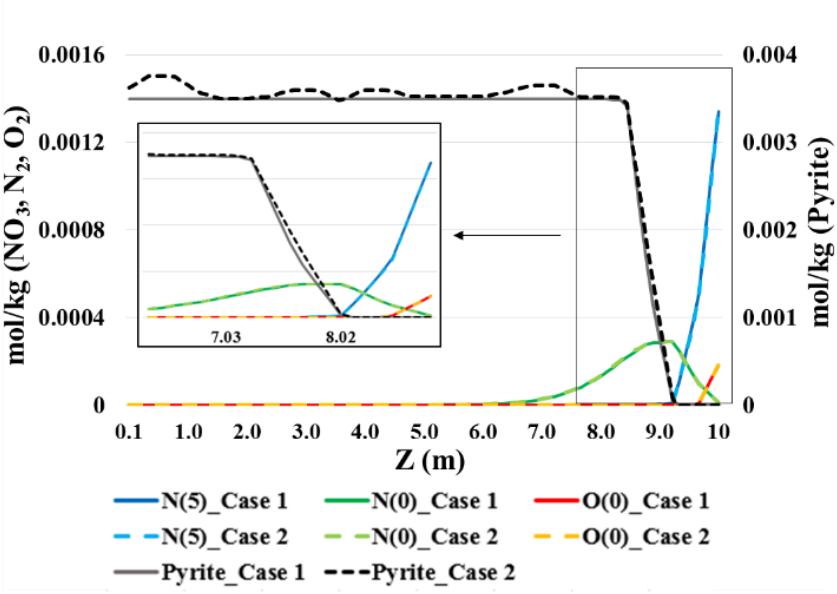


Figure 27 $NO_3^-$, $N_2$, $O_2$, and pyrite concentration changes after 5000 days along the profile x-x' (x=15m) for (a) Case 1 (homogeneous model) and (b) Case 2 (heterogeneous modelwith $\sigma^2 = 0.03$).

## 5.4.2. Influence of heterogeneous hydraulic conductivity fields

Scenario 2 shows how physical heterogeneity (represented by the spatial distribution of hydraulic conductivity) influences the chemical species distribution and, consequently, the nitrate reduction processes (simulation 2-5, See Table 12). Except parameters directly related to the hydraulic conductivity, all parameters are the same as the reference model (simulation 1). For each simulation, thirty realizations of the heterogeneous hydraulic conductivity field were modeled. Subsurface chemical reactive substances (pyrite) are assumed to have a uniform distribution with an initial concentration of 0.0035molkg$^{-1}$ in all simulations.

In Figure 28, the evolution of $NO_3$ plumes over 5000 time steps for different simulations having contrasting degrees of heterogeneity ($\sigma^2 \in [0.03,3]$) are shown. With increasing of the degree of physical heterogeneity, the plumes are irregular and spread into deep aquifer in both longitudinal and transversal direction (Figure 28 and Figure 29). The most heterogeneous model ($\sigma^2 = 3$) shows a greater variability of $NO_3$ concentration distribution and a larger area of pyrite depletion. As more pyrite is oxidized, a greater oxidizing area is distributed (not shown here).

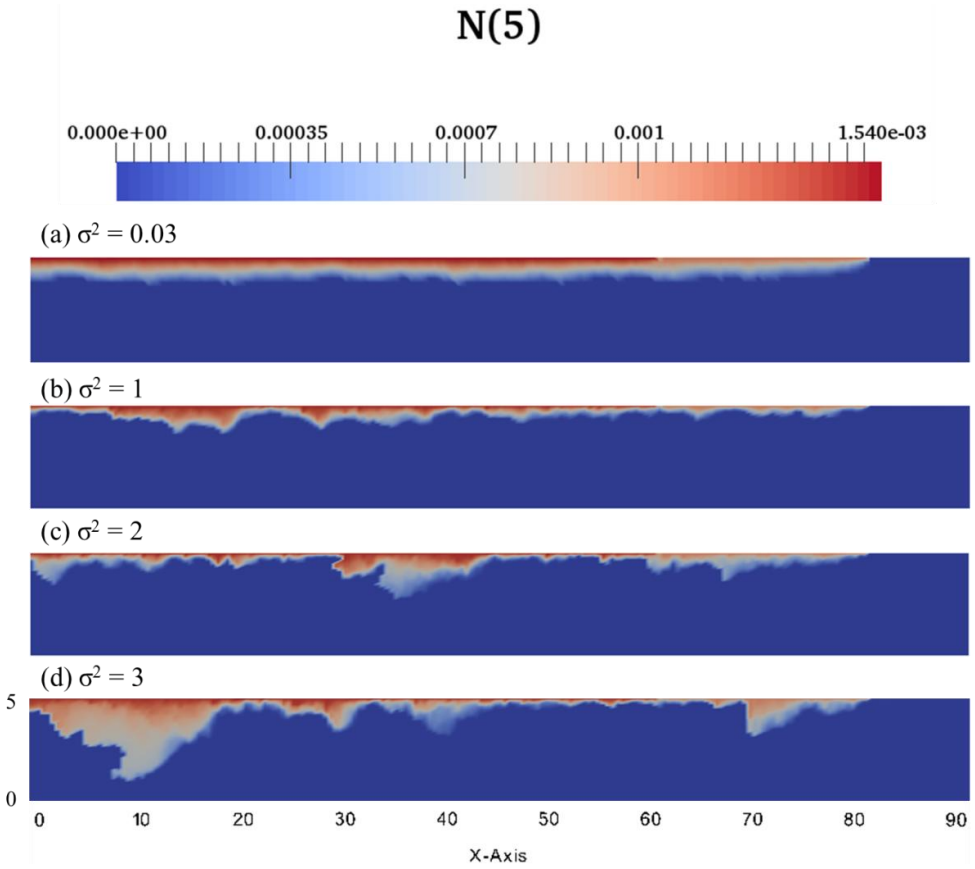


Figure 28 Evolution of $NO_3$ plumes in the end of the simulation.

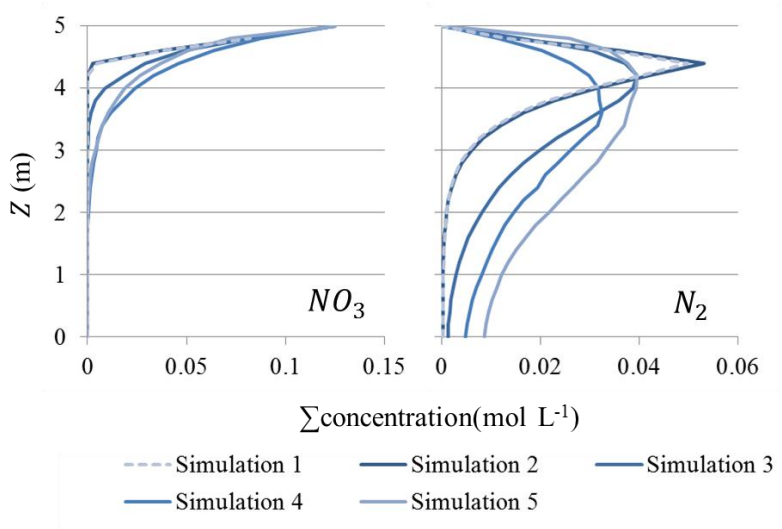


Figure 29 Sum of $NO_3$ and $N_2$ concentration on each depth. Simulation 1 refers to a homogeneous case (reference model) and Simulation 2-5 refer to the heterogeneity factor $\sigma^2$ = 0.03, 1, 2, and 3. Note that the calculated number is as average of twenty realizations in each case (from Jang et al. (2017))

The heterogeneous hydraulic conductivity fields produce preferential flow paths according to the prevailing high hydraulic conductivity and transport more chemical species including electron acceptors, e.g. oxygen and nitrate. It is clearly shown in Figure 30. The larger heterogeneity (also higher contrast in hydraulic conductivity) leads plume travel fast through the model domain which makes squeezing and stretching of the dissolved species, as well. Under such condition, nitrate reduction processes are initially confined to the high permeability areas where more chemical species are effectively transported. Therefore, it creates favorable conditions for the attenuation of nitrate contamination.

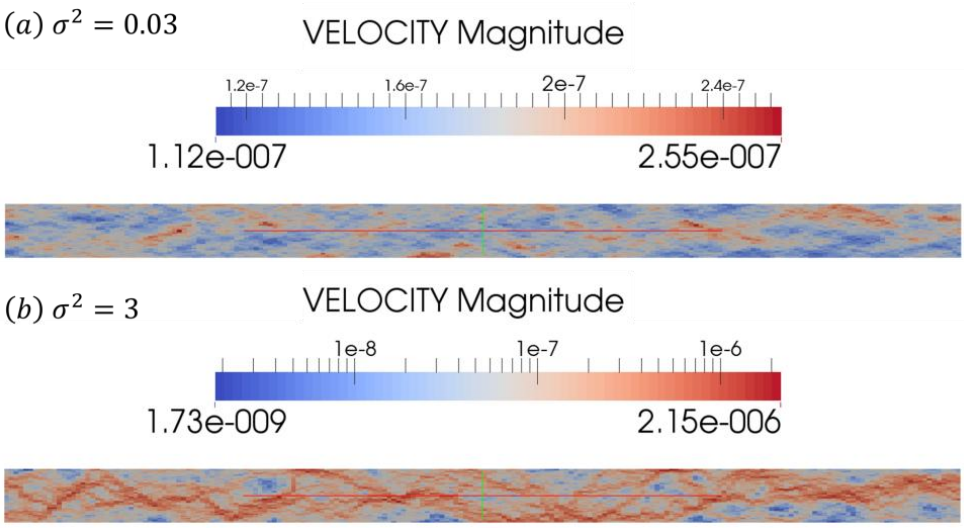


Figure 30 Velocity distribution in the heterogeneous hydraulic conductivity fields with (a) $\sigma^2 = 0.03$ and (b) $\sigma^2 = 3$. Individual realizations with the variance $\sigma^2$ show distinct distributions of flow systems attributed to randomly located preferential flow paths. Although the realizations within an ensemble might differ in their permeability structures, representative realizations were chosen for the discussion of results that the realizations show the typical flow patterns observed for the specific choice of heterogeneity parameters (from Jang et al. (2017))

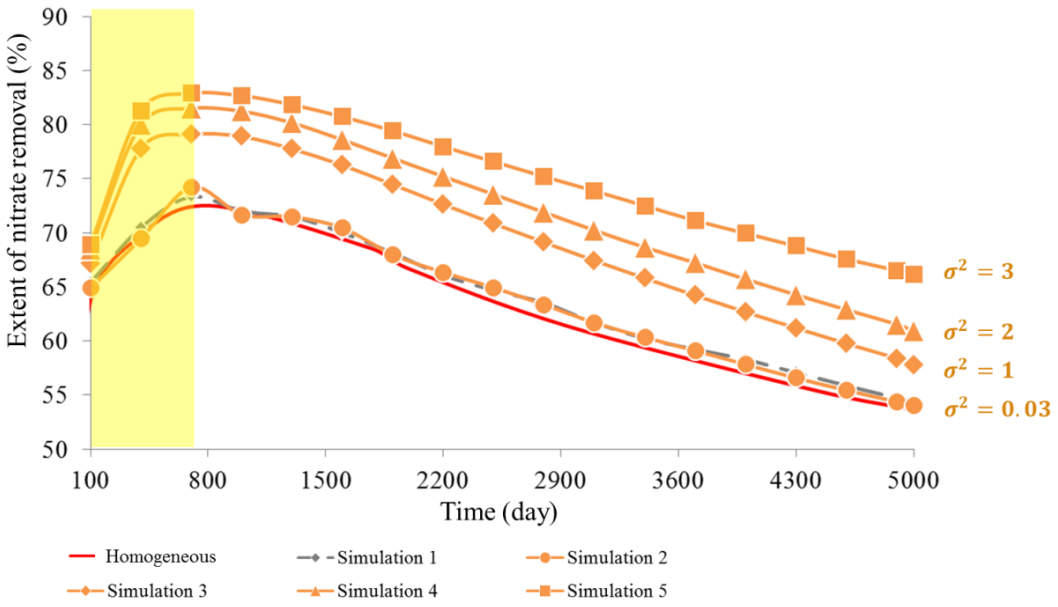


Figure 31 Extent of nitrate removal (%). Red line: homogeneous model (reference model). Orange line: physically-heterogeneous model. Grey line: physically-chemically heterogeneous model ($\sigma^2 = 0.03$) . Note that the calculated number is as average of twenty realizations in each case.

For the quantitative comparison, the extent of nitrate removal is calculated (Figure 31). Since the total simulation time (5000 days) and the chemical degradation potential are the same in all simulations (simulation 1-5), higher values indicate higher nitrate removal efficiency. Nitrate concentration changes are calculated and normalized by the nitrate tracer (non-reactive conservative species) (Eq. 5.4.1).

The graph shows that the calculated nitrate removal efficiencies start rising, peaking at around 700 days and gradually decrease with time in all simulations (Figure 31). The extent of nitrate removed ranges from 54.02% to 82.88% (Table 13). At the beginning of the simulation, entered nitrate successively reduced by pyrite oxidation in the high hydraulic conductivity zones (so called ―hotspots") until pyrite exhaustion. However, after the rapid depletion of pyrite in these highly reactive zones, they become the most vulnerable areas of nitrate accumulation. Finally, remaining pyrite is physically isolated from possible nitrate flow paths induced by the preferential flow and late injected nitrate may travel without reacting. More than a 15% increase in the nitrate removal efficiency

is seen in the most physically heterogeneous model ($\sigma^2 = 3$) as compared to the reference model (simulation 1) in the end of the simulation which can be explained by the enhanced mixing effect in the heterogeneous hydraulic conductivity fields (Cui et al., 2014; Sudicky et al., 1990). Mixing of reactive partners due to the macro-dispersion and transverse mixing enhances the nitrate removal. That is true of both the electron acceptors and the electron donors such as pyrite and chemoautotrophic energy sources, for example, reduced sulfide ($\sum H_2S = H_2S + HS^-$) and reduced Fe (inferred to be $Fe^{2+}$) provided by the oxidative formation of pyrite.

In some ways, the differences of the nitrate removals are relatively small compared to the heterogeneity variances changes. That means the exact value of the heterogeneity variance may not result in strong underestimations of the nitrate removals. However, ignoring the effect of the spatial variability of geological media can lead underestimation of the attenuation processes significantly if we compare the homogeneous and heterogeneous cases. The hydraulic conductivity ($ms^{-1}$) ranges roughly from 7.40E-07 to 1.50E-01 in the most physically heterogeneous case ($\sigma^2 = 3$) and 7.15E-6 to 1.00E-2 in the mild heterogeneous case ($\sigma^2 = 1$). The most heterogeneous case has 8.23% higher nitrate removal capacity than the mild heterogeneous case. Comparing between the mild and medium cases (between $\sigma^2 = 1$ and 2), the difference of the nitrate removal is at most 4.99% while the hydraulic conductivity variation span order of magnitude. However, as for the comparison with the homogeneous and the strong heterogeneous case, the strong heterogeneous field shows much higher nitrate removal capacity (21.65%)

### 5.4.3. Influence of heterogeneous chemical reactive substances distribution

In the third scenario, the availability of electron donors (ED) / acceptors (EA), which is crucial for the redox reactions, is assumed to be heterogeneously distributed. Unlike the physical aquifer heterogeneity, the chemical aquifer heterogeneity has been only examined in a few studies (Li et al., 2007; Mohamed et al., 2006; Tompson et al., 1996). To our knowledge, none of the studies have explored the spatial variability structure of pyrite in the subsurface except the fact that denitrification is highly variable and appears to be log-normally distributed (Groffman et al., 2009). Moreover, we are interested here in the influence of the heterogeneous distribution of chemically reactive substances compared to the physical aquifer heterogeneity, the spatial variability of the distribution of the electron donor has similar correlation structure to that of the heterogeneous hydraulic conductivity fields (Scenario 2). This assumption is also accepted by other previous studies (Mohamed et al., 2010; Mohamed et al., 2006). The mean initial pyrite concentration is constant for the four simulations (simulation 6-9) while spatial variance ($\sigma^2$) is varied ($\sigma^2 \in [0.03, 3]$) (see Table 12). To focus only the effect of heterogeneities in chemical properties, all simulations are assumed to have the same physical properties. Figure 32 shows the evolution of $NO_3$ plumes at the end of the simulation. Note that the figures only show the upper part of the aquifer where denitrification of groundwater nitrates generally occurs. As variance increases, more heterogeneous distributions of nitrate can be observed. However, this effect is much less than that induced by heterogeneous hydraulic conductivity fields (discussed in chapter 5.4.2). The shape of the produced nitrate plumes shows relatively linear patterns along shallow horizontal groundwater flow paths and exhibits a lesser degree of spreading in the transversal direction than the scenario 2 nitrate plumes (Figure 33).

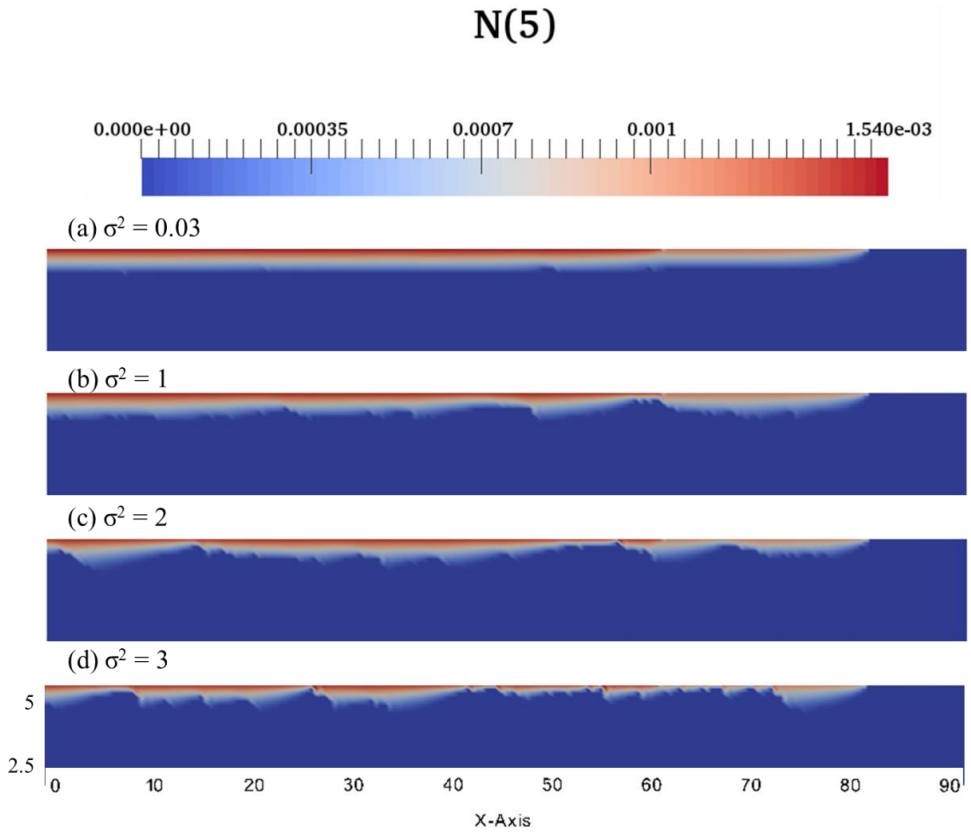


Figure 32 Evolution of $NO_3$ plumes at the end of the simulation(after 5000 days) (a) simulation 2 ($\sigma^2 = 0.03$), (b) simulation 3 ($\sigma^2 = 1$), (c) simulation 4 ($\sigma^2 = 2$), and (d) simulation 5 ($\sigma^2 = 3$

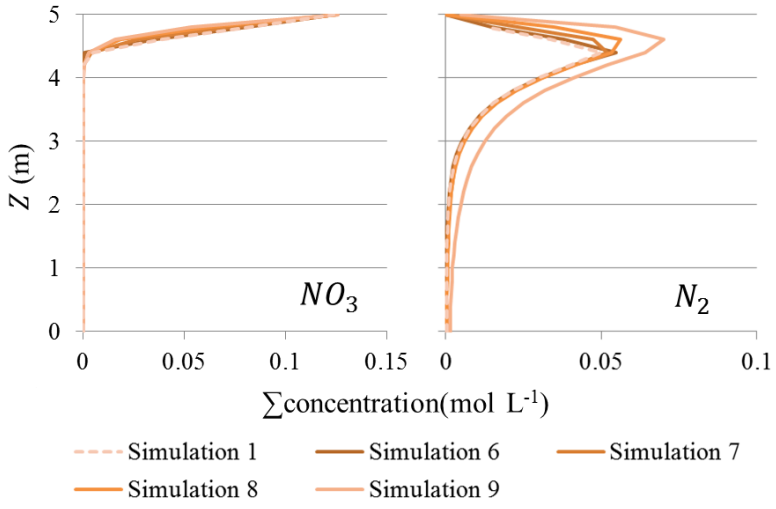


Figure 333 Sum of $NO_3$ and $N_2$ concentration on each depth. Simulation 1 refers to the homogeneous case (reference model) and Simulations 6-9 refer to the heterogeneity factor of 0.03, 1, 2, and 3. Note that the calculated as average of twenty realizations in each case. (from Jang et al. (2017))

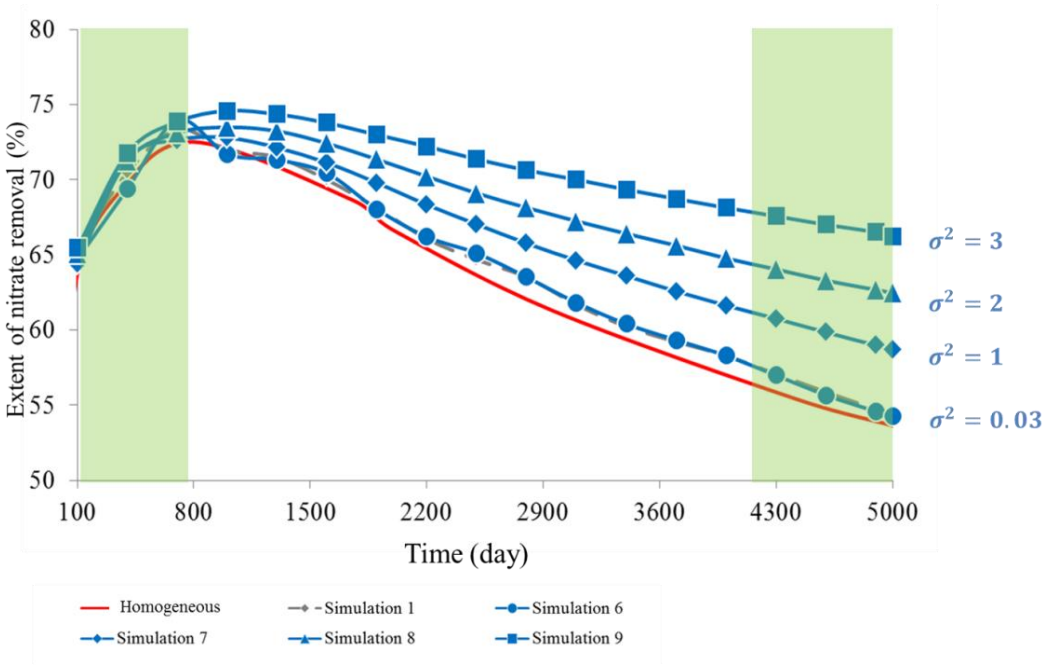


Figure 34 Extent of nitrate removal (%)

The chemical aquifer heterogeneity does not significantly alter nitrate removal efficiency over time between simulations until at around 700 days (Figure 34). However, as the simulation progresses (i.e. as pyrite is consumed during the denitrification process), the discrepancy between simulations increases. This finding is consistent with Li et al. (2007). They also reported that the effects of mineral spatial distributions on effective reaction rates were not significant when reactive mineral are abundant. Nitrate removal efficiencies from simulation 6 and 7 (weak and mild heterogeneous model) continue to fall steadily until the lowest point is reached by the end of the simulations while simulation 8 and 9 (medium and strong heterogeneous model) dropped slightly. The nitrate removal efficiencies of simulation 8 and simulation 9 are 14.14% and 18.99% higher than that of simulation 1 (reference model) at the end of the simulation (Table 13). This suggests that increasing the variance of the initial pyrite concentration distribution produces regions of extremely high and low pyrite concentration, and the high pyrite concentration in some regions from the most heterogeneous model (simulation 8 and 9) may compensate for the regions of lower pyrite.

Table 13 Calculated nitrate removal efficiencies (%)

| Scenario | Simulation | Time (day) | | |
|---|---|---|---|---|
| | | 700 | 2500 | 5000 |
| Scenario 1 (Reference model) | 1 | 74.58 | 65.43 | 53.93 |
| Scenario 2 | 2 | 74.21 | 64.93 | 54.02 |
| | 3 | 79.09 | 70.20 | 58.24 |
| | 4 | 81.49 | 74.57 | 63.89 |
| | 5 | 82.88 | 76.57 | 65.14 |
| Scenario 3 | 6 | 73.98 | 65.10 | 54.23 |
| | 7 | 72.75 | 67.07 | 58.66 |
| | 8 | 73.03 | 69.00 | 62.41 |
| | 9 | 73.85 | 71.37 | 66.22 |

## 5.4.4. Physical and chemical aquifer heterogeneities

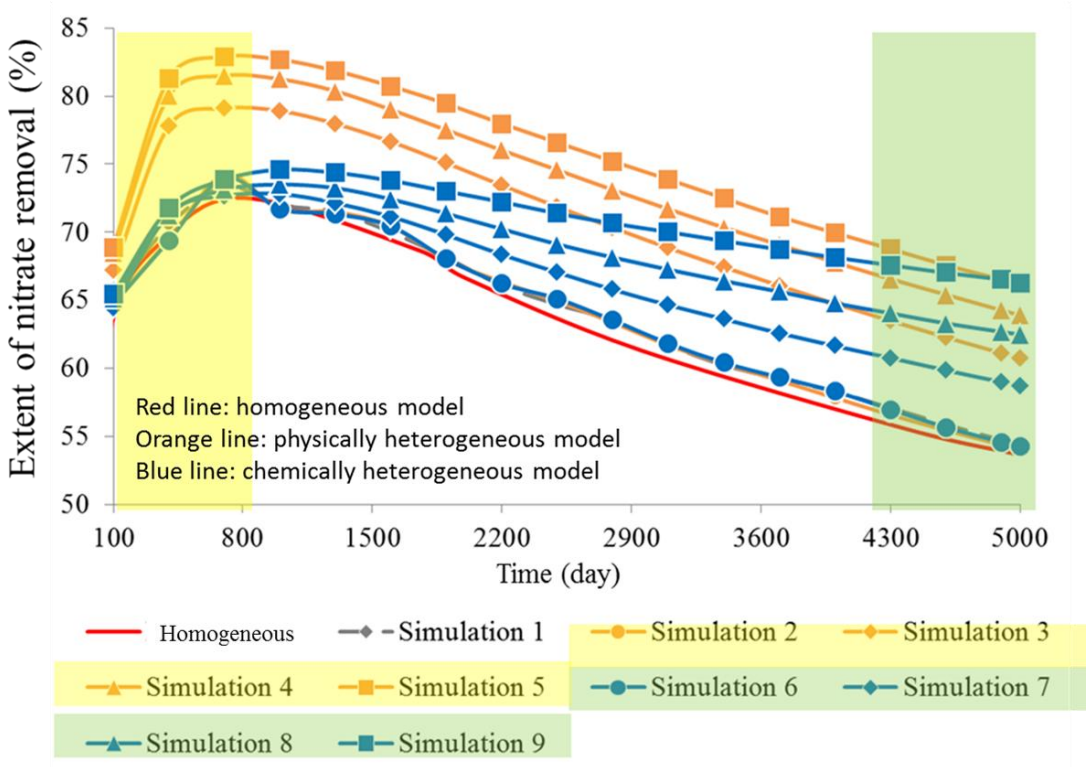


Figure 35 Calculated nitrate removal efficiencies between simulations

Figure 35 shows combined simulation results of scenario 2 and 3 and could be could be interpreted in several ways. First, scenario 2 representing physical aquifer heterogeneity (simulations 2-5, orange lines) shows higher nitrate removal efficiency compared to that of scenario 3 representing chemical heterogeneity (simulation 6-9, blue lines) until around 4000 days. Simulation 5 (the most physically-heterogeneous model) shows the highest nitrate removal efficiency. Heterogeneity with respect to hydraulic conductivity leads systematically to more nitrate removal.

Second, comparing results of simulation 5 and 9, it is seen that nitrate removal efficiency of the most chemically heterogeneous model exceeds or approximate that of the physical heterogeneity at around 4000 days. This finding indicates both physical and chemical aquifer heterogeneity significantly influence the nitrate reduction reaction but at different times. In the short term, physical aquifer heterogeneity plays a significantly more important role than chemical aquifer heterogeneity. However, ignoring chemical

aquifer heterogeneity can lead to an underestimation of the nitrate removal efficiencies in the long term. In scenario 2, the low amount of pyrite is the major limiting factor. The physical aquifer heterogeneity makes it possible to transport a large amount of nitrate to the remaining pyrite sources in the high permeable areas efficiently (also in the vertical direction due to preferential flow paths and large dispersion in high permeable zones). But this also means that the available pyrite in the entire domain will be depleted fast. As discussed in the Chapter 5.4.2, macro-dispersion (or differential advection resulting from hydraulic conductivity contrast) can be clearly observed in the highly heterogeneous flow field and it leads plume travel fast through the model domain and systematically to more nitrate removal (Figure 30). To address where denitrification occurs compared to the localization of the heterogeneity, nitrate tracer and pyrite concentration in the high and low velocity areas over simulation time (400 days) are shown in Figure 36. In the high permeability area (finite element node with a red point), pyrite and nitrate tracer are quickly exhausted and increased. It indicates that the highly heterogeneous flow field leads the higher hydrodynamic dispersion and enhances the contaminant transport which makes a better accessibility of the electron donors. In the meantime, transverse mixing of mobile dissolved species may play an important role in the low permeability areas. In scenario 3 (chemical aquifer heterogeneity), the homogeneous permeability field with low permeability is the major limiting factor which prevents nitrate to be transported to ―hot spots" efficiently. Since the groundwater flow direction is horizontal, the spread of the nitrate in the vertical direction is slow (transverse dispersion should be the main driving force in this scenario). As the increase of the heterogeneity of the electron donor concentration represented as chemical aquifer heterogeneity, the number of the "hotspots" i.e. zones with comparably higher reactivity, should also increase. Hence, the nitrate removal can still take place at comparably high rates after long time, when nitrate finally reaches these high reactive zones.

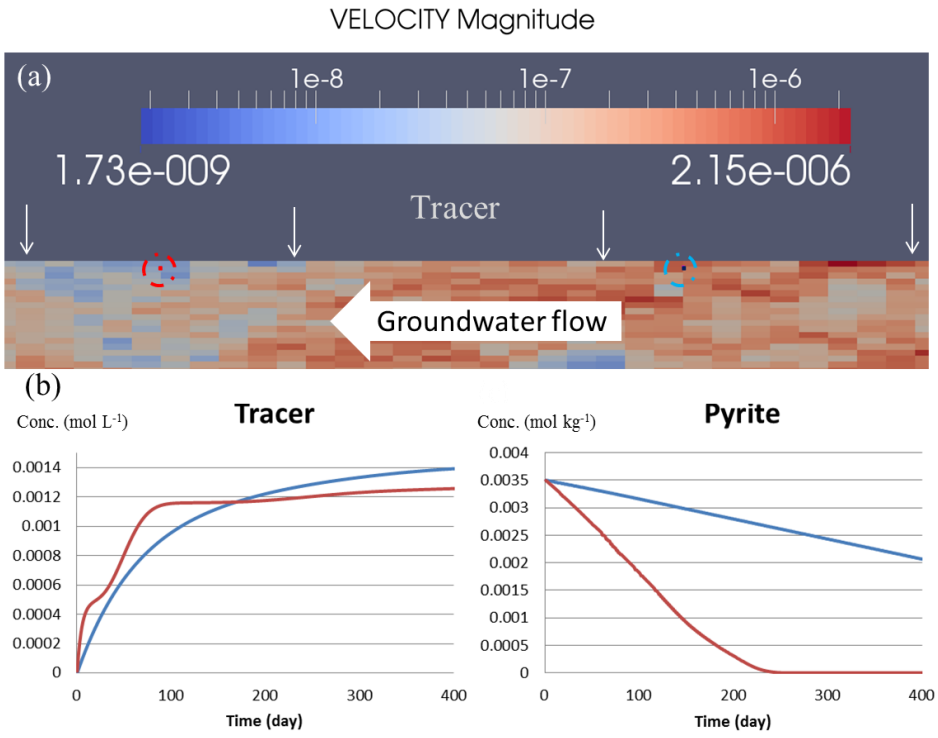


Figure 36 Nitrate tracer and pyrite concentration in the high and low velocity areas over simulation time (400days). (a) Velocity distribution and (b) Blue line: low velocity and Red line: high velocity area (Pyrite is homogeneously distributed with 0.0035mol)

Third, for each considered simulation, nitrate removal efficiencies of the heterogeneous models are higher than that of the reference model, indicating that the homogeneous model underestimates nitrate removal degradation and oval-estimation of remediation time. In this study, the range of heterogeneity is $\sigma^2 \in [0.03, 3]$. According to Höyng et al. (2015), hydraulic conductivity statistics for the natural aquifer analogs ranges between 1.19 and 5.77, and it is obvious that all natural structures have a certain degree of physical and chemical aquifer heterogeneity. That is, the homogeneous model is limited to manifesting the denitrification processes especially in the highly heterogeneous aquifer system.

# 5.5. The effect of correlation length

This chapter presents the effect of correlation length and anisotropy ratio of the random fields. The statistical factors, variance and correlation length, determine the strength of heterogeneity in the random fields. Increasing of the variance indicates that the range of hydraulic conductivity (or initial pyrite concentration) values is wider. Apart from the mean, and the variance (e.g. standard deviation), a third important factor of the random field is its degree of persistence. The correlation length measures the spatial persistence of the random field. Thus, the larger correlation length refers to the longer spatial persistence in the field.

According to Elfeki et al. (2012), correlation length is ―a measure of the distance which tells what extent the values are correlated in space". For example, if two points ($b_{x1,z1}$ and $b_{x2,z2}$) in the random field ($\tilde{b}$) are close together, they will be highly correlated, that is, if one is larger the other one is also likely to be large (Figure 37). If they are far away from one another, they will tend to be uncorrelated whether one is large or not has no (linear) influence on the size of the other. We can capture this idea with a correlation function $C(b_{x1,y1}, b_{x2,y2})$ which gives the correlation coefficient between $C\left(b_{y1,y1}\right)$ and $C\left(b_{y2,y2}\right)$ which decays as $l = |b_{x1,y1} - b_{x2,y2}|$ increase.

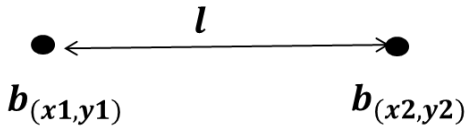


Figure 37 Two points ($b_{x1,z1}$ and $b_{x2,z2}$) in the random field ($\tilde{\boldsymbol{b}}$)

The exponential covariance model, characterized by a horizontal and vertical correlation length $\lambda_h$ and $\lambda_v$, was applied according to Eq. (5.1.1) and Eq. (5.1.2). Heterogeneous random fields are generated with varying horizontal correlation length ($\lambda_h$) from 1.5m (small scale), 3m (medium scale) and 10 m (large scale) while constant vertical correlation length ($\lambda_v$ = 1m).

## 5.5.1 Model set up

Heterogeneous aquifers are generated using the same mean and variance of the hydraulic conductivity and electron donor availability with different horizontal correlation lengths. With the exponential covariance function, the random fields for the hydraulic conductivity and the geochemical heterogeneity parameters can be generated with the arithmetic mean and variance and the correlation lengths in each direction. Twenty realizations were used for the simulation of each of the scenario explained below (Table 14) and examples of the simulation domain are depicted in Figure 38 and Figure 39.

Table 14 Summary of simulation parameters

| Scenario | Simulation | | Random variable | Variance of ($\sigma^2$) | | Correlation length (m) |
|---|---|---|---|---|---|---|
| | | | | *K* | *P* | |
| 1 | 1-1 | | *K* and *P* (uncorrelated) | 0.03 | 0.03 | 1.5 (Reference) |
| 2 | 2 | 2-1 | *K* | 0.03 | - | 1.5 |
| | | 2-2 | | 0.03 | - | 3 |
| | | 2-3 | | 0.03 | - | 10 |
| | 3 | 3-1 | *K* | 1 | - | 1.5 |
| | | 3-2 | | 1 | - | 3 |
| | | 3-3 | | 1 | - | 10 |
| | 4 | 4-1 | *K* | 2 | - | 1.5 |
| | | 4-2 | | 2 | - | 3 |
| | | 4-3 | | 2 | - | 10 |
| | 5 | 5-1 | *K* | 3 | - | 1.5 |
| | | 5-2 | | 3 | - | 3 |
| | | 5-3 | | 3 | - | 10 |
| 3 | 6 | 6-1 | *P* | - | 0.03 | 1.5 |
| | | 6-2 | | - | 0.03 | 3 |
| | | 6-3 | | - | 0.03 | 10 |
| | 7 | 7-1 | *P* | - | 1 | 1.5 |
| | | 7-2 | | - | 1 | 3 |
| | | 7-3 | | - | 1 | 10 |
| | 8 | 8-1 | *P* | - | 2 | 1.5 |
| | | 8-2 | | - | 2 | 3 |
| | | 8-3 | | - | 2 | 10 |
| | 9 | 9-1 | *P* | - | 3 | 1.5 |
| | | 9-2 | | - | 3 | 3 |
| | | 9-3 | | - | 3 | 10 |

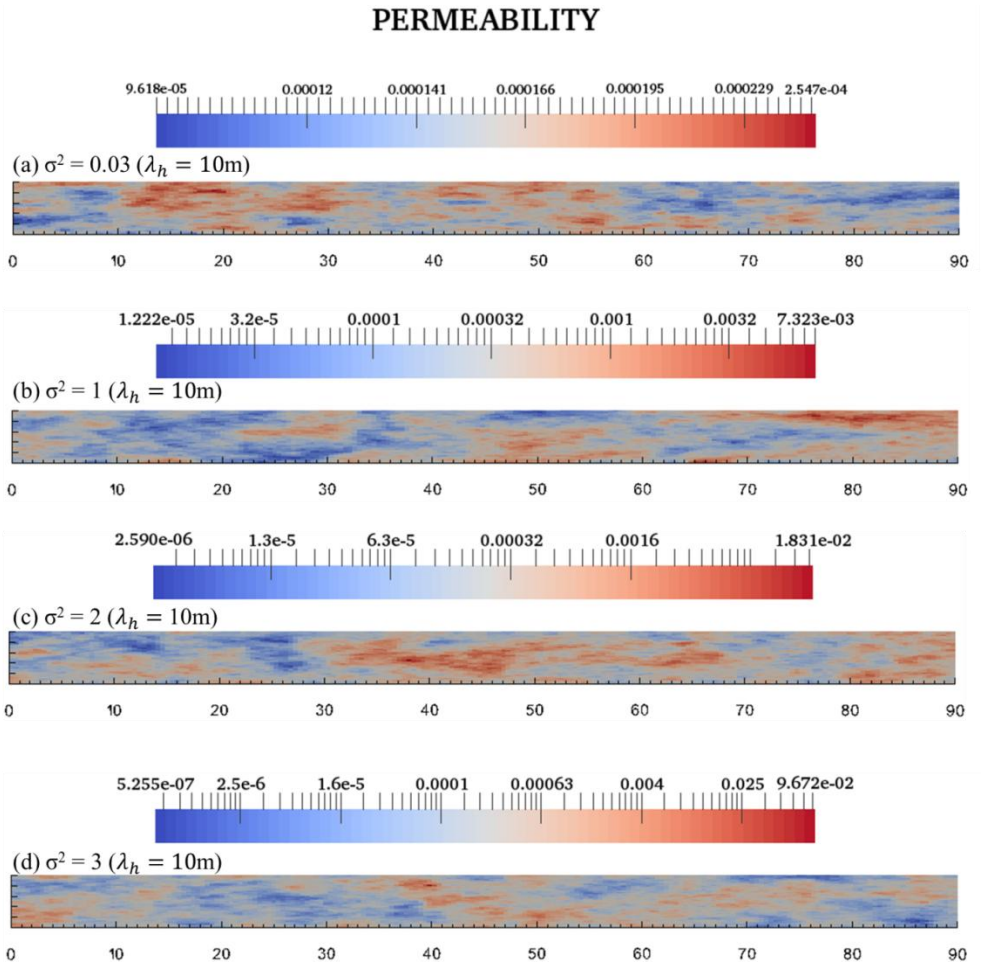


Figure 38 Distribution of hydraulic conductivity ($ms^{-1}$)

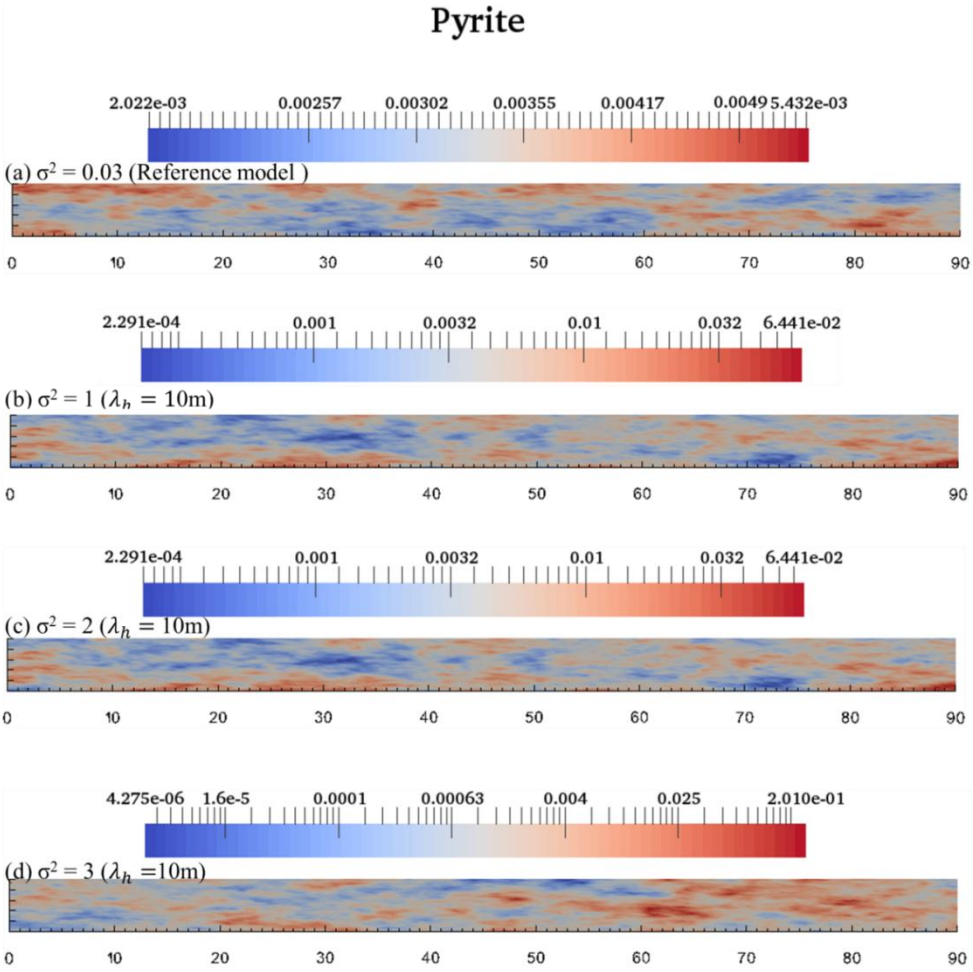


Figure 39 Distribution of pyrite (ED) concentration ($molkg^{-1}$).

## 5.5.2. Results and discussion

Figure 40 shows the simulation results for different correlation structures while keeping the variance at $\sigma^2 = 1$ (except the reference model which having the variance of 0.03 with horizontal correlation length $\lambda_h$ =1.5m). As discussed in Chapter 4.2, increasing value of the physical heterogeneity ($\sigma^2$) causes vertical dispersion. It can be seen that simulation with the small ($\lambda_h$=1.5m) and medium ($\lambda_h$ = 3m) correlation length cause local fluctuations in the nitrate concentration; while they do not significantly impact on the shape and the position of the nitrate plumes between simulations. However, if the correlation lengths get larger ($\lambda_h$ = 10m), more flatten nitrate plumes can be discovered.

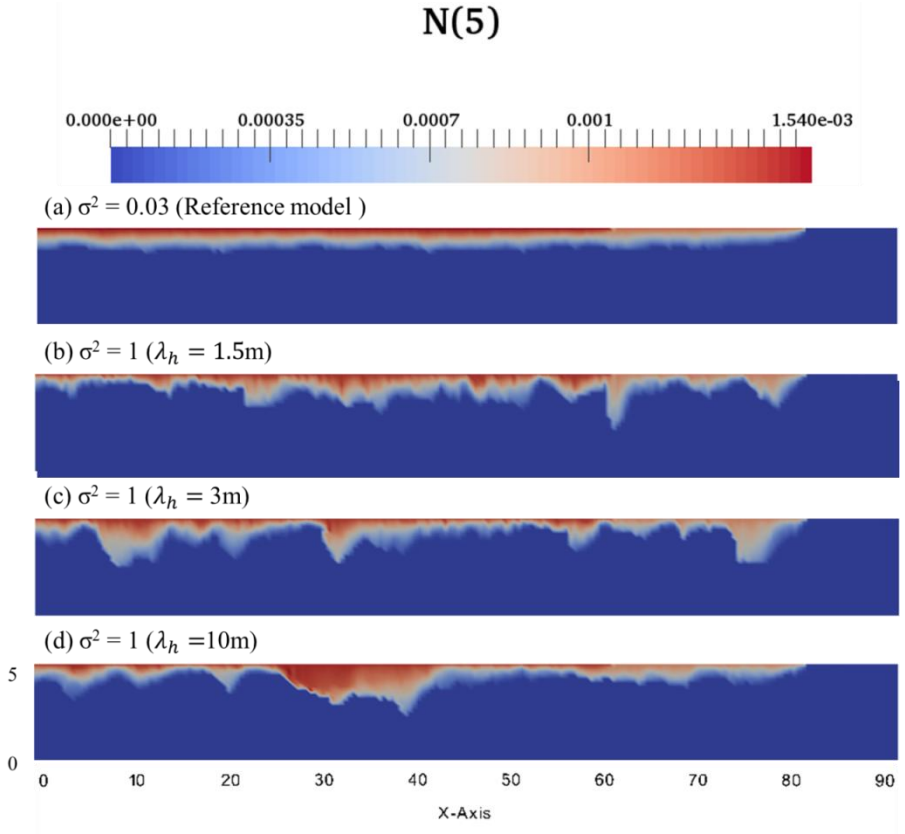


Figure 40 Distribution of nitrate concentration. (a) correlation length at 1.5m (Reference model), (b) correlation length at 1.5 m (small scale), (c) correlation length at 3m (medium scale), and (d) correlation length at 10m (large scale)

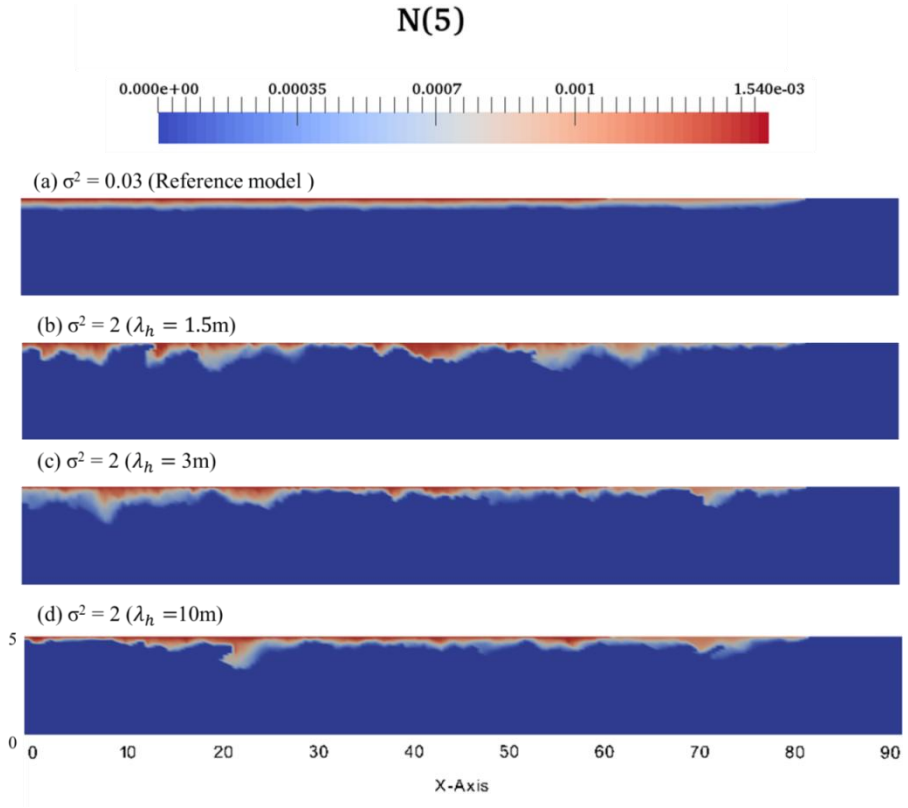


Figure 41 Distribution of nitrate concentration with heterogeneous permeability distribution. (a) correlation length at 1.5m (homogeneous model), (b) correlation length at 1.5 m (small scale), (c) correlation length at 3m (medium scale) and (d) correlation length at 10m (large scale)

Figure 41 visualizes the simulation results for different correlation structures while keeping the variance at $\sigma^2 = 2$. In this medium physical aquifer heterogeneity ($\sigma^2 = 2$), simulated realizations differ slightly from each other, and the concentration pattern of simulation result for the correlation length of 10m shows the most flatten nitrate distribution. However, the impact of the correlation structures plays a minor role. This is underlined by the calculated nitrate removal capacity (%) as well. The differences between realizations are also nearly identical between realizations (Figure 43).

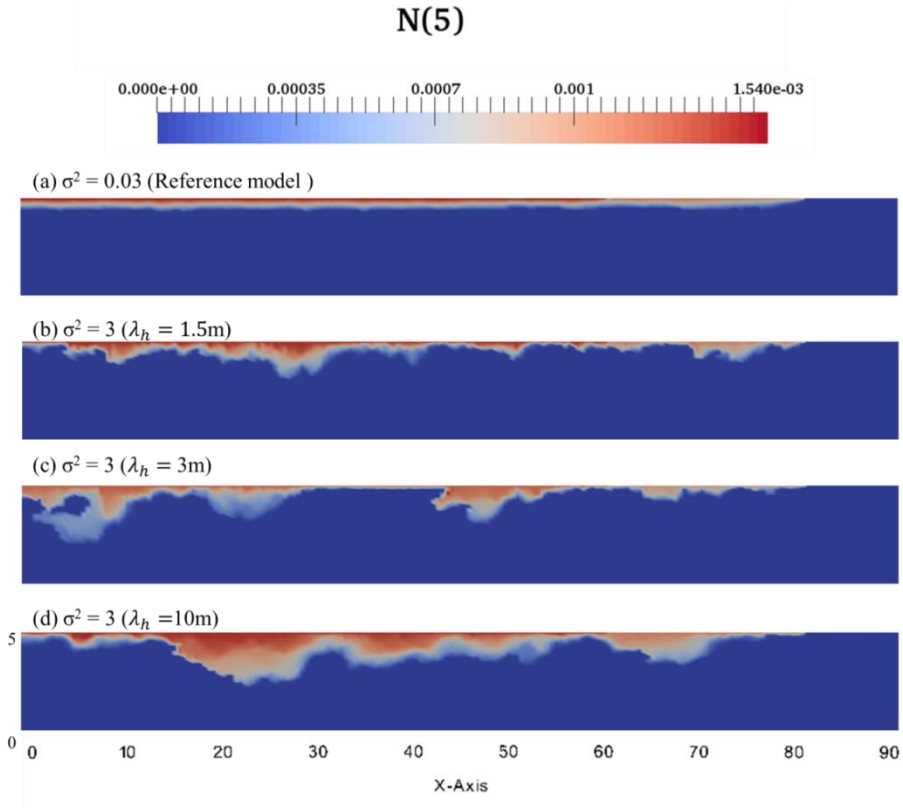


Figure 42 Distribution of nitrate concentration with heterogeneous permeability distribution. (a) correlation length at 1.5 m (small scale), (b) correlation length at 3m (medium scale) and (c) correlation length at 10m (large scale)

Figure 42 visualizes the simulation results for the most physically heterogeneous case ($\sigma^2$ = 3) with varying horizontal correlation lengths. Realizations differ strongly from each other and from the reference model. Local fluctuation is large and leads to significantly different nitrate plume patterns in the simulation results of largest scale correlation length of $\lambda_h$ = 10m. The differences to the reference simulation are largest. A higher amount of dissolved nitrate indicates a wider spread of nitrate plumes. This is supported by a lower relative nitrate removal capacity in the largest correlation length (Figure 43).

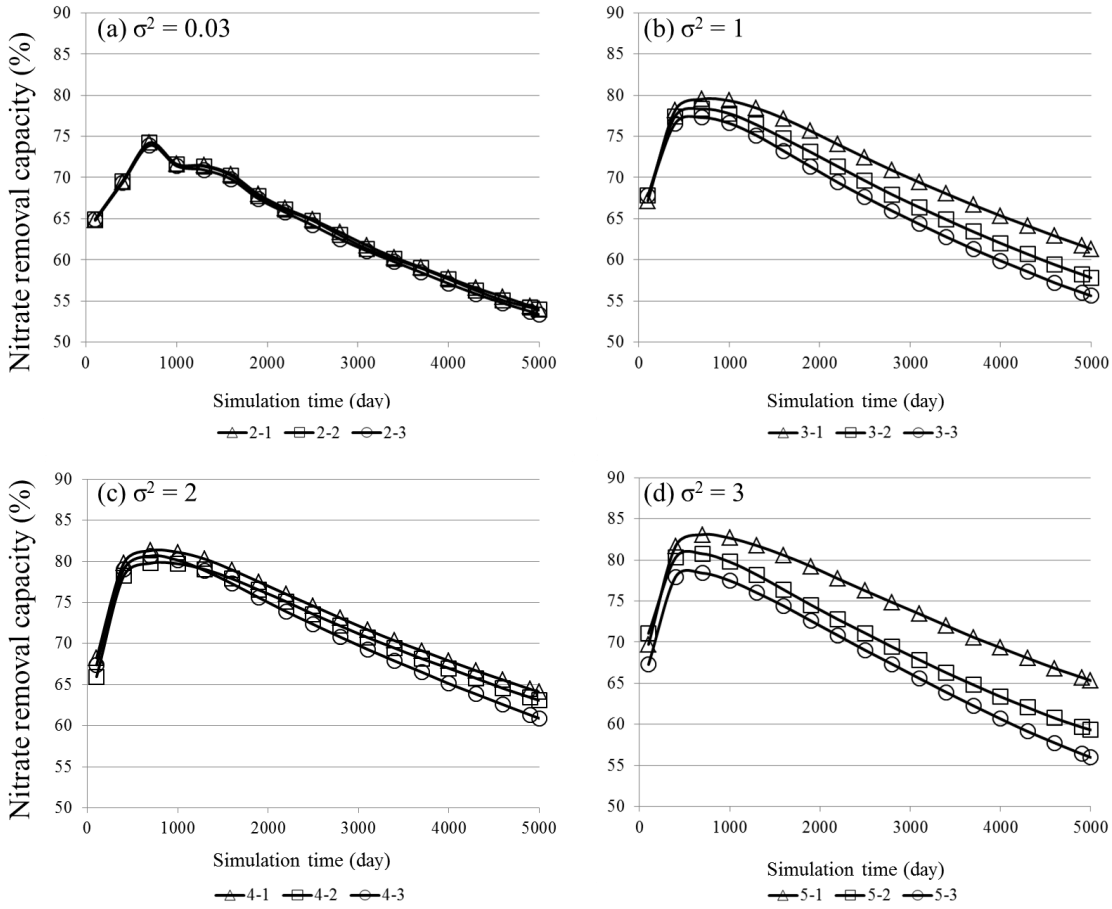


| Variance ($\sigma^2$) | Horizontal correlation length | | | Variance ($\sigma^2$) | Horizontal correlation length | | |
|---|---|---|---|---|---|---|---|
| | 1.5 m | 3 m | 10 m | | 1.5 m | 3 m | 10 m |
| 0.03 | 2-1 | 2-2 | 2-3 | 2 | 4-1 | 4-2 | 4-3 |
| 1 | 3-1 | 3-2 | 3-3 | 3 | 5-1 | 5-2 | 5-3 |

Figure 43 Extent of nitrate removal (%).Simulations with same heterogeneity variance and different correlation length (a)$\sigma^2 = 0.03$ (b) $\sigma^2 = 1$ (c) $\sigma^2 = 2$ (d) $\sigma^2 = 3$

In general, the nitrate reduction capacity has been decreased as increasing the horizontal correlation length scale (Figure 43 and Figure 44). When the physical aquifer heterogeneity is small (0.03) (Figure 43-(a)), the difference is very small and can be ignored. However, when the aquifer heterogeneity $\sigma^2$ is further increased ($\sigma^2 = 3$), the effect of the correlation length is larger (Figure 43-(d)).

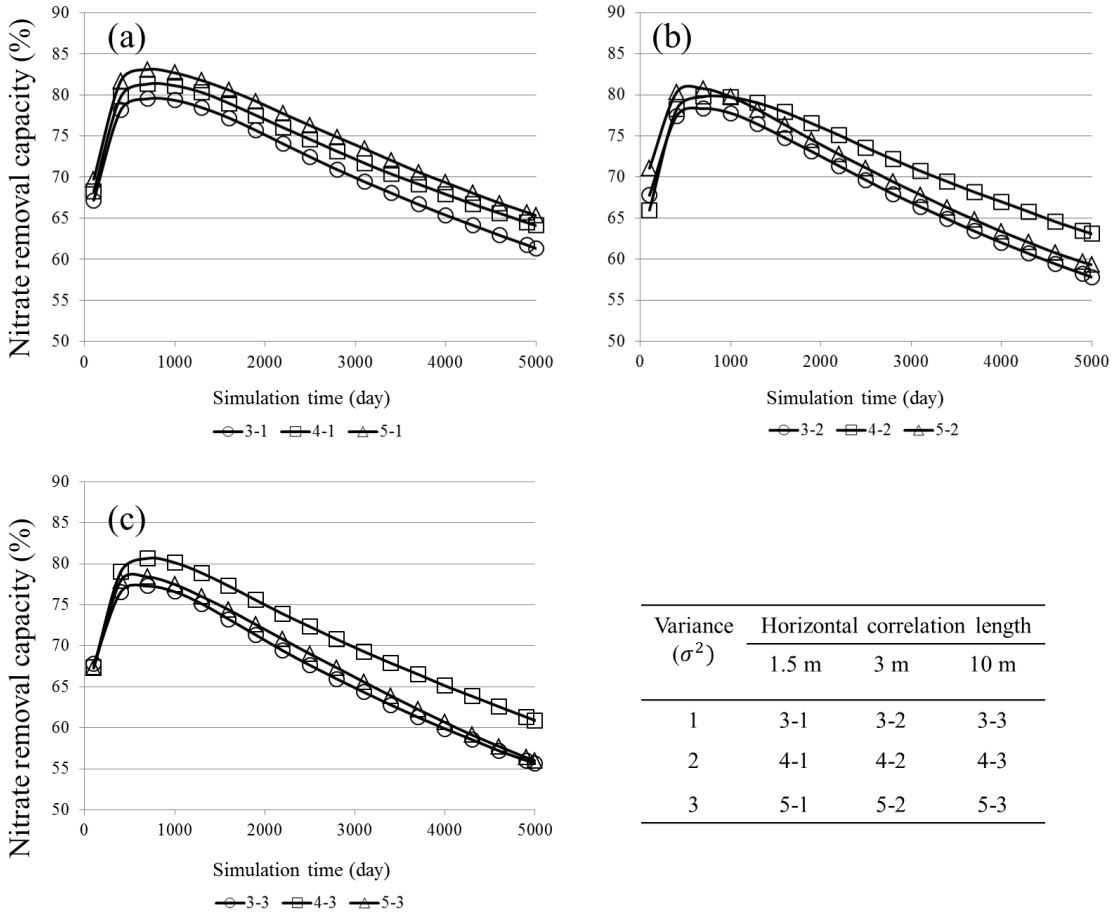


| Variance ($\sigma^2$) | Horizontal correlation length | | |
|---|---|---|---|
| | 1.5 m | 3 m | 10 m |
| 1 | 3-1 | 3-2 | 3-3 |
| 2 | 4-1 | 4-2 | 4-3 |
| 3 | 5-1 | 5-2 | 5-3 |

Figure 44 Extent of nitrate removal (%). Simulations with same correlation length and different heterogeneity variance (a)$\lambda$ = 1.5m (b) $\lambda$ = 3m (c) $\lambda$ = 10m

Table 15 Calculated nitrate removal efficiencies (%)

| Simulation | Time (day) | | |
|---|---|---|---|
| | 700 | 2500 | 5000 |
| 2-1 | 74.21 | 64.90 | 54.04 |
| 2-2 | 74.21 | 64.76 | 53.90 |
| 2-3 | 73.87 | 64.19 | 53.34 |
| 3-1 | 79.52 | 72.43 | 61.31 |
| 3-2 | 79.33 | 69.61 | 57.81 |
| 3-3 | 77.28 | 67.63 | 55.62 |
| 4-1 | 81.31 | 74.57 | 64.09 |
| 4-2 | 79.77 | 73.56 | 63.09 |
| 4-3 | 80.66 | 73.32 | 60.91 |
| 5-1 | 83.08 | 76.25 | 65.32 |
| 5-2 | 80.75 | 71.10 | 59.32 |
| 5-3 | 78.39 | 69.01 | 55.97 |

# 6. SUMMARY

This study describes the influence of physical and chemical aquifer heterogeneity on the redox reactions, with a focus on nitrate reduction processes. The physical and chemical aquifer heterogeneities are represented by heterogeneous hydraulic conductivity and initial requisite electron donor distribution, respectively. The coupling interface OGS#IPhreeqc is applied to pyrite-driven denitrification of nitrate-contaminated groundwater scenarios. Groundwater flow and mass transport are simulated by OGS while the geochemical calculations (kinetic and equilibrium reactions) are carried out by PHREEQC geochemical solver. Stochastic realizations of aquifer heterogeneity parameters are realized by using a geostatistical approach.

The resulting coupled model reproduces nitrate reduction processes including dissolution/precipitation of pyrite and goethite, and consumption of nitrate. It also captures fairly well the sequence of redox reactions; the initial decrease in oxygen followed by the reduction in nitrate (Chapter 4.2.1 and Chapter 5.4.1). From the heterogeneity scenario results, physical aquifer heterogeneity (i.e. heterogeneous hydraulic conductivity fields) significantly influences the fate of chemical species and, consequently, nitrate reduction reactions. The larger heterogeneity (also higher contrast in hydraulic conductivity) makes preferential flow paths and leads plumes travel fast through the domain which makes squeezing and stretching of the dissolved species. Under such condition, nitrate reduction processes are initially confined to the high permeability zones which are also zones of high contaminant flux. Therefore, it creates favorable conditions for the attenuation of nitrate. Also, the enhanced mixing of reactive partners due to the macro-dispersion and transverse mixing increases the nitrate removal. In this case, the amount of electron donors is the major limiting factor (Chapter 5.4.2). With the abundant electron donors, the influence of the spatial variation in the concentration of the electron donors does not significantly alter the nitrate removal efficiency of the system. However, ignoring chemical aquifer heterogeneity can lead to an underestimation of nitrate removals in long-term behavior. It is worth to mention that the homogeneous flow fields with low permeability, which prevents nitrate

to be transport to ―hot spots (i.e. zones with comparably higher reactivity)" efficiently, is the limiting factor for chemically heterogeneous fields. Since the water flow direction is horizontal, the spread of the chemical species in the vertical direction is very slow. In this case, the transversal dispersion is an important mechanism which determines the contaminants to be effectively transported to the ―hot spots". As the spatial variability of the electron donor concentration increases, the number of the ―hotspots" should also increases. Hence, denitrification can still take place at comparably high rates in the highly heterogeneous system after a long time until the electron donor becomes exhausted in these functional zones. That means nitrate removal efficiencies will also be spatially variable but overall efficiency of the system will be sustained if longer time scales are considered and nitrate fronts reach these high reactivity zones (Chapter 5.4.3). Under such conditions, the nitrate removal efficiencies of the chemical aquifer heterogeneity exceed or approximate those of the physical aquifer heterogeneity. This can be evidence that the most influential aquifer heterogeneity factor may change over time. That means physical aquifer heterogeneity is more important concerning short-term effects and chemical heterogeneity regarding long-term behavior. Moreover, for each considered simulation, the homogeneous model is limited to manifesting the denitrification processes especially in the highly heterogeneous aquifer system since it underestimates the nitrate removal efficiency, and therefore, overestimates the time required for remediation (Chapter 5.4.4). The change of the horizontal correlation length and anisotropy ratio is significantly important in the highly heterogeneous system ($\sigma^2 = 3$). The effect of a decreased nitrate removal efficiency is given for increasing the horizontal correlation length ($\lambda_h$ =1.5m to 10m) in the both physically and chemically heterogeneous fields (Chapter 5.5).

Our simulation results highlight that appropriate characterization of variance and correlation length of physical and chemical properties within the aquifer is important to predict the movement and behavior of nitrate and quantify the impact of uncertainty of numerical groundwater simulation as well.

# 7. CONCLUSION AND OUTLOOK

Determining the environmental risk associated with groundwater contamination problems has been common research issue. This involves investigating the fate and transport of the contaminant in the subsurface including physical-, chemical- and biological processes. Numerical reactive transport modeling commonly used to make such a prediction regarding water flow and contaminant degradation processes. Due to the scarcity of the field information and strong variability of properties in space, however, most exiting reactive transport models assume the subsurface properties as a single value for the entire or part of the domain. The effect of the aquifer heterogeneity is often overlooked despite the fact that these imperfect representations lead to errors in model results.

Fate and transport of groundwater contaminants (e.g. nitrate) in natural formations are strongly influenced by spatial heterogeneity such as hydrological and geochemical aquifer characteristics. The amount of nitrate reduction in the subsurface, for example, mainly depends on the local geochemical environments (e.g. spatial distribution of the reactive substances as electron donors) and the groundwater patterns (e.g. hydraulic conductivity fields) as the nitrate needs to be transported. The main objective of this work is to describe the influence of physical and chemical aquifer heterogeneity on the nitrate removal processes and identify the most influential heterogeneity factors affecting the nitrate fate and redox transformation. In this presented work, a nitrate reactive transport with coupled hydrological-geochemical aquifer heterogeneity has been achieved by OGS#IPhreeqc simulation. To account for the heterogeneous subsurface characteristics, stochastic approach is applied to generate a series of heterogeneous realizations.

Our finding, in short, is that the most influential aquifer heterogeneity affecting nitrate removal capacity can change over time. Physically dynamic aquifers need careful consideration when modeling especially for a short-term prediction, since errors may become magnified. However, ignoring chemical aquifer heterogeneity can lead to an

underestimation of nitrate removal efficiencies in long-term behavior. These characteristics should be considered when using the concept of coupled physical and chemical aquifer heterogeneity in modeling and designing long-term remediation and risk assessment.

The model set used in this study is a simplification of processes and certainly not the case in the natural aquifer systems. In fact, nitrate reduction processes in the natural system are controlled by more complicated laws with spatial and temporal variations. More studies are also needed before firm conclusions can be reached about the influence of physical and chemical aquifer heterogeneity. Despite this, simplifying approach allows the individual evaluation of the influence of the hydrological and chemical heterogeneity on the contaminant fate and transport. The results give a feasible explanation about the trend of nitrate removal efficiency changes and the most influential aquifer heterogeneity factors for redox transformation, as well.

This work contributes the understanding of the influence of physical and chemical aquifer heterogeneity on the nitrate transport and redox transformation processes, however; any other reactive multi-species transport problems (e.g. predicting migration and natural attenuation of organic and inorganic pollutants in the subsurface environment) also can be applied and discussed by using the reactive transport model.

# List of publication

## ISI publications

**Eunseon Jang**, Wenkui He, Heather Savoy, Peter Dietrich, Olaf Kolditz, Yoram Rubin, Christoph Schüth and Thomas Kalbacher (2017), Identifying the influential aquifer heterogeneity factor on nitrate reduction processes by numerical simulation, Advances in Water Resources, 99, 38-52, DOI: 10.1016/j.advwatres.2016.11.007

Renchao Lu, Norihiro Watanabe, Wenkui He, **Eunseon Jang**, Hua Shao, Olaf Kolditz, and Haibing Shao (2017), Calibration of water-granite interaction with pressure solution in a flow-through fracture under confining pressure, Environ Earth Sci, 76 (417), DOI:10.1007/s12665-017-6727-1

Wenkui He, Christof Beyer., Jan H. Fleckenstein, **Eunseon Jang**, Olaf Kolditz, Dmitri Naumov, and Thomas Kalbacher (2015), A parallelization scheme to simulate reactive transport in the subsurface environment with OGS#IPhreeqc 5.5.7-3.1.2, Geosci. Model Dev., 8 (10), 3333-3348, DOI: 10.5194/gmd-8-3333-2015.

## Other publication

**Eunseon Jang** (2017) "Reactive Nitrate Transport Model". In : OpenGeoSys Tutorial: Computational Hydrology II: Groundwater Quality Modeling. SpringerBriefs in Earth System Sciences, Springer International Publishing, Berlin, Heidelberg, pp 35-52.

# Appendix I: PHREEQC input definition

To simulate reactive transport modeling using OGS#IPhreeqc, several input files are needed. Each of files is responsible for defining certain aspect of the model. Apart from the PHREEQC database file (*phreeqc.dat*) and heterogeneity distribution files (*hetero_*.txt*), all other input files share the same name but with different file endings (Listing. A.1). In this appendix, the structure and contents of PHREEQC input file for setting up reactive transport modules OGS#IPhreeqc are described.

Listing A.1: Input files and descriptions.

| Input files | Explanation |
|---|---|
| denitrification.pcs | Process definition |
| denitrification.gli | Geometry |
| denitrification.msh | Finite element mesh |
| denitrification.num | Numerical properties |
| denitrification.tim | Time discretization |
| denitrification.ic | Initial condition |
| denitrification.bc | Boundary condition |
| denitrification.st | Source/sink term |
| denitrification.mcp | Component properties |
| denitrification.mfp | Fluid properties |
| denitrification.mmp | Medium properties |
| denitrification.msp | Solid properties |
| denitrification.out | Output configuration |
| denitrification.pqc | PHREEQC input definition |
| phreeqc.dat | PHREEQC database |
| hetero_PERMEABILITY.txt | Hydraulic conductivity distribution file* |
| hetero_PYRITE.txt | Pyrite concentration distribution file* |

*To write heterogeneous random fields, generated by exponential covariance model using R, to an OGS project, distribution file is used to write the hydraulic conductivity and pyrite concentration distribution for each element and node. These distribution files are only necessary for the heterogeneous model.

*PHREEQC input definition (denitrification.pqc)*

*denitrification.pqc* file is based on a PHREEQC input file. There are several minor changes to be executed by OGS#IPhreeqc.

1) #comp: At the right-hand side of each component, this command has to be added and should be defined in *denitrification.mcp* file. Concentration of the each component does not affect the system instead, the real concentration values of the component have to be defined in the initial and boundary condition files (*denitrification.ic* and *denitrification.bc*)
2) #ende: This keyword has to be added after each PHREEQC module (e.g. SOLUTION, EQUILIBIUM_PHASES, RATES, PRINT).
3) There is no need to include the transport modules of PHREEQC since the transport processes will be calculated by OGS.

Listing A.2: Define solution and Equilibrium phases (*denitrification.pqc*)

```
SOLUTION 1
units mol/kgw
temp 25.000000
pH 7 charge # comp 1
pe 4.0  # comp 2
N(5) 0 # comp 3
N(0) 0 # comp 4
O(0) 0 # comp 5
S(6) 0 # comp 6
S(-2) 0 # comp 7
Fe(2) 0 # comp 8
Fe(3) 0 # comp 9
Ca 0 # comp 10
C 0 # comp 11
#ende

EQUILIBRIUM_PHASES 1
    Calcite   0 10  # comp 16
    Goethite  0 10  # comp 17
#ende
```

Equilibrium reactions are defined by EQUILIBRIUM_PHASE. Rate expressions of geochemical reactions that not reach equilibrium in the modeled time frame can be calculated with the embedded BASIC interpreter in PHREEQC. There are two data blocks and user can specify its rate equations. In the RATES data block, the mathematical expression of the kinetic reactions is defined. In the KINETICS data block, the parameters controlling the reaction rates set in the RATES block are defined, further which phase or chemical species reacts, their stoichiometric coefficients and at last parameters controlling the iterations of the Runge-Kutta algorithm. User can decide with the keyword ―INCREMENTAL_REACTIONS", whether every time step starts at time zone and so the results of the previous one does not affect the next time step, or that the results of the previous time step are the starting point of the next iteration. A more detailed information for the general PHREEQC input data can be found Parkhurst and Appelo (1999), and OGS (also OGS#IPhreeqc) input file description can be found here https://svn.ufz.de/ogs/wiki/public/doc-auto.

Listing A.3: Define Kinetic reactions (*denitrification.pqc*)

```
KINETICS
Pyrite  # comp 18
    -formula  FeS2  1
    -m        0.57412
    -m0       0.57412
    -tol      1e-008
Organic_C  # comp  19
    -formula  CH2O  1
    -m        0.57412
    -m0       0.57412
    -tol      1e-008
-steps       21000 in 1 steps # seconds
#ende

RATES
    Pyrite
-start
   1 A = 15e3*m0
   10 if SI("Pyrite") >0 then goto 100
   20 fH = MOL("H+")
   30 fFe2 = (1 + TOT("Fe(2)")/1e-6)
   40 if MOL("O2") < 1e-6 then goto 80
   50 rO2 = 10^-8.19*MOL("O2")*fH^-0.11
   60 rO2_Fe3=6.3e-4 *TOT("Fe(3)")^0.92*fFe2^-0.43
   70 goto 90
   80 rem
   81 rFe3= 1.9e-6*TOT("Fe(3)")^0.28*fFe2^-0.52*fH^-0.3
   90 rate = A* (m/m0)^0.67 *(rO2 + rO2_Fe3 + rFe3) * (1-SR("Pyrite"))
   100 Save rate*time
-end

Organic_C
  -start
   10 if (m <= 0) then goto 200
   20  mO2 = mol("O2")
   30  mNO3 = tot("N(5)")
   40  mSO4 = tot("S(6)")
   50   rate = 7.5e-5*mO2/(2.94e-4 + mO2) + 2.12e-5*mNO3/(1.55e-4 + mNO3)
   60   rate = rate + 1.e-7*mSO4/(1.e-4 + mSO4)
   70  moles = rate * m * (m/m0) * time
   80 if (moles > m) then moles = m
   200 save moles
  -end
#ende
```

Listing A.4: Define output (*denitrification.pqc*)

```
PRINT
 -reset true
 -selected_output true
#ende

SELECTED_OUTPUT
-file phout_sel.dat
-high_precision
-reset false
#ende

USER_PUNCH
10 PUNCH TOT("N(5)"), TOT("N(3)"), TOT("N(0)"), TOT("Fe(2)"), TOT("Fe(3)"), TOT("O(0)")
20 PUNCH -LA("H+"), -LA("e-")
30 PUNCH KIN("Pyrite"), KIN("Organic_C"), EQUI("Calcite"), EQUI("Goethite")
#ende
END
#STOP
```

# Appendix II: Generating the spatial fields

First, load a gstat library.

```
library(gstat)
```

Create 200*50 grids and define the min - and max - of x-axis and y-axis (for example, 90m for x-direction and 10m for z-direction) unit is meter.

```
x_dim <- 200
y_dim <- 50
x_range <- c(0,90)
y_range <- c(0,10)
paste("Grid spacing - ",
      "x:", diff(x_range)/x_dim, "m,", #The grid spacings
      " y:", diff(y_range)/y_dim, "m",sep="")

```

Specify the mean value and different correlation length scales for the x- and y- axis. Note that we set the mean to a negative value since hydraulic conductivity is generally log-normally distributed (Freeze, 1975).

```
mean <- -5.65499231
var <- 3
scale_x <- 1.5 #meters
scale_y <- 1 #meters
```

Convert it into a data frame.

```
grid <- expand.grid(x=seq(x_range[1], x_range[2], length.out=x_dim),
                    y=seq(y_range[1], y_range[2], length.out=y_dim))
gridded(grid) <- ~x+y
```

Defining the spatial model and performing the simulations.

```
gauss <- gstat(formula=I~1, dummy=TRUE, beta=mean, nmax=10,
               model=vgm(psill=var, model="Exp", range=scale_x,
                         anis=c(90,scale_y/scale_x)))
gauss_field <- predict(gauss,grid,nsim=1)
field <- gauss_field$sim1
whole_field <- SpatialPixelsDataFrame(points=coordinates(gauss_field),
                                      data=as.data.frame(field))

```

where formula defines the dependent variable (l) as a linear model of the independent variable. For ordinary and simple kriging, the formula l~1 can be used which is necessary to define a beta parameter as well. For the universal kriging, if l is linearly dependent on x - and y – axis, then the formula l~ x+y can be applied. Here, the simple kriging is applied (formula = l~1). dummy is a logical value, and it has to be TRUE for the unconditional simulation. beta is applied only for simple kriging. It is a vector with the trend coefficients. If no independent variables are assigned, the model only contains the trend coefficients. Variogram model (model) is defined by vgm with sill, range, and nugget parameters, and variogram type (e.g. exponential, Gaussian, and spherical and son on). Anisotropy can also be defined by using anis and nmax allows defining the number of nearest observations that should be used for the kriging predictions or simulation. To write this field to an OGS project, distribution file is used to write the hydraulic conductivity values for each element.

```
setwd("C:/Users/jange/Documents/WORK2015/Hessian/FINAL")
distribution <- paste(seq(0,(length(whole_field)-1),1),
                      exp(whole_field$field))
fileText <- c("#MEDIUM_PROPERTIES_DISTRIBUTED",
              "$MSH_TYPE",
              " NONE",
              "$MMP_TYPE",
              " PERMEABILITY",
              "$DIS_TYPE",
              " ELEMENT",
              "$DATA",
              as.character(distribution))
write.table(fileText, file=paste("hetero_PERMEABILITY.txt",sep=""),
            row.names=FALSE, col.names=FALSE, quote=FALSE)

project_name <- "pds"  #the ogs project name
if(file.exists(paste(project_name,"-original.mmp",sep=""))==FALSE)
  file.copy(paste(project_name,".mmp",sep=""), paste(project_name,"-original.mmp",sep=""))
properties <- readLines(paste(project_name,"-original.mmp",sep=""))
end <- grep("MEDIUM_PROPERTIES",properties,value=FALSE)[2]-1
perm <- grep("PERMEABILITY_TENSOR",properties[1:end],value=FALSE)
prop_text <- c(properties[1:perm],
               "  ISOTROPIC 1.0",
               " $PERMEABILITY_DISTRIBUTION",
               "  hetero_PERMEABILITY.txt",
               properties[(perm+2):end],
               "#STOP")
writeLines(prop_text,paste(project_name,".mmp",sep=""))
```

# Reference


Androulakakis, A., 2012. Nitrate in groundwater (using the example of the Hessian Ried). In: N. Bernstein and M. Ben-Hur (Editors), Binational Student Conference: Soil, Water and Environment. Volcani Center, Isreal and Darmstadt Technical University, Germany.

Appelo, C.A.J. and Postma, D., 2005. Geochemistry, groundwater and pollution. CRC press.

Atchley, A.L., Maxwell, R.M. and Navarre-Sitchler, A.K., 2013. Using streamlines to simulate stochastic reactive transport in heterogeneous aquifers: Kinetic metal release and transport in CO2 impacted drinking water aquifers. Advances in Water Resources, 52: 93-106.

Bailey, R.T., Baù, D.A. and Gates, T.K., 2012. Estimating spatially-variable rate constants of denitrification in irrigated agricultural groundwater systems using an Ensemble Smoother. Journal of Hydrology, 468: 188-202.

Bailey, R.T., Morway, E.D., Niswonger, R.G. and Gates, T.K., 2013. Modeling Variably Saturated Multispecies Reactive Groundwater Solute Transport with MODFLOW-UZF and RT3D. Groundwater, 51(5): 752-761.

Bailey, R.T., Romero, E.C. and Gates, T.K., 2015. Assessing best management practices for remediation of selenium loading in groundwater to streams in an irrigated region. Journal of Hydrology, 521: 341-359.

Bauer, S. et al., 2013. Impacts of the use of the geological subsurface for energy storage: an investigation concept. Environmental earth sciences, 70(8): 3935-3943.

Bauer, S. et al., 2012. Mass Transport. In: O. Kolditz, U.-J. Görke, H. Shao and W. Wang (Editors), Thermo-Hydro-Mechanical-Chemical Processes in Porous Media: Benchmarks and Examples. Springer Berlin Heidelberg, Berlin, Heidelberg, pp. 201-231.

Bayer, P., Comunian, A., Höyng, D. and Mariethoz, G., 2015. High resolution multi-facies realizations of sedimentary reservoir and aquifer analogs. Scientific Data, 2: 150033.

Bea, S.A. et al., 2013. Identifying key controls on the behavior of an acidic-U (VI) plume in the Savannah River Site using reactive transport modeling. Journal of contaminant hydrology, 151: 34-54.

Bear, J. and Bachmat, Y., 1990. Introduction to modeling of transport phenomena in porous media, 4. Springer Science & Business Media.

Beauchamp, E., Trevors, J. and Paul, J., 1989. Carbon sources for bacterial denitrification, Advances in soil science. Springer, pp. 113-142.

Beisman, J.J., Maxwell, R.M., Navarre-Sitchler, A.K., Steefel, C.I. and Molins, S., 2015. ParCrunchFlow: an efficient, parallel reactive transport simulation tool for physically and chemically heterogeneous saturated subsurface environments. Computational Geosciences, 19(2): 403-422.

Beller, H.R. et al., 2006. Whole-genome transcriptional analysis of chemolithoautotrophic thiosulfate oxidation by Thiobacillus denitrificans under aerobic versus denitrifying conditions. Journal of bacteriology, 188(19): 7005-7015.

Bellin, A., Rinaldo, A., Bosma, W.J.P., van der Zee, S.E.A.T.M. and Rubin, Y., 1993. Linear equilibrium adsorbing solute transport in physically and chemically heterogeneous porous formations: 1. Analytical solutions. Water Resources Research, 29(12): 4019-4030.

Bellin, A., Salandin, P. and Rinaldo, A., 1992. Simulation of dispersion in heterogeneous porous formations: Statistics, first-order theories, convergence of computations. Water Resources Research, 28(9): 2211-2227.

Beyer, C., Li, D., De Lucia, M., Kühn, M. and Bauer, S., 2012. Modelling CO2-induced fluid–rock interactions in the Altensalzwedel gas reservoir. Part II: coupled reactive transport simulation. Environmental Earth Sciences, 67(2): 573-588.

Beyer, C., Popp, S. and Bauer, S., 2016. Simulation of temperature effects on groundwater flow, contaminant dissolution, transport and biodegradation due to shallow geothermal use. Environmental Earth Sciences, 75(18): 1244.

Bierkens, M.F.P. and Geer, F.C.v., 2012. Stochastic Hydrology, Utrecht University, Netherlands.

Böhlke, J.K. and Denver, J.M., 1995. Combined Use of Groundwater Dating, Chemical, and Isotopic Analyses to Resolve the History and Fate of Nitrate Contamination in Two Agricultural Watersheds, Atlantic Coastal Plain, Maryland. Water Resources Research, 31(9): 2319-2339.

Bolster, D. et al., 2009. Probabilistic risk analysis of groundwater remediation strategies. Water Resources Research, 45(6): W06413.

Bosma, W.J.P. and van der Zee, S.E.A.T.M., 1993. Transport of reacting solute in a one-dimensional, chemically heterogeneous porous medium. Water Resources Research, 29(1): 117-131.

Carrayrou, J., Mosé, R. and Behra, P., 2004. Operator-splitting procedures for reactive transport and comparison of mass balance errors. Journal of Contaminant Hydrology, 68(3–4): 239-268.

Centler, F. et al., 2010. GeoSysBRNS—A flexible multidimensional reactive transport model for simulating biogeochemical subsurface processes. Computers & Geosciences, 36(3): 397-405.

Central Intelligence Agency, 2013. The World Factbook 2013-14. Government Printing Office.

Chae, G.-T. et al., 2009. Hydrochemical and stable isotopic assessment of nitrate contamination in an alluvial aquifer underneath a riverside agricultural field. Agricultural Water Management, 96(12): 1819-1827.

Charlton, S.R. and Parkhurst, D.L., 2011. Modules based on the geochemical model PHREEQC for use in scripting and programming languages. Computers & Geosciences, 37(10): 1653-1663.

Chin, D.A., 1997. An assessment of first-order stochastic dispersion theories in porous media. Journal of Hydrology, 199(1–2): 53-73.

Christensen, T.H. et al., 2000. Characterization of redox conditions in groundwater contaminant plumes. Journal of Contaminant Hydrology, 45(3–4): 165-241.

Comly, H.H., 1945. Cyanosis in infants caused by nitrates in well water. Journal of the American Medical Association, 129(2): 112-116.

Critchley, K., Rudolph, D., Devlin, J. and Schillig, P., 2014. Stimulating in situ denitrification in an aerobic, highly permeable municipal drinking water aquifer. Journal of contaminant hydrology, 171: 66-80.

Cui, Z., Welty, C. and Maxwell, R.M., 2014. Modeling nitrogen transport and transformation in aquifers using a particle-tracking approach. Computers & Geosciences, 70: 1-14.

Davies, C.W., 1962. Ion Association, London: Butterworths.

de Dreuzy, J.-R., Beaudoin, A. and Erhel, J., 2007. Asymptotic dispersion in 2D heterogeneous porous media determined by parallel numerical simulations. Water Resources Research, 43(10).

Eckert, P. and Appelo, C.A.J., 2002. Hydrogeochemical modeling of enhanced benzene, toluene, ethylbenzene, xylene (BTEX) remediation with nitrate. Water Resources Research, 38(8): 5-1-5-11.

Elfeki, A.M., Uffink, G. and Lebreton, S., 2012. Influence of temporal fluctuations and spatial heterogeneity on pollution transport in porous media. Hydrogeology Journal, 20(2): 283-297.

Elfeki, A.M., Uffink, G.J. and Barends, F.B., 1997. Groundwater Contaminant Transport: Impact of heterogenous characterization: a new view on dispersion. CRC Press.

Engesgaard, P. and Kipp, K.L., 1992. A geochemical transport model for redox-controlled movement of mineral fronts in groundwater flow systems: A case of nitrate removal by oxidation of pyrite. Water resources research, 28(10): 2829-2843.

Essaid, H.I. and Bekins, B.A., 1997. BIOMOC, A multispecies solute-transport model with biodegradation.

European Commission, 2008. Groundwater protection in Europe - The new Groundwater Directive : consolidating the EU regulatory framework Office for Official Publications of the European Communities.

European Union, 1998. Council Directive 98/83/EC Off. J. Eur. Com. L 330:32-54. EU, Brussels.

Fan, A.M. and Steinberg, V.E., 1996. Health Implications of Nitrate and Nitrite in Drinking Water: An Update on Methemoglobinemia Occurrence and Reproductive and Developmental Toxicity. Regulatory Toxicology and Pharmacology, 23(1): 35-43.

Fiori, A., Jankovic, I. and Dagan, G., 2011. The impact of local diffusion upon mass arrival of a passive solute in transport through three-dimensional highly heterogeneous aquifers. Advances in Water Resources, 34(12): 1563-1573.

Freeze, R.A., 1975. A stochastic-conceptual analysis of one-dimensional groundwater flow in nonuniform homogeneous media. Water Resources Research, 11(5): 725-741.

Graham, W.D. and McLaughlin, D.B., 1991. A stochastic model of solute transport in groundwater: Application to the Borden, Ontario, Tracer Test. Water Resources Research, 27(6): 1345-1359.

Groffman, P. et al., 2009. Challenges to incorporating spatially and temporally explicit phenomena (hotspots and hot moments) in denitrification models. Biogeochemistry, 93(1-2): 49-77.

Gu, C., Anderson, W. and Maggi, F., 2012. Riparian biogeochemical hot moments induced by stream fluctuations. Water Resources Research, 48(9): n/a-n/a.

Gusman, A.J. and Mariño, M.A., 1999. Analytical modeling of nitrogen dynamics in soils and ground water. Journal of Irrigation and Drainage Engineering, 125(6): 330-337.

Hansen, A.L., Gunderman, D., He, X. and Refsgaard, J.C., 2014. Uncertainty assessment of spatially distributed nitrate reduction potential in groundwater using multiple geological realizations. Journal of Hydrology, 519, Part A: 225-237.

Hayakawa, A., Hatakeyama, M., Asano, R., Ishikawa, Y. and Hidaka, S., 2013. Nitrate reduction coupled with pyrite oxidation in the surface sediments of a sulfide-rich ecosystem. Journal of Geophysical Research: Biogeosciences, 118(2): 639-649.

He, W., 2016. Reactive transport modeling at hillslope scale with high performance computing methods, Technische Universität Dresden, Dresden.

He, W. et al., 2015. A parallelization scheme to simulate reactive transport in the subsurface environment with OGS#IPhreeqc 5.5.7-3.1.2. Geosci. Model Dev., 8(10): 3333-3348.

Heaton, T.H.E. and Vogel, J.C., 1981. "Excess air" in groundwater. Journal of Hydrology, 50: 201-216.

Heinelt, H., Swyngedouw, E. and Getmis, P., 2002. Achieving Sustainable and Innovative Policies through Participatory Governance in a Multi-level Context - Interim Report on water supply, Research project funded by the European community under the 5th frameowrk program (Contract n HPSE-CT-1999-00028).

Houlding, S., 2000. Practical geostatistics: modeling and spatial analysis. Manual, 1. Springer Science & Business Media.

Höyng, D., Prommer, H., Blum, P., Grathwohl, P. and Mazo D'Affonseca, F., 2015. Evolution of carbon isotope signatures during reactive transport of hydrocarbons in heterogeneous aquifers. Journal of Contaminant Hydrology, 174: 10-27.

IPNI, IPNI Nitrogen Notes, International Plant Nutrition Institute (IPNI). http://www.ipni.net/publication/nitrogen-en.nsf/0/668099AE825517CB85257DD600054B8C/$FILE/NitrogenNotes-EN-5.pdf (accessed 05.07.2017).

Jang, E. et al., 2017. Identifying the influential aquifer heterogeneity factor on nitrate reduction processes by numerical simulation. Advances in Water Resources, 99: 38-52.

Juncher Jørgensen, C., Jacobsen, O.S., Elberling, B. and Aamand, J., 2009. Microbial Oxidation of Pyrite Coupled to Nitrate Reduction in Anoxic Groundwater Sediment. Environmental Science & Technology, 43(13): 4851-4857.

Kalbus, E., Schmidt, C., Molson, J.W., Reinstorf, F. and Schirmer, M., 2009. Influence of aquifer and streambed heterogeneity on the distribution of groundwater discharge. Hydrol. Earth Syst. Sci., 13(1): 69-77.

Kehew, A.E., 2001. Applied Chemical Hydrogeology. Prentice Hall.

Kim, K.-H. et al., 2015. Quantification of nitrate sources in groundwater using hydrochemical and dual isotopic data combined with a Bayesian mixing model. Agriculture, Ecosystems & Environment, 199: 369-381.

Kinzelbach, W., 1988. The random walk method in pollutant transport simulation, Groundwater flow and quality modelling. Springer, pp. 227-245.

Kinzelbach, W., Schäfer, W. and Herzer, J., 1991. Numerical modeling of natural and enhanced denitrification processes in aquifers. Water Resources Research, 27(6): 1123-1135.

Kludt, C. et al., 2013. Process-oriented investigation of the nitrate-removal-capacity of the aquifers in the Hessian Ried, EGU General Assembly 2013.

Kludt, C. et al., 2016. Identification of denitrification processes and prognoses of denitrification potential in the sediments of the Hessian Ried. Grundwasser: 1-15.

Knipp, E., 2012. Charakterisierung des Nitratabbaupotenzials an Bohrkernproben aus dem Hessischen Ried - Methodenvalidierung zur Lokalisierung regionaler Abbauhorizonte, Technical University of Darmstadt, Darmstadt, Germany.

Kolditz, O. et al., 2012. OpenGeoSys: an open-source initiative for numerical simulation of thermo-hydro-mechanical/chemical (THM/C) processes in porous media. Environmental Earth Sciences, 67(2): 589-599.

Korom, S.F., 1992. Natural denitrification in the saturated zone: A review. Water Resources Research, 28(6): 1657-1668.

Kosakowski, G. and Watanabe, N., 2014. OpenGeoSys-Gem: A numerical tool for calculating geochemical and porosity changes in saturated and partially saturated media. Physics and Chemistry of the Earth, Parts A/B/C, 70–71: 138-149.

Li, D., Bauer, S., Benisch, K., Graupner, B. and Beyer, C., 2013. OpenGeoSys-ChemApp: a coupled simulator for reactive transport in multiphase systems and application to CO2 storage formation in Northern Germany. Acta Geotechnica, 9(1): 67-79.

Li, L., Peters, C. and Celia, M., 2007. Effects of mineral spatial distribution on reaction rates in porous media. Water resources research, 43(1).

Li, R. and Merchant, J.W., 2013. Modeling vulnerability of groundwater to pollution under future scenarios of climate change and biofuels-related land use change: A case study in North Dakota, USA. Science of The Total Environment, 447: 32-45.

Liao, L., Green, C.T., Bekins, B.A. and Böhlke, J.K., 2012. Factors controlling nitrate fluxes in groundwater in agricultural areas. Water Resources Research, 48(6): n/a-n/a.

Ludwig, F., 2011. Regional variation of chemical groundwater composition in Hessen, Germany, and its relation to the aquifer geology, Albert-Ludwigs-Universität Freiburg.

MacQuarrie, K.T.B., Sudicky, E.A. and Robertson, W.D., 2001. Numerical simulation of a fine-grained denitrification layer for removing septic system nitrate from shallow groundwater. Journal of Contaminant Hydrology, 52(1–4): 29-55.

Maggi, F. et al., 2008. A mechanistic treatment of the dominant soil nitrogen cycling processes: Model development, testing, and application. Journal of Geophysical Research: Biogeosciences, 113(G2): n/a-n/a.

Miotliński, K., 2008. Coupled Reactive Transport Modeling of Redox Processes in a Nitrate-Polluted Sandy Aquifer. Aquatic Geochemistry, 14(2): 117-131.

Mohamed, M., Hatfield, K., Hassan, A. and Klammler, H., 2010. Stochastic evaluation of subsurface contaminant discharges under physical, chemical, and biological heterogeneities. Advances in Water Resources, 33(7): 801-812.

Mohamed, M.M., Hatfield, K. and Hassan, A.E., 2006. Monte Carlo evaluation of microbial-mediated contaminant reactions in heterogeneous aquifers. Advances in water resources, 29(8): 1123-1139.

Mohamed , M.M.A., Hatfield, K. and Hassan, A.E., 2006. Monte Carlo evaluation of microbial-mediated contaminant reactions in heterogeneous aquifers. Advances in Water resources, 29(8): 1123-1139.

Mueller, D.K., Hamilton, P.A., Helsel, D.R., Hitt, K.J. and Ruddy, B.C., 1995. Nutrients in ground water and surface water of the United States; an analysis of data through 1992. 95-4031.

Murakami, H., 2010. Development of a bayesian geostatistical data assimilation method and application to the Hanford 300 Area, University of California at Berkeley.

Murphy, L.L., 2006. The effects of viscosity and subsurface heterogeneity on a braine barrier approach to DNAPL remediation, University of North Carolina at Chapel Hill.

NIER, 2012. Groundwater Pollution and Background Quality in Cropping-Livestock Farming Complex Areas.

Nolan, B.T., Ruddy, B.C., Hitt, K.J. and Helsel, D.R., 1997. Risk of Nitrate in groundwaters of the United States a national perspective. Environmental science & technology, 31(8): 2229-2236.

Otero, N., Torrentó, C., Soler, A., Menció, A. and Mas-Pla, J., 2009. Monitoring groundwater nitrate attenuation in a regional system coupling hydrogeology with multi-isotopic methods: The case of Plana de Vic (Osona, Spain). Agriculture, Ecosystems & Environment, 133(1–2): 103-113.

Oyarzun, R., Arumí, J., Salgado, L. and Mariño, M., 2007. Sensitivity analysis and field testing of the RISK-N model in the Central Valley of Chile. Agricultural Water Management, 87(3): 251-260.

Park, C.-H., Beyer, C., Bauer, S. and Kolditz, O., 2008. A study of preferential flow in heterogeneous media using random walk particle tracking. Geosciences Journal, 12(3): 285-297.

Parkhurst, D.L. and Appelo, C., 2013. Description of input and examples for PHREEQC version 3: a computer program for speciation, batch-reaction, one-dimensional transport, and inverse geochemical calculations. 2328-7055, US Geological Survey.

Parkhurst, D.L. and Appelo, C.A.J., 1999. User's guide to PHREEQC (Version 2) : a computer program for speciation, batch-reaction, one-dimensional transport, and inverse geochemical calculations. 99-4259.

Parsons, S., 2005. Advanced Oxidation Processes for Water and Wastewater Treatment. Water Intelligence Online, 4.

Pebesma, E.J., 2004. Multivariable geostatistics in S: the gstat package. Computers & Geosciences, 30(7): 683-691.

Pebesma, E.J. and Wesseling, C.G., 1998. Gstat: a program for geostatistical modelling, prediction and simulation. Computers & Geosciences, 24(1): 17-31.

Petzoldt, T. and Rinke, K., 2007. Simecol: An Object-Oriented Framework for Ecological Modeling in R. Journal of Statistical Software: 1548-7660.

Peyrard, D. et al., 2011. Longitudinal transformation of nitrogen and carbon in the hyporheic zone of an N-rich stream: A combined modelling and field study. Physics and Chemistry of the Earth, Parts A/B/C, 36(12): 599-611.

Piper, A.M., 1944. A graphic procedure in the geochemical interpretation of water-analyses. Eos, Transactions American Geophysical Union, 25(6): 914-928.

Postma, D., Boesen, C., Kristiansen, H. and Larsen, F., 1991. Nitrate Reduction in an Unconfined Sandy Aquifer: Water Chemistry, Reduction Processes, and Geochemical Modeling. Water Resources Research, 27(8): 2027-2045.

Preiß, I., 2013. Anwendbarkeit einer Screeningmethode zur Bestimmung des Nitratabbaupotenzials mittels Redoxprofilmessungen in Grundwassermessstellen im Hessischen Ried, Technische Universität Darmstadt.

R Core Team, 2014. R: A language and environment for statistical computing. R Foundation for Statistical Computing, R Foundation for Statistical Computing, Vienna, Austria.

Regnier, P., Jourabchi, P. and Slomp, C., 2003. Reactive-transport modeling as a technique for understanding coupled biogeochemical processes in surface and subsurface environments. Netherlands Journal of Geosciences/Geologie en Mijnbouw, 82(1).

Rinke, K. et al., 2013. Reservoirs as sentinels of catchments: the Rappbode Reservoir Observatory (Harz Mountains, Germany). Environmental Earth Sciences, 69(2): 523-536.

Rivett, M.O., Buss, S.R., Morgan, P., Smith, J.W. and Bemment, C.D., 2008. Nitrate attenuation in groundwater: a review of biogeochemical controlling processes. Water research, 42(16): 4215-4232.

Rubin, Y., 1990. Correction to ―Stochastic modeling of macrodispersion in heterogeneous porous media" by Yoram Rubin. Water Resources Research, 26(10): 2631-2631.

Rubin, Y., 2003. Applied stochastic hydrogeology. Oxford University Press.

Sappa, G., Barbieri, M., Ergul, S. and Ferranti, F., 2012. Hydrogeological Conceptual Model of Groundwater from Carbonate Aquifers Using Environmental Isotopes (<sup>18</sup>O, <sup>2</sup>H) and Chemical Tracers: A Case Study in Southern Latium Region, Central Italy. Journal of Water Resource and Protection, Vol.04No.09: 22.

Scholl, M.A., 2000. Effects of heterogeneity in aquifer permeability and biomass on biodegradation rate calculations—Results from numerical simulations. Ground Water, 38(5): 702-712.

Schulze-Makuch, D., 2009. Advection, Dispersion, Sorption, Degradation, Attenuation. Groundwater-Volume II: 55.

Shao, H., Kulik, D.A., Berner, U., Kosakowski, G. and Kolditz, O., 2009. Modeling the competition between solid solution formation and cation exchange on the retardation of aqueous radium in an idealized bentonite column. Geochemical Journal, 43(6): e37-e42.

Simmons, C.T., Fenstemaker, T.R. and Sharp Jr, J.M., 2001. Variable-density groundwater flow and solute transport in heterogeneous porous media:

approaches, resolutions and future challenges. Journal of Contaminant Hydrology, 52(1–4): 245-275.
Singh, A.K., Raj, B., Tiwari, A.K. and Mahato, M.K., 2013. Evaluation of hydrogeochemical processes and groundwater quality in the Jhansi district of Bundelkhand region, India. Environmental Earth Sciences, 70(3): 1225-1247.
Singleton, M.J. et al., 2007. Saturated Zone Denitrification: Potential for Natural Attenuation of Nitrate Contamination in Shallow Groundwater Under Dairy Operations. Environmental Science & Technology, 41(3): 759-765.
Smith, L. and Freeze, R.A., 1979. Stochastic analysis of steady state groundwater flow in a bounded domain: 2. Two-dimensional simulations. Water Resources Research, 15(6): 1543-1559.
Soetaert, K. and Meysman, F., 2012. Reactive transport in aquatic ecosystems: Rapid model prototyping in the open source software R. Environmental Modelling & Software, 32(0): 49-60.
SRU, 2015. The implementation of the Water Frameowrk Directive in Germany with regard to nitrogen inputs from agriculture, German Advisory Council on the Environment, Berlin.
Steefel, C.I., 2009. CrunchFlow. Software for modeling multicomponent reactive flow and transport, User's manual.
Steefel, C.I. et al., 2014. Reactive transport codes for subsurface environmental simulation. Computational Geosciences, 19(3): 445-478.
Sudicky, E.A., 1986. A natural gradient experiment on solute transport in a sand aquifer: Spatial variability of hydraulic conductivity and its role in the dispersion process. Water Resources Research, 22(13): 2069-2082.
Sudicky, E.A., Schellenberg, S.L. and MacQuarrie, K.T.B., 1990. Assessment of the behaviour of conservative and biodegradable solutes in heterogeneous porous media. In: J. Cushman (Editor), Dynaics of Fluids in Hierarchical Porous Formations. Academic Press.
Sun, F., 2011. Computational Hydrosystem Anslysis: Applications to the Meijiang and Nankou Catchments in China, Technische Universität Dresden, Dresden, Germany.
Sun, F. et al., 2011. Groundwater drawdown at Nankou site of Beijing Plain: model development and calibration. Environmental Earth Sciences, 64(5): 1323-1333.
Sun, F. et al., 2012. Groundwater deterioration in Nankou—a suburban area of Beijing: data assessment and remediation scenarios. Environmental Earth Sciences, 67(6): 1573-1586.
Tarki, M., Dassi, L. and Jedoui, Y., 2012. Groundwater composition and recharge origin in the shallow aquifer of the Djerid oases, southern Tunisia: implications of return flow. Hydrological Sciences Journal, 57(4): 790-804.
Tompson, A.F.B., Schafer, A.L. and Smith, R.W., 1996. Impacts of Physical and Chemical Heterogeneity on Cocontaminant Transport in a Sandy Porous Medium. Water Resources Research, 32(4): 801-818.
Torrentó, C., Cama, J., Urmeneta, J., Otero, N. and Soler, A., 2010. Denitrification of groundwater with pyrite and Thiobacillus denitrificans. Chemical Geology, 278(1–2): 80-91.

Torrentó, C. et al., 2011. Enhanced denitrification in groundwater and sediments from a nitrate-contaminated aquifer after addition of pyrite. Chemical Geology, 287(1–2): 90-101.

Twomey, K.M., Stillwell, A.S. and Webber, M.E., 2010. The unintended energy impacts of increased nitrate contamination from biofuels production. Journal of Environmental Monitoring, 12(1): 218-224.

UNEP, 2013. Global Environment Outlook 2000, 1. Routledge.

USEPA, 2009. National Primary Drinking Water Regulations United States Environmental Protection Agency.

Wang, W., Kosakowski, G. and Kolditz, O., 2009. A parallel finite element scheme for thermo-hydro-mechanical (THM) coupled problems in porous media. Computers & Geosciences, 35(8): 1631-1641.

Widdowson, M.A., Molz, F.J. and Benefield, L.D., 1988. A numerical transport model for oxygen- and nitrate-based respiration linked to substrate and nutrient availability in porous media. Water Resources Research, 24(9): 1553-1565.

Williamson, M.A. and Rimstidt, J.D., 1994. The kinetics and electrochemical rate-determining step of aqueous pyrite oxidation. Geochimica et Cosmochimica Acta, 58(24): 5443-5454.

Wriedt, G. and Rode, M., 2006. Modelling nitrate transport and turnover in a lowland catchment system. Journal of Hydrology, 328(1): 157-176.

Xie, M., Kolditz, O. and Moog, H.C., 2011. A geochemical transport model for thermo-hydro-chemical (THC) coupled processes with saline water. Water Resources Research, 47(2).

Xu, Z., Hu, B.X., Davis, H. and Cao, J., 2015. Simulating long term nitrate-N contamination processes in the Woodville Karst Plain using CFPv2 with UMT3D. Journal of Hydrology, 524: 72-88.

Yabusaki, S.B. et al., 2011. Variably saturated flow and multicomponent biogeochemical reactive transport modeling of a uranium bioremediation field experiment. Journal of Contaminant Hydrology, 126(3–4): 271-290.

Zan, F. et al., 2011. Phosphorus distribution in the sediments of a shallow eutrophic lake, Lake Chaohu, China. Environmental Earth Sciences, 62(8): 1643-1653.

Zech, A., Zehner, B., Kolditz, O. and Attinger, S., 2016. Impact of heterogeneous permeability distribution on the groundwater flow systems of a small sedimentary basin. Journal of Hydrology, 532: 90-101.

Zhang, Y.-C. et al., 2013. Model-Based Integration and Analysis of Biogeochemical and Isotopic Dynamics in a Nitrate-Polluted Pyritic Aquifer. Environmental Science & Technology, 47(18): 10415-10422.

Zhang, Y.-C., Slomp, C.P., Broers, H.P., Passier, H.F. and Van Cappellen, P., 2009. Denitrification coupled to pyrite oxidation and changes in groundwater quality in a shallow sandy aquifer. Geochimica et Cosmochimica Acta, 73(22): 6716-6726.

Zinder, B., Furrer, G. and Stumm, W., 1986. The coordination chemistry of weathering: II. Dissolution of Fe(III) oxides. Geochimica et Cosmochimica Acta, 50(9): 1861-1869.